**CIRCULATION AND EXCHANGE IN THE SAGINAW BAY-LAKE HURON SYSTEM:
OBSERVATIONS AND NUMERICAL MODELING**

By

Tuan Duc Nguyen

A DISSERTATION

Submitted to
Michigan State University
in partial fulfillment of the requirements
for the degree of

Civil Engineering - Doctor of Philosophy

2014

ABSTRACT

CIRCULATION AND EXCHANGE IN THE SAGINAW BAY-LAKE HURON SYSTEM:
OBSERVATIONS AND NUMERICAL MODELING

By

Tuan Duc Nguyen

Knowledge of lake circulation is essential for addressing many issues ranging from water quality to human and ecosystem health. Lake Huron, the third largest of the Great Lakes by volume, has been significantly affected by natural and anthropogenic activities. Since Lake Huron is a connecting waterway between the upper and lower Great Lakes, understanding Lake Huron circulation and thermal structure is also important for questions involving the lower lakes.

In this study, we use a three-dimensional, unstructured grid hydrodynamic model to examine circulation, thermal structure, ice cover extent, and exchange in the Saginaw Bay - Lake Huron system during summer months for 3 consecutive years (2009-2011) and winter months for 2 years (2010 and 2013). The model was tested against ADCP observations of currents, data from a Lagrangian drifter experiment in the Saginaw Bay, observations of temperature from thermistor chains, and temperature data from the National Data Buoy Center stations. Mean circulation was predominantly cyclonic in the main basin of Lake Huron with current speeds in the surface layer being highest in August in summer and in January in winter. Circulation in the Saginaw Bay was characterized by the presence of an anti-cyclonic gyre at the mouth of the outer bay and two recirculating cells within the inner bay for both seasons. The ice cover data extracted from Moderate Resolution Imaging Spectroradiometer (MODIS) with relatively high spatial resolution and from the Great Lakes Ice Atlas were used to test against results obtained from an ice model. The results show that the ice model was able to simulate lake circulation and ice cover extent in winter season reasonably well. The percent coverage of ice reached a

maximum of 38.3% and 38.7% in mid-February in 2010 and beginning of March in 2013 respectively. New estimates are provided for the mean flushing times (computed as the volume of the bay divided by the rate of inflow) and residence times (computed as e-folding flushing times treating the bay as a continuously stirred tank reactor) for Saginaw Bay for summer and winter seasons. The average flushing time (over the three months of summer and for all three years) was 23.0 days for the inner bay and 9.9 days for the entire bay. The corresponding values for the winter season are 43.2 days and 15.6 days respectively. The mean e-folding flushing time was 62 days for summer and 64.7 days for winter for the inner bay and 115 days for the summer and 114.2 days for the winter conditions for the entire bay. Empirical relations between the mean residence time and river discharge were proposed. To characterize the behavior of river plumes in the inner Saginaw Bay, the absolute diffusivity values in the along-shore and cross-shore directions were calculated using data from GPS-enabled Lagrangian drifters and simulation results based on particle transport models.

To my parents, my wife, and my lovely children

ACKNOWLEDGEMENTS

TABLE OF CONTENTS

LIST OF TABLES

LIST OF FIGURES

Chapter 1

Introduction

1.1   Problem description

Knowledge of circulation patterns in lakes and oceans is essential to addressing a number of issues ranging from water quality to ecosystem modeling. Knowledge of lake circulation has proven to be indispensable in prediction of pollution from point sources or industrial discharge into large bodies of water. In addition, currents are a primary factor in understanding many environmental issues such as harmful algal blooms, dead zones, and so on.

Lake Huron is a large aquatic system and the third largest of the Great Lakes by volume. Lake Huron encompasses three distinct basins (Gerogian Bay, North Channel, and the main basin which includes Saginaw Bay) as shown in Figure 1, with several islands (St. Joseph Island, Bois Blanc Island, Drummond Island, Cockburn Island, Clapperton Island, Manitoulin Island, Fitzwilliam Island, Charity Island, etc.) and bays (Georgian Bay, Saginaw Bay, Thunder Bay). The prominent bathymetric feature in Lake Huron is the mid-lake ridge that extends southeastward from Thunder Bay at Alpena on the west side across to Point Clark on the east side. The ridge (Alpena-Amberley Ridge or AAR) separates the lake into the southwestern and

northeastern basins. The shallower southwestern basin has a maximum depth of about 90 m while the deeper northeastern basin has a maximum depth of about 200 m. In addition to the complex topography, the wind strongly influences circulation in Lake Huron.

As in the other Great Lakes, Lake Huron has been significantly affected by natural and anthropogenic activities. The Lake is affected by water quality degradation, invasion of zebra mussels [*Fahnenstiel et al.*, 1995; *Heath et al.*, 1995; *Bierman et al.*, 2005; *Fishman et al.*, 2009], toxic contaminants and eutrophication in some localized areas [*Nalepa et al.*, 2007]. Water quality problems such as persistance of Escherichia coli [*Alm et al.*, 2006], and mercury contamination [*Marvin et al.*, 2004] are also pertinent issues. In addition, recent awareness of the water level declining in the Lake Michigan-Huron system has made it necessary to study and compare the circulation and exchanges with the past. Shallow areas and embayments such as Saginaw Bay are believed to have increased benthic algal growth from invasive mussel [*Hecky et al.*, 2004]. Lake Huron is a connecting water way between the upper and lower lakes in the Great Lakes. Therefore, all of these contaminants will impact not only Lake Huron ecosystem but also the ecosystems of the lower lakes. Knowledge of the water movement and temperature distribution are of critical importance.

Saginaw Bay is an important part of Lake Huron that receives flow from the Saginaw River. The Saginaw Bay - Lake Huron system is significantly impacted by human activities and figures prominently in the list of Areas of Concern [Great Lakes Water Quality Agreement, 1978]. The Saginaw River, which drains an area of over 16,000 km^2, is the major source to the Bay with an average discharge of about 100 m^3/s [*Danek and Saylor*, 1977]. The Bay is 87 km long, and the width varies between 20 km and 46 km. The Bay is often divided into the inner and outer regions based on topographic features and water circulation patterns (Figure 3a). The

bay has extensive shallows averaging 4.0m and 12.0m in depth in the inner and outer bays, respectively.

The Saginaw Bay is of particular interest because it is the region that anthropogenic activities interact most strongly with the Bay environment. A significant portion of the total loading from industrial activity is released along the Saginaw River. Persistent contamination of the water column and bottom sediment has resulted in degraded water quality. It is well-known that embayed regions tend to accumulate contaminants due to their long residence times [*Nixon et al., 1996*]. Offshore transport and mixing with lake waters are the dominant process for reduction in concentrations of contaminants in embayed regions attached to large lakes [*Ge, et al.*, 2012; *Thupaki, et al.*, 2010]. While mixing is dominated by small-scale hydrodynamics and shear [*Lawrence et al.*, 1995; *Spydell et al.*, 2007], advective exchange between Saginaw Bay and Lake Huron is strongly influenced by large-scale circulation patterns.

Figure 1: Map of Lake Huron showing the important physical features: Manitoulin Basin; Bay City Basin; NC: North Channel; Alpena- Amberley Ridge; Georgian Bay. (source: http://www.ngdc.noaa.gov/).

1.2   Summer Circulation and Thermal Structure

The large scale circulation in Lake Huron was first described by *Harrington* [1894], who used data from drift bottle studies to conclude that circulation pattern is generally counterclockwise in the main basin of Lake Huron. While drift bottles have higher error than modern Lagrangian drifter designs due to stokes-drift, wind forces, and lack of real-time GPS tracking, many of the conclusions Harrington arrived at have been supported by later observations. *Sloss and Saylor* [1976] used observational datasets from extensive current mooring measurements to confirm that while the northern two-thirds of the lake is dominated by counterclockwise circulation during summer, the shallower southern part shows a much more complex circulation pattern. They also found that stratification during summer allowed the inertial component to dominate open lake circulation.

Although, Lake Huron and Michigan are considered one ecosystem due to their hydraulic connectivity, Lake Huron has been poorly studied when compared to Lake Michigan. A number of studies have used numerical models to examine circulation in Lake Huron. *Sheng and Rao* [2006] used a three-dimensional hydrodynamic model based on the primitive equation, *z*-level CANDIE ocean model to simulate large-scale circulation and temperature distribution in Lake Huron. Using a nested-grid methodology, they were able to resolve small-scale hydrodynamics in the Georgian Bay region. More recently, *Anderson and Schwab* [2013] used the unstructured grid Finite Volume Coastal Ocean Model (FVCOM) to develop a Lake Michigan-Huron model to simulate currents in the Straits of Mackinac. *Bai et al.,* [2013] also implemented the sigma-coordinate, unstructured grid ocean model (GL-FVCOM) in all five Great Lakes with 21 terrain following layers in the vertical to simulate circulation and thermal structure for 1993-2008. Physical features such as shallow depths and complex bathymetry in addition to the presence of a

sill near the entrance of the Bay City Basin (BCB) produce a complex circulation pattern within the Saginaw Bay. As a result, hydrodynamic models using coarse grids will not be able to adequately resolve circulation within the Saginaw Bay.

Figure 2: Aerial view of the Saginaw Bay area showing the upstream region along the Saginaw River, the river mouth, and the Shelter Island (*Photo credit* : Doc Searls)

Circulation in Lake Huron shows more spatial variation than other large lakes of comparable size in North America (e.g., Lake Superior and Lake Michigan) due to the presence of several islands, bays and other complex physical features. Studies using numerical models to examine circulation in Lake Huron have used multi-resolution (nested) structured grids [*Sheng and Rao*, 2006] or coarse-resolution unstructured grids [*Bai et al.*, 2013]. In order to reduce the numerical

error in simulating the thermocline and horizontal pressure gradient terms, *Sheng and Rao* [2006] used the *z*-level ocean model CANDIE [*Sheng et al.*, 1998]. Accurately representing the physical features of the lake basin in the computational domain is necessary in order to simulate currents, thermal structure as well as large-scale hydrodynamics.

Using time-series analyses and numerical simulations, *Allender* [1975] and *Allender and Green* [1976] determined that circulation within the bay is coupled to large-scale circulation in Lake Huron. Using a combination of Lagrangian drifter observations from current meters deployed in Saginaw Bay, *Danek and Saylor* [1977] and *Saylor and Danek* [1976] determined the circulation patterns inside Saginaw Bay for different wind directions. They found that when wind direction was parallel to axis of the bay, exchange rate between the inner and outer bay was $3700 m^3$/s. More recently, in their analysis of the seasonal circulation in the Great Lakes, *Beletsky et al.,*[1999] observed that mean currents during winter are higher than during summer months. Based on the surface current measurements, they also inferred the presence of a return flow out of Georgian Bay at deeper depths. *Schertzer et al.,*[2008] have compiled the mean circulation, inter-lake exchange and climatology for Lake Huron.

Most of the previous studies described the circulation in Lake Huron based on observational data that is limited in space and time. Description of the annual pattern of circulation in Lake Huron is impossible because of a lack of sufficient observations [*Schertzer et al.,*2008] and overall the system is still poorly understood. Therefore, using a numerical model to obtain a more detailed knowledge of both spatial and temporal dynamics of water movement in the lake shows great promise.

1.3   Winter Circulation and Ice Cover Extents

The limited literature on the winter circulation of Lake Huron includes ice extents while the annual cycle of ice formation and loss affects physical processes within the lake and the ecosystem of the lake [*Assel,* 2005]. The winter season is characterized by nearly homogeneous water in Lake Huron as in the other Great Lakes. The circulation during cold weather has received very little attention not only in Lake Huron, but in all of the Great Lakes as well. The main reason is due to lack of observational data during the winter season.

One of the first attempts to describe winter circulation in Lake Huron was carried out by *Saylor and Miller [1979].* In their study they used twenty-one current moorings deployed in Lake Huron during the winter of 1974-1975 for approximately 6 months. They concluded that there is a strong cyclonic flow throughout the winter with current speeds that ranged from 1 to 7cm/s with a mean of 3cm/s. Because of isothermal conditions in the water column, the winter currents are barotropic [*Beletsky et al., 1999*]. It has been known that the Great Lakes have considerable influence on the regional climate *[Bates and Giorgi, 1993; Scott and Huff, 1996]*. *Rao and Murty* [1970] used a homogeneous, vertically integrated numerical model to conclude that winter circulation in Lake Ontario was driven by wind.

The hydrology of the Great Lakes can affect local meteorological conditions in the long term. For example, *Scott and Huff [1996]* estimated that lake-effect precipitation increased 90% downwind of Lake Huron in the winter time. In addition, understanding the major effects of colder weather on the lake are crucial in predicting water movement patterns and water temperature structure. More recently, *Fujisaki et al.,[2012]* used the Princeton Ocean Model (POM) which included ice processes to investigate the seasonal variation of ice cover on Lake Erie. The study showed that the packed ice cover slowed down the surface water velocity. To our

knowledge, simulation of lake processes beneath the ice cover in three dimensions has not been attempted. Therefore, there are large gaps in our understanding of lake circulation, thermal structure, ice cover extent, and the water exchange rates between Saginaw Bay and the main lake in the winter.

1.4   Residence and Flushing Times

Residence and flushing times of an estuary are important variables used to estimate the rate of removal of pollutants from the bay. As concluded by *Monsen et al.*, [2002], first-order transport time scales such as residence times and flushing times within the bay are useful for understanding and interpreting the fate and transport of contaminants, nutrient budgets, the occurrence of harmful algal blooms and for comparing processes and rates across different ecosystems.

There have been a few studies of the mean residence time in Saginaw Bay and Lake Huron system. *Quinn [1992]* estimated the residence time defined as the time it takes to replace the water volume of Lake Huron as 22 years. *Saylor and Danek*, [1976] calculated an exchange rate between the inner bay and outer bay of 3700m^3/s and a mean residence time of 26.5 days for the inner bay. The residence time of any bay may vary with several factors such as wind direction, and river inflow. Since the Saginaw bay is shallow, the residence time is strongly influenced by wind. As *Saylor and Danek*, [1976] pointed out, the residence time of water in the bay is much longer with the winds perpendicular to the axis of the bay. In an earlier study *Dolan [1975]* calculated a residence time of 110 days for the inner bay based on a time-variable chloride model.

Until now, there have been no observational studies on residence time in Saginaw Bay since the early work cited above. A 3D lake-wide numerical model with additional water quality models provides a great opportunity to study residence time and flushing time for the bay in detail for both the summer and winter seasons. This research will estimate the residence time based on different methods that are presented in Chapter 5.

Significant progress has been made in recent years in characterizing the transport time scales for surface water bodies using hydrodynamic and transport models [*Andutta et al.*, 2013; *Camacho and Martin*, 2013; *Phelps et al.*, 2013; *Hsu et al.*, 2013; *Wan et al.*, 2013; *Liu et al.*, 2012; *Andrado´ttir et al.*, 2012; *Jouon et al.*, 2006]. Although some estimates of residence times are available for the Saginaw Bay [*Dolan*, 1975; *Saylor and Danek*, 1976], they are nearly 40 years old and much has changed in terms of our ability to observe and model natural systems since then. Recent concerns associated with environmental issues in the Saginaw Bay highlight the need for accurate estimates of transport timescales in the bay and one of the objectives of this work is to fill this gap. Furthermore, identifying the spatial patterns of residence time throughout Saginaw Bay for the forecasting water quality is critical. Terms such as residence time and flushing time, however, are defined and used in many different ways in the literature. Following the suggestions of *Monsen et al.* [2002] and *Bolin and Rodhe* [1973] who recommend that the terms be defined precisely and used with care to avoid confusion, we define these transport time scales in the next chapter and describe how they are calculated.

1.5   Goals of the Thesis

The aim of this study was to characterize summer and winter circulation, thermal structure and ice cover extent in the Lake Huron - Saginaw Bay system and to quantify residence and flushing times within the bay. This was performed using a combination of field and satellite-based observations and high-resolution, three-dimensional, unstructured grid numerical model.

1.6   Structure of the Thesis

Chapter 1: Introduction

Chapter 2: Field Observations and Analysis

Chapter 3: Summer Circulation and Thermal Structure

Chapter 4: Ice Cover, Winter Circulation and Thermal Structure

Chapter 5: Residence Time in the Saginaw Bay and Lake Huron System

Chapter 6: Conclusions

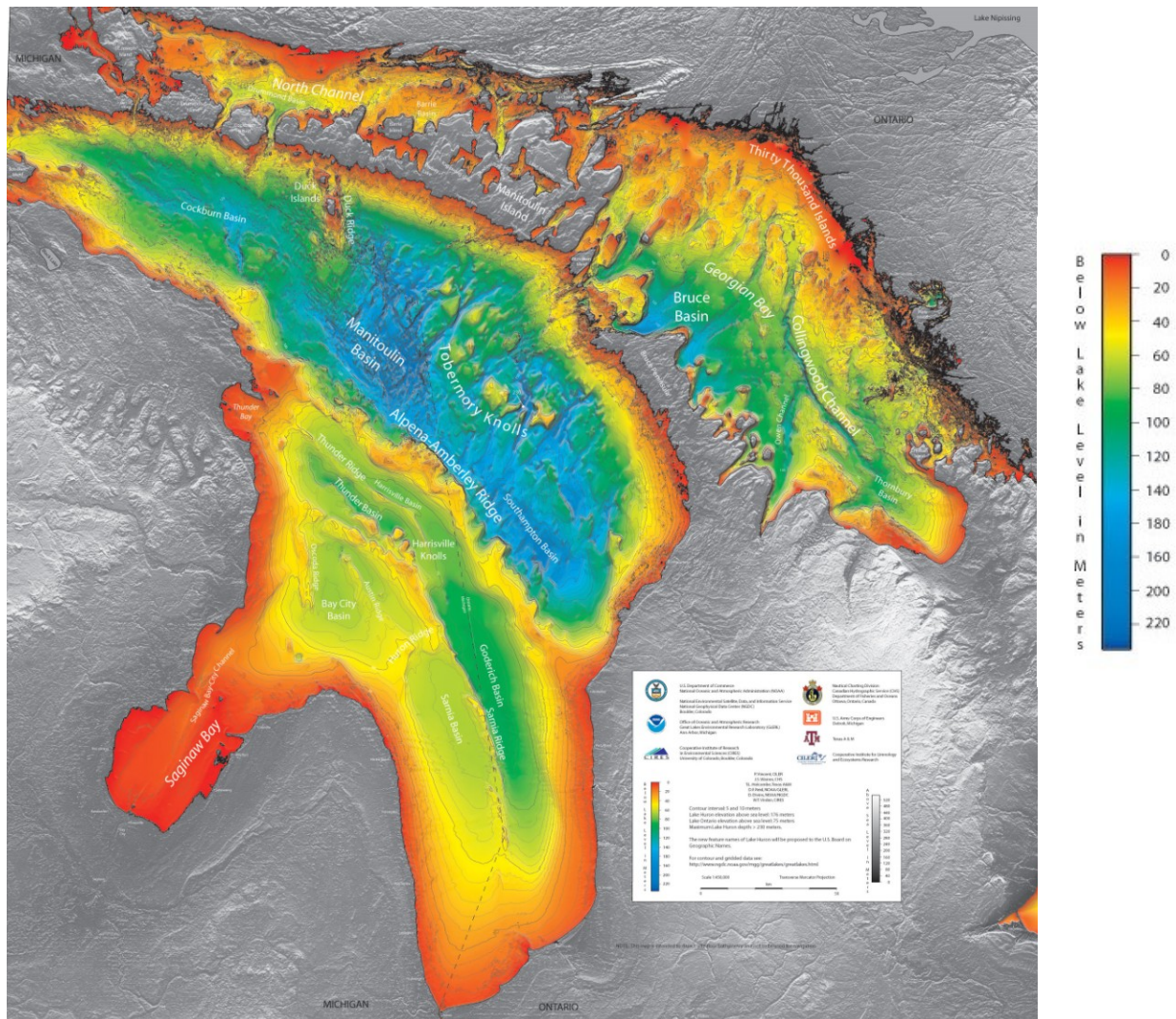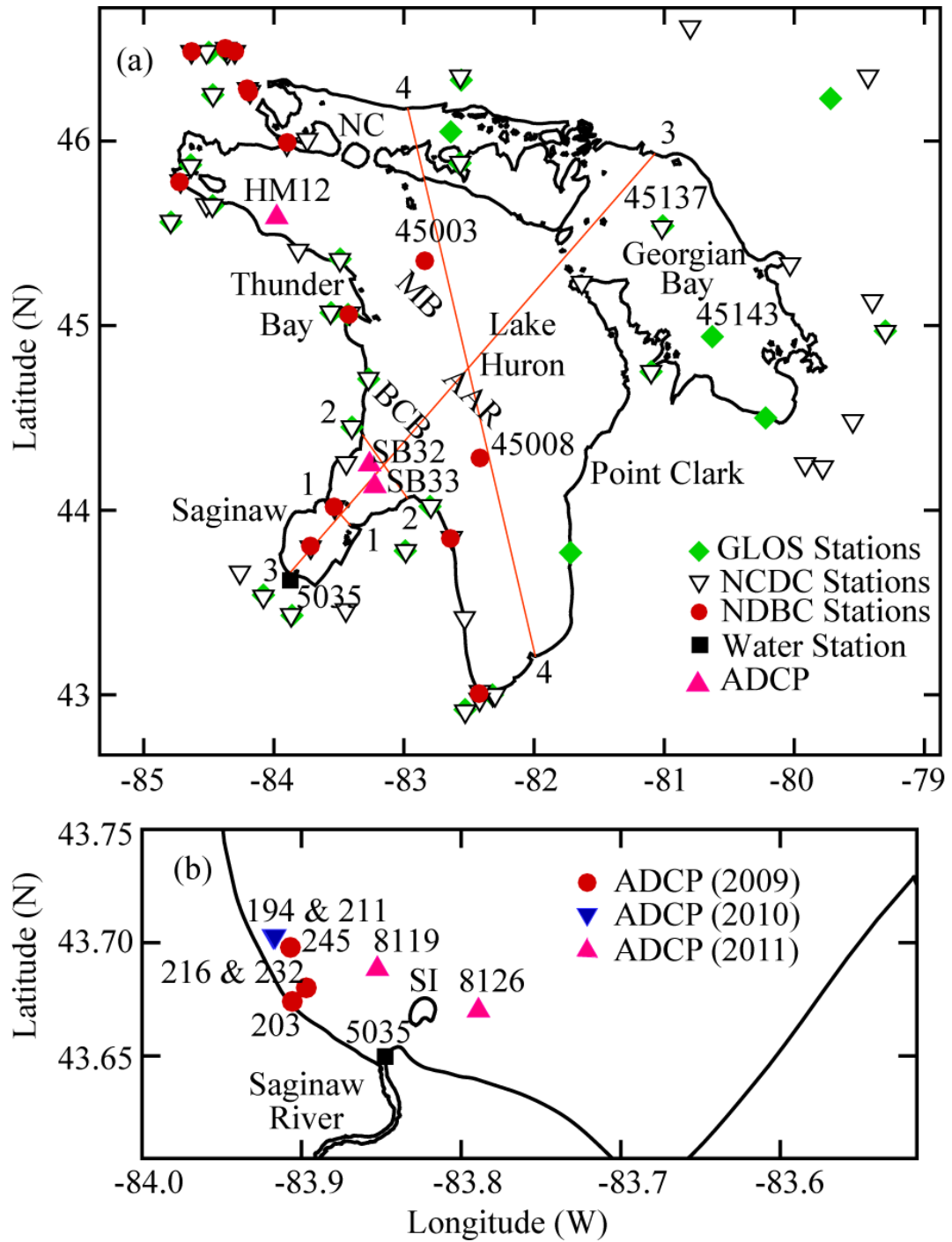**Figure 3:** (a) Map of Lake Huron showing the important physical features. MB: Manitoulin Basin; BCB: Bay City Basin; NC: North Channel; AAR: Alpena- Amberley Ridge. (b) Map of Saginaw Bay showing the ADCP locations. SI: Shelter Island. 1-1 and 2-2 in Figure 3(a) are the inner and outer Saginaw Bay transects respectively and 3-3 and 4-4 are transects for which vertical temperature profiles are shown.

Chapter 2

Field Observations and Analysis

2.1 Observational Data

Observational datasets have a very important role in terms of understanding natural processes and to validate the numerical model. The hydrodynamic model could not be tested without adequate data to serve as input and also for calibration purposes. The areas of interest for this study are Lake Huron and Saginaw Bay. Field observations were undertaken in the vicinity of Saginaw River mouth and Saginaw Bay mouth as shown in the Figure 3.

The field work was conducted to collect current velocity, and water temperature throughout the water column. It has been known that the primary factors that affect circulation in lakes are wind, temperature, bathymetry, and tributary flows. Therefore, in order to obtain a better understanding of the fundamental hydrodynamics and river plume, several drifters were released adjacent to the Saginaw River mouth. The observational data outlined above are used to compare the results from hydrodynamic model and estimate diffusivity using Lagrangian drifters and particle transport model. Here we present in detail the field data in the next section.

2.1.1 Currents

The field work was conducted to collect current velocity data in both summer and winter seasons. The observational investigations in summer were carried out between July and September of 2009, 2010, and 2011 using Nortek (www.nortekusa.com) Aquadopp current profilers (2000 kHz). The ADCPs were set up in a bottom-resting, upward-looking configuration, at different locations within the Bay and programmed to record current data with a bin-size of 0.25m and ensemble length of 900s or 1800s to collect an extensive observational dataset in the near-shore region of Saginaw River mouth (Figure 3). This region is characterized by very shallow water depths (average depth 2.5m).

There are two observational investigations which contribute to winter datasets for the year 2010 and 2013. The first field work was conducted in the winter 2010 in which the RD Instruments ADCPs were deployed in the Saginaw Bay mouth as shown in Figure 3a as SB32 and SB33 stations. The second observational investigation was collected in the winter 2013. A Teledyne – RD Instruments (http://rdinstruments.com) Workhorse Sentinel ADCP (600 kHz frequency) was deployed in the area of Hammond Bay with a water depth of about 27m. The observational dataset provided a time series of water current and temperature in the water column. Deployment locations and additional details are listed in Table 1.

Table 1: Details of ADCP deployments in Lake Huron

Deployment Date	Location	Longitude	Latitude	Depth(m)
07/22/09 - 08/04/09	203	-83.90235	43.673233	3.0
08/04/09-08/18/09	216	-83.897016	43.680066	2.0
08/20/09-09/02/09	232	-83.897016	43.680066	2.9
09/02/09-09/16/09	245	-83.91055	43.699066	3.3
10/14/09-05/26/10	SB32	-83.2609	44.2699	27.0
10/20/09-05/26/10	SB33	-83.2069	44.1434	29.0
07/13/10-07/27/10	194	-83.917683	43.702916	2.4
07/30/10-08/12/10	211	-83.916666	43.702916	2.5
07/27/11-08/28/11	8119	-83.8525	43.688333	3.6
07/27/11-08/28/11	8126	-83.789166	43.670000	4.0
11/09/12-05/19/13	HM12	-84.05447	45.5264	27.0

2.1.2   Temperature

One of the primary factors affecting lake circulation is water temperature in the lake (via the density gradient term in the momentum equation). As with other large lakes, Lake Huron is stratified during summer time and has nearly homogeneous temperature during winter time. Description of the thermal distribution and evolution in Lake Huron is one of the goals of the study. Thus, the observational investigation which measures water temperature throughout the

water column is very useful to validate the results from the hydrodynamic model. In this study, we used the temperature data measured by GLERL scientists using thermistor chains. Time series measurements of water temperature were collected at 2 stations (SB32, SB33 as shown in Figure 3) located along the boundary of outer Saginaw Bay during the summer of 2009 and the winter of 2010. Details of the measurements at the individual stations are presented below in which the sensor positions are in meters above the bottom.

Table 2 : Details of Thermistor deployments in Lake Huron				
Deployment Date	**Location**	**Longitude**	**Latitude**	**The sensor positions (m)**
07/16/2009 - 05/25/2010	SB32	-83.2609	44.2699	[1.0;5.0;9.0;13.0;17.0;21.0;23.0]
07/16/2009 - 05/25/2010	SB33	-83.2069	44.1434	[1.0;5.0;9.0;13.0;17.0;21.0;23.0; 25.0;27.0;29.0]

2.1.3   Lagrangian Drifters

Lagrangian drifters have been widely used in the studies of oceans and large lakes. The observational data was particularly valuable to estimate the flow field spatially and to validate the hydrodynamic model. Based on the Lagrangian data the diffusion coefficient can be estimated providing a better understanding of both fundamental hydrodynamics and environmental transport issues.

Multiple drifters were deployed between the Saginaw River mouth and Shelter Island (SI) (Figure 3b) for three days in end of July 2011. Deployment dates and start locations are given in

Table 3. The drifters were originally designed by Michael McCormick of the Great Lakes Environmental Research Laboratory (GLERL), Ann Arbor, Michigan. The drifters used in the present study were constructed following the original design using a fiberglass and plywood cross frame with vinyl drogues (area of $20'' \times 35''$) to reduce latency as shown in Figure 4. Location of drifters were tracked in real-time using Trackpack ® GPS transmitters programmed to report their location every 30 min. The transmitters were encased in a water resistant housing and the manufacturer reported uncertainty in GPS location to be approximately 5m.

Drifter ID	Deployment locations		Deployment time	Picking up time	Duration of travel
	Longitude	Latitude			(hour)
Day 1- Drifter 1	-83.846734	43.655956	07/27/2011 18:44	07/28/2011 18:44	24
Day 1- Drifter 2	-83.842742	43.661277	07/27/2011 18:21	07/28/2011 18:51	23
Day 1- Drifter 3	-83.839867	43.661309	07/27/2011 18:23	07/27/2011 23:53	5
Day 2- Drifter 1	-83.840640	43.661288	07/28/2011 20:21	07/29/2011 18:21	22
Day 2- Drifter 2	-83.839266	43.661374	07/28/2011 20:23	07/29/2011 17:53	21
Day 3- Drifter 1	-83.843365	43.658445	07/29/2011 18:44	08/01/2011 07:44	61
Day 3- Drifter 2	-83.837743	43.662919	07/29/2011 19:23	07/30/2011 03:53	8

Table 3: Details of Lagrangian drifter deployments in Saginaw Bay
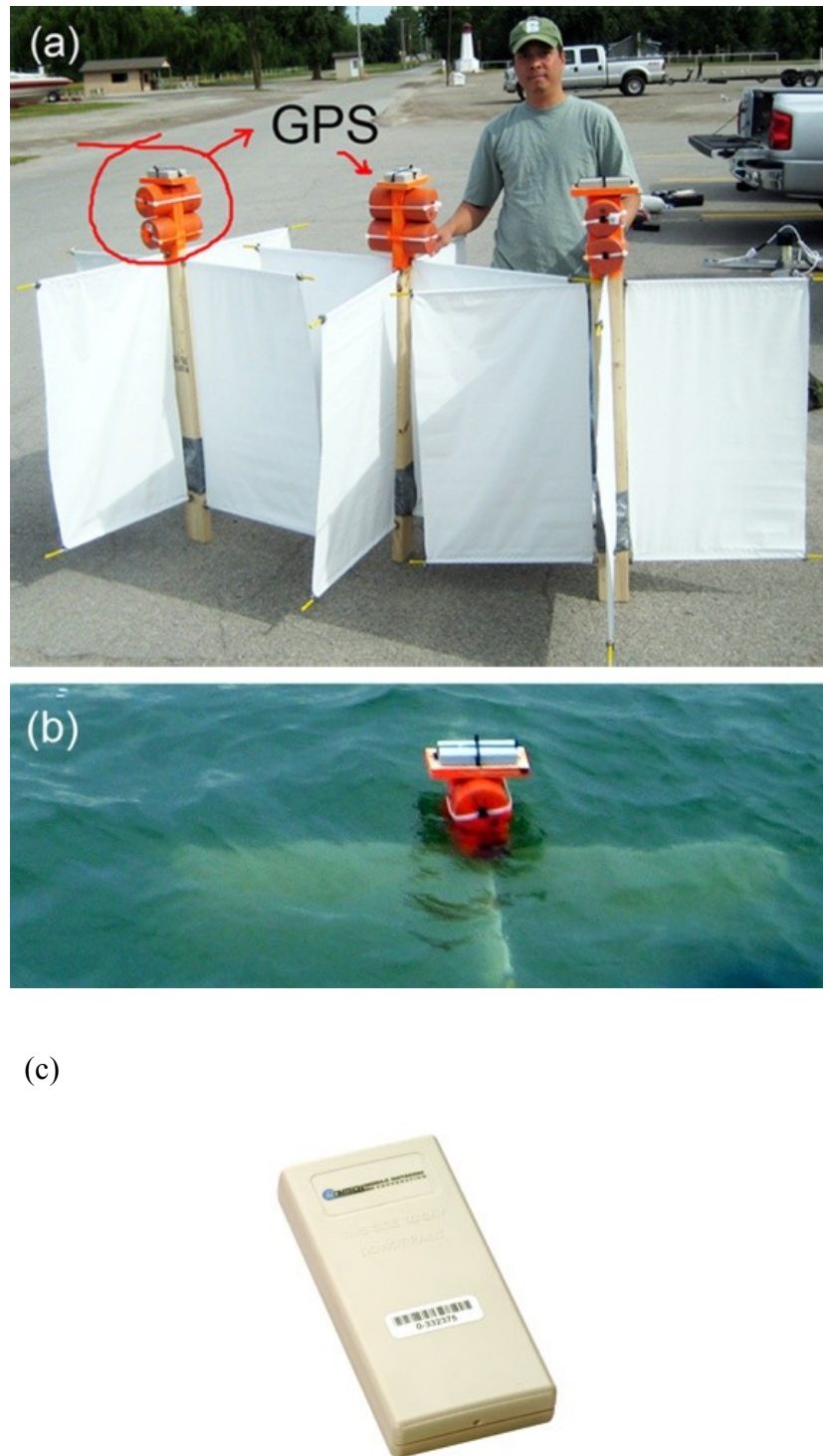
Figure 4: Photograph showing (a) the Lagrangian drifters, (b) a drifter in water, and (c) the Trackpack® GPS

2.2   Numerical Model

The three-dimensional unstructured grid numerical model (FVCOM) is used to describe circulation and thermal structure in Lake Huron and Saginaw Bay. Since Lake Huron has complex topographic features, the use of a variable resolution mesh seems to be a suitable approach. With the flexibility of unstructured meshes the model is able to represent complex coastlines to a high degree of accuracy. The model solves the hydrodynamic primitive equations using the hydrostatic assumption in the vertical direction with the Boussinesq simplification for convective flows. The continuity, momentum, and temperature equations are shown in Equation 1 to Equation 5.

$$\frac{\partial u}{\partial x} + \frac{\partial v}{\partial y} + \frac{\partial w}{\partial z} = 0 \qquad (1)$$

$$\frac{\partial u}{\partial t} + u\frac{\partial u}{\partial x} + v\frac{\partial u}{\partial y} + w\frac{\partial u}{\partial z} - fv = -\frac{1}{\rho_0}\frac{\partial P}{\partial x} + \frac{\partial}{\partial z}\left(K_M\frac{\partial u}{\partial z}\right) + F_u \qquad (2)$$

$$\frac{\partial v}{\partial t} + u\frac{\partial v}{\partial x} + v\frac{\partial v}{\partial y} + w\frac{\partial v}{\partial z} + fu = -\frac{1}{\rho_0}\frac{\partial P}{\partial y} + \frac{\partial}{\partial z}\left(K_M\frac{\partial v}{\partial z}\right) + F_v \qquad (3)$$

$$\frac{\partial P}{\partial z} = -\rho g \qquad (4)$$

$$\frac{\partial T}{\partial t} + u\frac{\partial T}{\partial x} + v\frac{\partial T}{\partial y} + w\frac{\partial T}{\partial z} = \frac{\partial}{\partial z}\left(K_H\frac{\partial T}{\partial z}\right) + F_T \qquad (5)$$

Here x, y, and z are the Cartesian coordinates; (u, v, w) are velocity components in horizontal and vertical directions, respectively; ρ is the density; ρ_0 is the reference density; T is the

temperature; P is the pressure; f is the Coriollis parameter; g is the acceleration due to gravity.

The horizontal momentum diffusion terms $(F_u, F_v,)$ have the form:

$$F_u = \frac{\partial}{\partial x}\left(2A_m \frac{\partial u}{\partial x}\right) + \frac{\partial}{\partial y}\left(A_m \left(\frac{\partial u}{\partial y} + \frac{\partial v}{\partial x}\right)\right) \qquad (6)$$

$$F_v = \frac{\partial}{\partial y}\left(2A_m \frac{\partial v}{\partial y}\right) + \frac{\partial}{\partial x}\left(A_m \left(\frac{\partial u}{\partial y} + \frac{\partial v}{\partial x}\right)\right) \qquad (7)$$

$$F_T = \frac{\partial}{\partial x}\left(A_h \frac{\partial T}{\partial x}\right) + \frac{\partial}{\partial y}\left(A_h \frac{\partial T}{\partial y}\right) \qquad (8)$$

Vertical eddy viscosity and diffusivity (K_M, K_H) are modeled using the Mellor-Yamada 2.5 level turbulence closure scheme [*Mellor and Yamada*, 1982; *Galperin et al.*, 1988]. The horizontal diffusion coefficients A_m are calculated using the Smagorinsky turbulence closure model [*Smagorinsky*, 1963].

$$A_m = C\Delta x \Delta y \frac{1}{2}\left[\left(\frac{\partial u}{\partial x}\right)^2 + \frac{1}{2}\left(\frac{\partial u}{\partial y} + \frac{\partial v}{\partial x}\right)^2 + \left(\frac{\partial v}{\partial y}\right)^2\right] \qquad (9)$$

The horizontal eddy diffusivity A_h is related to the eddy viscosity A_m via the turbulent Prandtl number. $P_r = {A_m}/{A_h} = 1.0$ was used in this study after carefully testing the effect of this number on model results. Details of the governing equations and boundary conditions can be found elsewhere (e.g., *Chen et al.,* [2003]).

The surface boundary condition for temperature is given as follows:

$$\frac{\partial T}{\partial z} = \frac{1}{\rho c_p K_h} [Q_n(x, y, t) - SW(x, y, t)] \qquad (10)$$

The bottom boundary condition for temperature is given as follows:

$$\frac{\partial T}{\partial z} = -\frac{A_H \tan(\alpha)}{K_h} \frac{\partial T}{\partial n} \qquad (11)$$

where $Q_n(x, y, t)$ is the surface net heat flux, $SW(x, y, t)$ is the shortwave radiation flux incident at the water surface, c_p is the specific heat of water, A_H is the horizontal thermal diffusion coefficient, α is the slope of the bottom.

The surface and bottom boundary conditions for velocity u and v are:

$$K_m \left(\frac{\partial u}{\partial z}, \frac{\partial v}{\partial z}\right) = \frac{1}{\rho_0} \left(\tau_{sx}, \tau_{sy}\right) \qquad (12)$$

$$K_m \left(\frac{\partial u}{\partial z}, \frac{\partial v}{\partial z}\right) = \frac{1}{\rho_0} \left(\tau_{bx}, \tau_{by}\right) \qquad (13)$$

where $\left(\tau_{sx}, \tau_{sy}\right)$ and $\left(\tau_{bx}, \tau_{by}\right)$ are the x and y components of surface wind and bottom stresses. The horizontal computational domain consists of non-overlapping unstructured triangular meshes. The calculated horizontal velocity components are placed at the centroids of triangle. While all scalar components are calculated at the nodes of triangle. More details about the model can be found in the study of *Chen et al.,*[2003].

2.3   Uncertainty of measurements

Observational datasets were used in this study for driving and testing the numerical model. Therefore, the accuracy of data plays a very important role for developing accurate numerical models. The quality of meteorological data such as air temperature, wind speed, wind direction, water surface temperature, and dew point is controlled by the National Data Buoy Center (NDBC) and the National Climatic Data Center (NCDC). Here we present in detail the accuracy of observational data used in this study in the Table 4.

Table 4: Accuracy of the measurements			
No	**Parameters**	**Unit**	**Accuracy**
1	Air Temperature	Degree	+/- 1.0 C
2	Wind Speed	m/s	+/- 1.0
3	Wind Direction	Degree	+/- 10
4	Dew Point	Degree	+/- 1.0 C
5	Water Surface Temperature	Degree	+/- 1.0 C
6	ADCP velocity	cm/s	+/- 0.3% or +/- 0.3 cm/s
7	Drifter Tracks	m	5.0

Chapter 3

Summer Circulation and Thermal Structure

3.1   Introduction

Concerns associated with climate change impacts and the increased incidences of anthropogenic stressors have necessitated an accurate characterization of circulation and thermal structure in Lake Huron to obtain a better understanding of circulation, thermal structure and residence times.

Although there have been many studies focusing on circulation in Lake Huron and Saginaw Bay using observational datasets or numerical models (*Sloss and Saylor* [1976]; *Allender and Green* [1976] ; *Danek and Saylor* [1977]; *Beletsky et al.,* [1999] ; *Sheng and Rao* [2006]; *Schertzer et al.,* [2008] ; *Bai et al.,* [2013]) the circulation and temperature distribution in Lake Huron are still far from being understood. For example, without information about circulation and results from hydrodynamic models, it is impossible to solve the issues related to water quality. Furthermore, most of the previous studies described the circulation in Lake Huron based on observational data that is limited in space and time.

In this chapter, we use a three-dimensional, unstructured grid hydrodynamic model with a nesting model to examine circulation and thermal structures in the Saginaw Bay - Lake Huron

system during the summer months for three consecutive years (2009-2011). The model was tested against ADCP observations of currents, data from a Lagrangian drifter experiment in the Saginaw Bay and temperature data from the National Data Buoy Center stations. Using data from a Lagrangian drifter release conducted near the mouth of Saginaw River, we also calculate absolute particle diffusion rates within the inner Saginaw Bay near the mouth of the Saginaw River. The results from the numerical model are then used to calculate volumetric exchange rates for both the inner and outer Saginaw Bay and to estimate first-order transport time scales such as the residence time/flushing time and their inter-annual variability. The new estimated flushing time and residence time will be presented in the Chapter 5.

3.2   Numerical model

3.2.1   Model configuration

The three-dimensional unstructured grid numerical model (FVCOM, *Chen et al.*, [2003]) is used to describe circulation and thermal structure in Lake Huron and Saginaw Bay. The model solves the hydrodynamic primitive equations (1-5) presented in the previous chapter.

Two separate hydrodynamic models: (a) the Lake-wide Model (LWM) and (b) Saginaw Bay Model (SBM) (including the Saginaw River mouth) were setup to resolve large-scale, lake-wide circulation and circulation within the Saginaw Bay respectively.

The unstructured meshes for LWM and SBM were created using the Surface Water Modeling System (SMS, www.aquaveo.com) and bathymetry at node locations was interpolated from the 6 arc-second bathymetry data downloaded from the NOAA National Geophysical Data Center, Geophysical Data System (GEODAS) website (http://www.ngdc.noaa.gov/mgg/gdas/). In order

to obtain the bathymetry at node locations we used a MATLAB (The Mathworks Inc., Natick, MA, 2013) program based on the `TriScatteredInterp` function to interpolate from the 6 arc-seconds bathymetry data to node locations using the Natural neighbor interpolation method (Figure 5). The method allows us to get more accurate interpolated bathymetry data. The LWM computational domain was treated as a closed boundary and inflow through the Straits of Mackinac, St.Mary's River or other tributaries and outflow to Lake St.Clair via the St.Clair River were not included in the numerical model. The computational meshes used to resolve the hydrodynamics and evolution of thermal structure in Lake Huron and Saginaw Bay are shown in Figure 8 and Figure 9b, respectively.
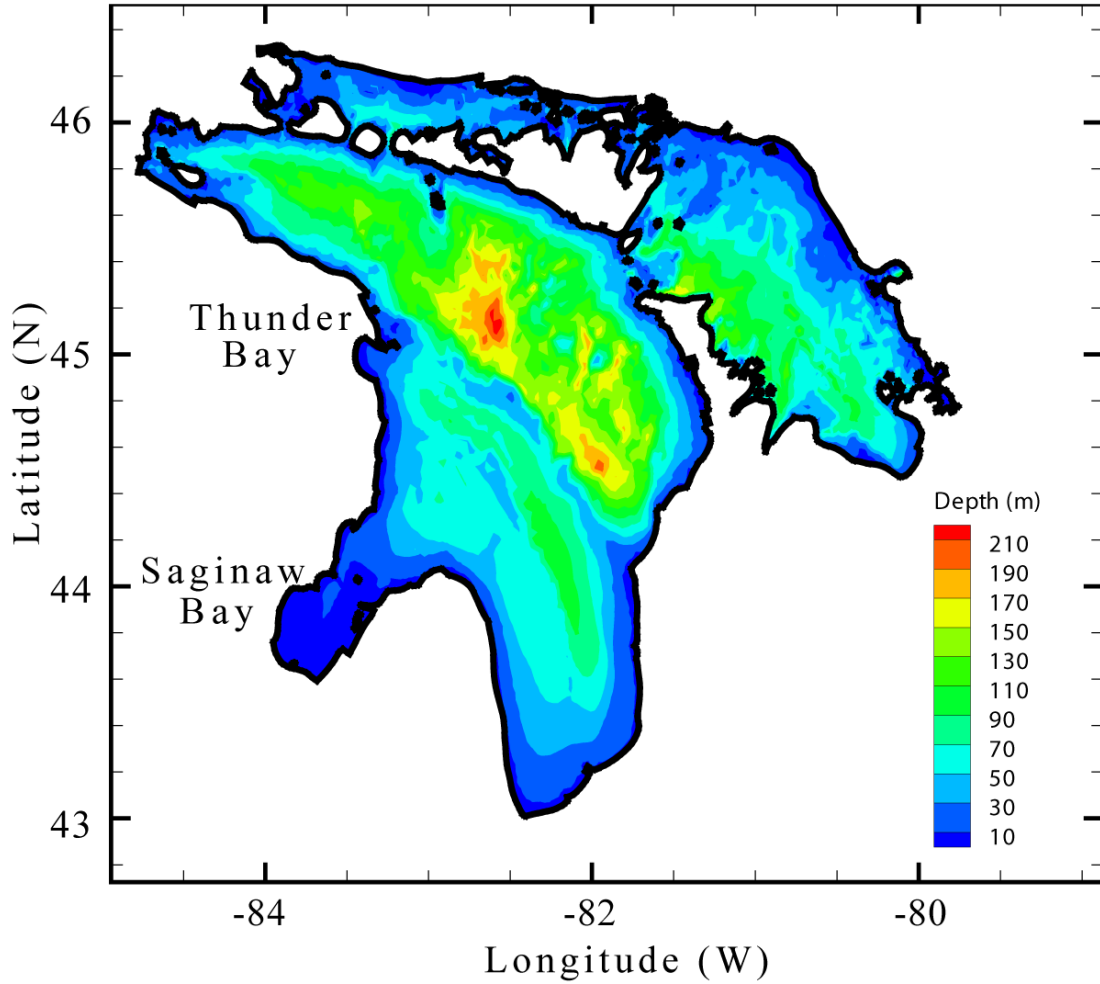
Figure 5: Map of Lake Huron showing the bathymetry interpolated from data downloaded from the NOAA National Geophysical Data Center, Geophysical Data System (GEODAS).

The LWM uses an unstructured grid with 9611 nodes and 17619 triangular elements in the horizontal (average element size =2.5 km). In general, the LWM's horizontal model resolution increases from the center of the main lake, where it is as coarse as 5 km, toward the coastlines with higher resolution near important features of about 2.0 km. With the horizontal resolution as shown in the Figure 6, most of the cells are into the range of 2-3 km.
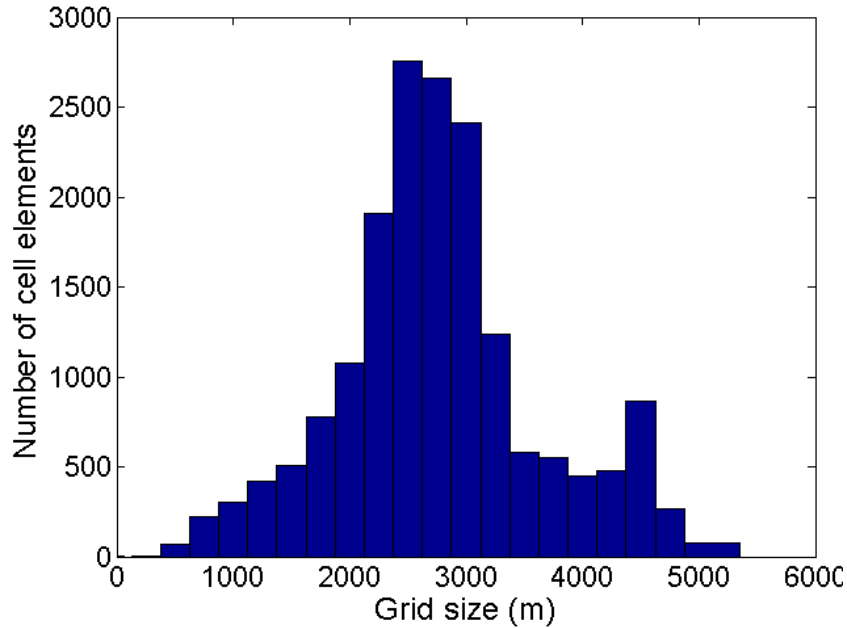
Figure 6: A histogram of model grid size of Lake Huron Model (LWM)

Circulation in Saginaw Bay is influenced by large-scale, lake-wide circulation. The SBM uses an unstructured grid with 8236 nodes and 15575 triangular elements (average element size approximately 200m) in the horizontal (Figure 7). The minimum element size of 45m is used near the Saginaw River mouth. Coupling between the LWM and SBM is one-way. Simulated hourly water levels and velocities at the boundary of the SBM, taken from the LWM, were used to drive the SBM. Discharge from the Saginaw River, though considered negligible to LWM circulation and hydrodynamics, was used to provide a flux boundary condition in the SBM. Daily discharge rates measured at the USGS gaging station on the Saginaw River (#04157000) (http://waterdata.usgs.gov/) were used to provide the boundary condition at the Saginaw River mouth in the SBM model.
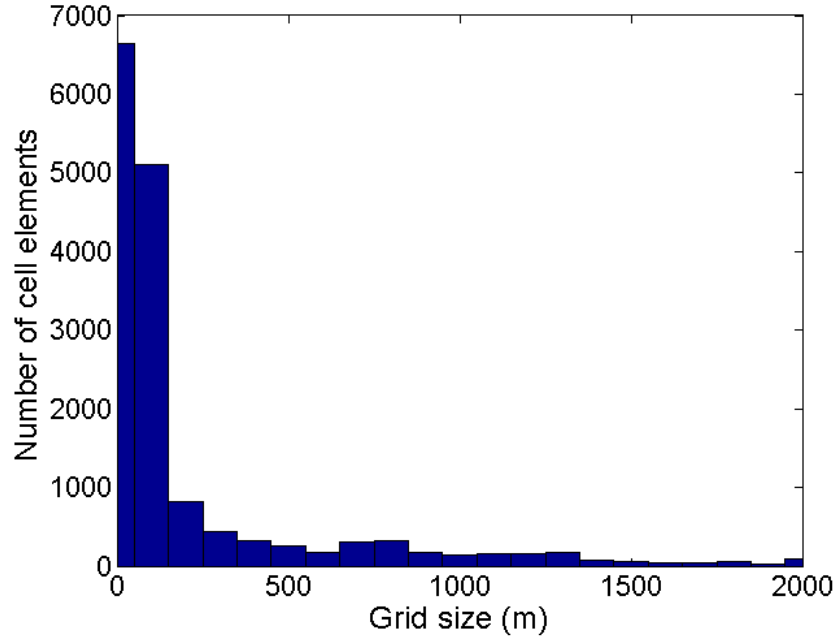
Figure 7: A histogram of model grid size of the Saginaw Bay Model (SBM)

The two models (LWM and SBM) for Lake Huron and Saginaw Bay have 21 vertical sigma levels. The centers of the sigma levels are located at ([-0.0158; -0.0520; -0.0952; -0.1422; -0.1921; -0.2443; -0.2984; -0.3542; -0.4116; -0.4703; -0.5297; -0.5884; -0.6458; -0.7016; -0.7557; -0.8079; -0.8578; -0.9048; -0.9480; -0.9842]). This model setup will allow accurate representation of the vertical temperature stratification. Based on the well-known Courant-Friedrichs -Levy (CFL) stability criterion, the external and internal time steps used are 4s and 10s for the LWM and 1s and 10s for the SBM, respectively.
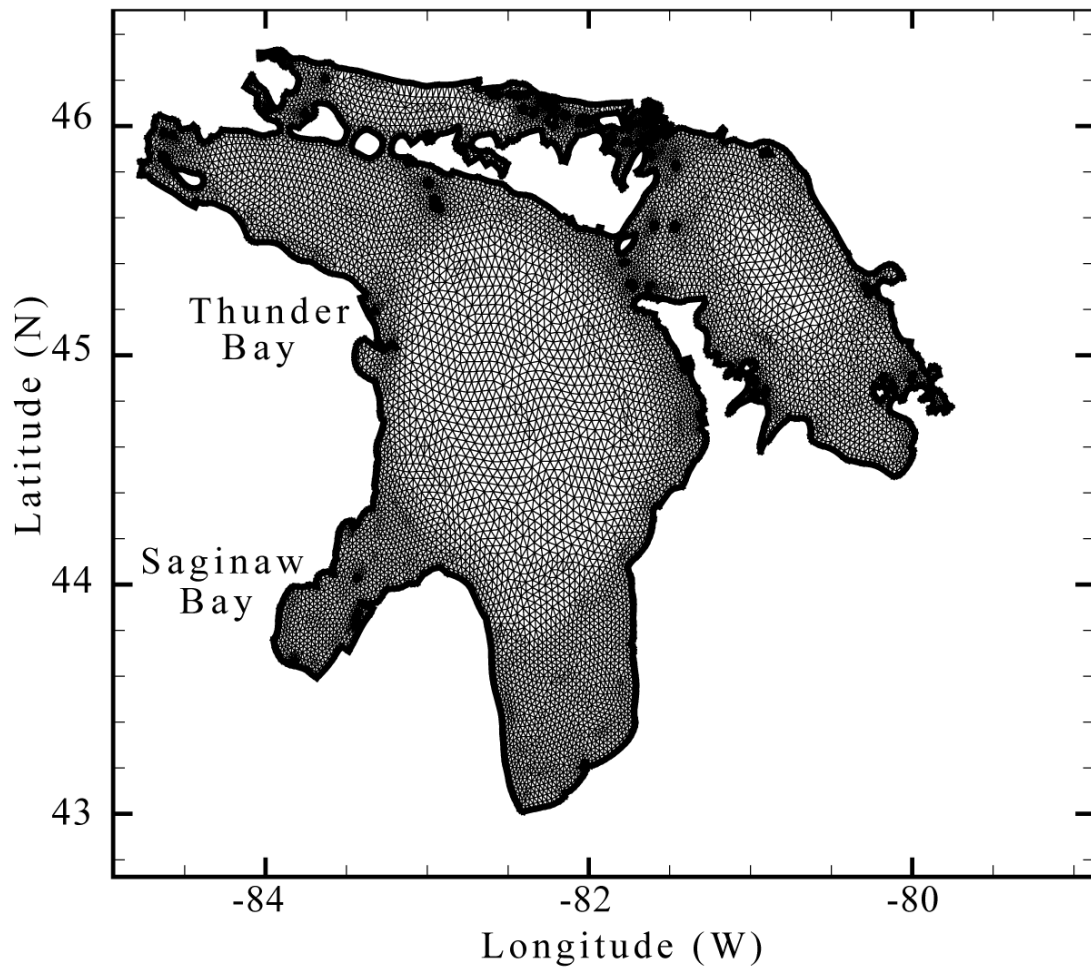
Figure 8: The computational mesh used for the Lake Huron model (LWM)
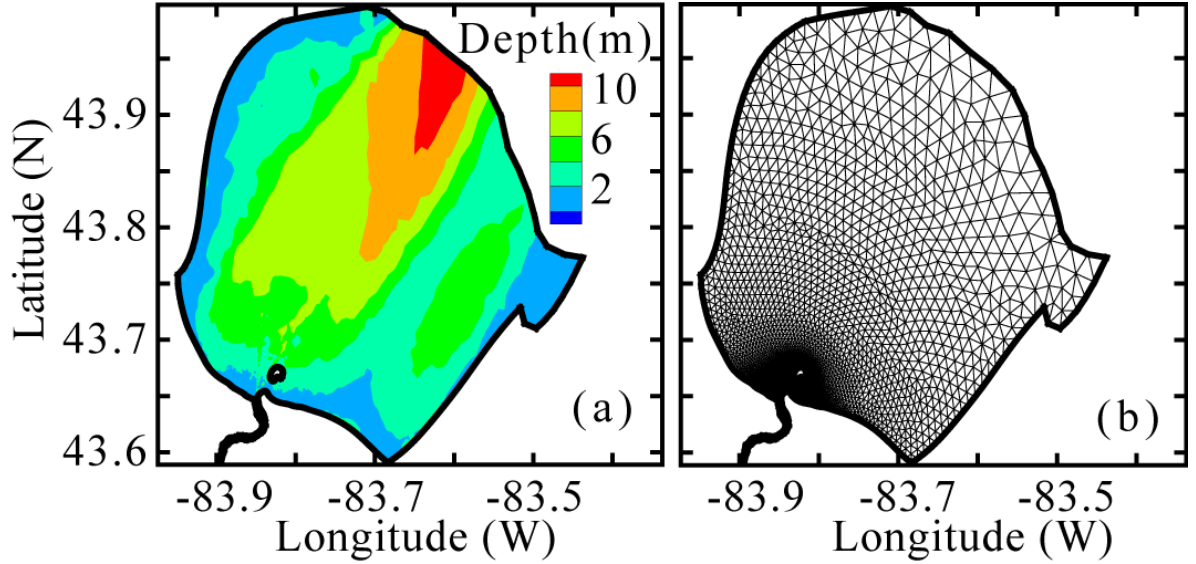
Figure 9: Bathymetry and computational mesh of the Saginaw Bay model (a and b).

3.2.2 Meteorological Data

The model was driven by the surface winds, heat fluxes, and river discharge. The major difficulty with meteorological data over Lake Huron is that most of the National Data Buoy Center Stations (NDBC) are located along the U.S shorelines in the west and the southwest and very few are located along the Canadian shorelines in the northeast and eastern regions. In this study we used meteorological data from the NDBC Stations and from the Great Lakes Observation System (GLOS) (http://data.glos.us/obs/) to drive the hydrodynamic model.

The Hourly standard meteorological data such as wind speed, wind direction, and air temperature for the model simulation periods in 2009, 2010, and 2011 were downloaded from 14 National Data Buoy Center Stations (NDBC) (http://www.ndbc.noaa.gov/) around Lake Huron. In addition, hourly meteorological data from 27 stations were also obtained from the Great Lakes Observation System (GLOS). The quality of meteorological data is controlled by the National Data Buoy Center (NDBC) and the National Climatic Data Center (NCDC)

31

). The GLOS, NCDC, and NDBC stations used in this study

are shown in Figure 3. Meteorological station locations and parameters in which were measured

at each station are presented in the Table 5, 6, and 7. In the Tables, WSPD is the wind speed,

WDIR is the wind direction, TA is the air temperature, WT is the surface water temperature,

DEWP is the dew point, and CC is the cloud cover. In order to get overwater fields data from

meteorological datasets, three main steps are required: (1) height adjustments to a common 10m

height over the water surface, (2) overland/overwater adjustments, and (3) interpolation. The

methods and procedures are described more thoroughly by *Schwab* [1999]. The observed

meteorological datasets such as wind speed, air temperature, cloud cover and relative humidity

were interpolated to the computational domain using a smoothened nearest neighbor method

[*Schwab*, 1999]. Surface heat flux, *HFLX*, is calculated as

$$HFLX = SW + LW + H_{sensible} + H_{latent} \qquad (14)$$

The incoming shortwave radiation was calculated as described by *Bunker* [1976]:

$$SW = SW_{clrsky}(1 - kc) \qquad (15)$$

where SW_{clrsky} is the clear-sky shortwave radiation, calculated using methods described by

Annear and Wells, [2007]. The cloud cover c is converted from NCDC description and k is an

empirical parameter. A value of 0.7 was used for k in this study based on [*Schwab*, 1999]. The

incoming long-wave radiation was calculated following [*Parkinson and Washington*, 1979]:

$$LW = \sigma T_a^4\left(1 - 0.261e^{\left(-7.77\times10^{-4}(273-T_a)^2\right)}\right)(1 + 0.275c) \qquad (16)$$

Where σ is the Stefan-Boltzmann constant (5.67×10^{-8} W m^{-2} K^{-4}); T_a is the air temperature; c is cloud cover. Hourly wind and heat flux values were used to force the hydrodynamic models (LWM and SBM) used in this study. The sensible ($H_{sensible}$) and latent (H_{latent}) heat transfers are calculated at each grid point based on a bulk aerodynamic formulation COARE 2.6 developed by *Fairall et al.,* [1996]. Lake-wide summer circulation for three years (2009, 2010, and 2011) was simulated using the large-scale hydrodynamic model (LWM). In order to avoid problems with initialization of the stratified temperature, the model simulations were started on May 1 with a uniform vertical temperature profile determined from observations at 4 NDBC buoys (45003, 45008, 45137, and 45143).

Table 5: NDBC Meteorological station locations

Station ID	Location	Latitude	Longitude	Period of data availability	Parameters
45003	NDBC Buoy	45.351	-82.840	05-06-2009 to 11-30-2009 01-01-2010 to 12-31-2010 04-30-2011 to 12-07-2011 04-05-2012 to 12-31-2012	WSPD;WDIR; TA;WT;
45008	NDBC Buoy	44.283	-82.416	05-07-2009 to 11-30-2009 01-01-2010 to 12-31-2010 04-30-2011 to 12-14-2011 03-31-2012 to 12-21-2012	WSPD;WDIR; TA;WT;
APNM4	Alpena Harbor Light, MI	45.060	-83.424	01-01-2009 to 06-20-2013	WSPD;WDIR; TA;
DTLM4	De Tour Village, MI	45.992	-83.897	01-01-2009 to 06-20-2013	WSPD;WDIR; TA;
FTGM4	Fort Gratiot, MI	43.007	-82.423	01-01-2009 to 06-20-2013	WSPD;WDIR; TA;
GSLM4	Gravelly Shoals Light MI	44.018	-83.537	01-02-2009 to 06-30-2013	WSPD;WDIR; TA;
HRBM4	Harbor Beach, MI	43.847	-82.643	01-01-2009 to 06-30-2013	WSPD;WDIR; TA;
LTRM4	Little Rapids, MI	46.485	-84.300	01-01-2009 to 06-30-2013	WSPD;WDIR;
MACM4	Mackinaw City, MI	45.778	-84.725	03-18-2009 to 06-30-2013	WSPD;WDIR; TA;
PTIM4	Point Iroquois, MI	46.485	-84.632	01-01-2009 to 06-30-2013	WSPD;WDIR; TA;
RCKM4	Rock Cut, MI	46.265	-84.192	01-01-2009 to 06-30-2013	WSPD;WDIR;
SBLM4	Saginaw Bay Light #1, MI	43.806	-83.719	01-01-2009 to 06-30-2013	WSPD;WDIR; TA;
SWPM4	S.W. Pier, MI	46.502	-84.373	01-01-2009 to 06-30-2013	WSPD;WDIR; TA;
WNEM4	West Neebish, MI	46.283	-84.205	01-01-2009 to 12-31-2012	WSPD;WDIR; TA;

<p style="text-align: center;">**Table 6:** GLOS Meteorological station locations</p>

Station	Station ID	Latitude	Longitude	Period of data availability	Parameters
45137	45137	45.54	-81.01	07-15-2009 to 11-31-2009 05-01-2010 to 11-19-2010 05-01-2011 to 11-30-2011	WSPD;WDIR; TA;WT;
45143	45143	44.94	-80.63	07-15-2009 to 11-31-2009 05-01-2010 to 11-22-2010 05-01-2011 to 11-30-2011	WSPD;WDIR; TA;WT;
45149	45149	43.54	-82.07	07-15-2009 to 11-31-2009 05-04-2010 to 11-17-2010	WSPD;WDIR; TA;WT;
45151	45151	-79.37	44.50	07-15-2009 to 10-06-2009 05-17-2010 to 11-02-2010	WSPD;WDIR; TA;WT;
45152	45152	-79.72	46.23	07-15-2009 to 10-15-2009 05-08-2010 to 10-13-2010 05-15-2011 to 10-28-2011	WSPD;WDIR; TA;WT;
45154	45154	-82.64	46.05	07-15-2009 to 10-16-2009 05-07-2010 to 11-28-2010 05-12-2011 to 11-14-2011	WSPD;WDIR; TA;WT;
Sault Ste. Marie	ANJ	46.48	-84.36	07-15-2009 to 12-31-2009 01-01-2010 to 11-30-2010 05-01-2011 to 11-30-2011 06-01-2012 to 06-20-2013	WSPD;WDIR; TA;DEWP;
Alpena County Regional Airport	APN	45.07	-83.56	07-15-2009 to 12-31-2009 01-01-2010 to 11-30-2010 05-01-2011 to 11-30-2011 06-01-2012 to 06-20-2013	WSPD;WDIR; TA;DEWP;
Huron County Memorial Airport	BAX	43.78	-82.99	07-15-2009 to 12-31-2009 01-01-2010 to 11-30-2010 05-01-2011 to 11-30-2011 06-01-2012 to 06-20-2013	WSPD;WDIR; TA;DEWP;
Cheboygan	CYGM4	45.65	-84.47	07-15-2009 to 12-31-2009 01-01-2010 to 11-30-2010 05-01-2011 to 11-30-2011 06-01-2012 to 06-20-2013	WSPD;WDIR;
Saginaw County H.W. Browne Airport	HYX	43.43	-83.86	07-15-2009 to 12-31-2009 01-01-2010 to 11-30-2010 05-01-2011 to 11-30-2011 06-01-2012 to 06-20-2013	WSPD;WDIR; TA;DEWP;
MBS International Airport	MBS	43.54	-84.08	07-15-2009 to 12-31-2009 01-01-2010 to 11-30-2010 05-01-2011 to 11-30-2011 06-01-2012 to 06-20-2013	WSPD;WDIR; TA;DEWP;

Table 6 (cont'd)

Station	Station ID	Latitude	Longitude	Period of data availability	Parameters
Mackinac Island Airport	MCD	45.87	-84.64	07-15-2009 to 12-31-2009 01-01-2010 to 11-30-2010 05-01-2011 to 11-30-2011 06-01-2012 to 06-20-2013	WSPD;WDIR; TA;DEWP;
Oscoda-Wurtsmith Airport	OSC	44.45	-83.40	07-15-2009 to 12-31-2009 01-01-2010 to 11-30-2010 05-01-2011 to 11-30-2011 06-01-2012 to 06-20-2013	WSPD;WDIR; TA;DEWP;
Port Hope	P58	44.02	-82.80	07-15-2009 to 12-31-2009 01-01-2010 to 11-30-2010 05-01-2011 to 11-30-2011 06-01-2012 to 06-20-2013	WSPD;WDIR; TA;DEWP;
St. Clair County International	PHN	42.92	-82.53	07-15-2009 to 12-31-2009 01-01-2010 to 11-30-2010 05-01-2011 to 11-30-2011 06-01-2012 to 06-20-2013	WSPD;WDIR; TA;DEWP;
Pellston Regional Airport of Emmet County Airport	PLN	45.56	-84.79	07-15-2009 to 12-31-2009 01-01-2010 to 11-30-2010 05-01-2011 to 11-30-2011 06-01-2012 to 06-20-2013	WSPD;WDIR; TA;DEWP;
Presque Isle Light	PRIM4	45.36	-83.49	07-15-2009 to 12-31-2009 01-01-2010 to 11-30-2010 05-01-2011 to 11-30-2011 06-01-2012 to 06-20-2013	WSPD;WDIR;
Sturgeon Point	SPTM4	44.71	-83.27	01-01-2010 to 11-30-2010 05-01-2011 to 11-30-2011 06-01-2012 to 06-20-2013	WSPD;WDIR; TA;DEWP;CC
Collingwood Automatic Weather Reporting System	WCO	44.50	-80.22	07-15-2009 to 12-31-2009 01-01-2010 to 11-30-2010 05-01-2011 to 11-30-2011 06-01-2012 to 06-20-2013	WSPD;WDIR; TA;DEWP;
Goderich Automatic Weather Reporting System	WGD	43.77	-81.72	07-15-2009 to 12-31-2009 01-01-2010 to 11-30-2010 05-01-2011 to 11-30-2011 06-01-2012 to 06-20-2013	WSPD;WDIR; TA;DEWP;

Table 6 (cont'd)

Station	Station ID	Latitude	Longitude	Period of data availability	Parameters
Ont	YAM	46.48	-84.50	01-01-2010 to 11-30-2010 05-01-2011 to 11-30-2011 06-01-2012 to 06-20-2013	WSPD;WDIR; TA;DEWP;CC
Elliot Lake Supplementary Aviation Weather Reporting	YEL	46.33	-82.56	07-15-2009 to 12-31-2009 01-02-2010 to 11-30-2010 04-01-2011 to 11-30-2011	WSPD;WDIR; TA;DEWP;
Ont	YQA	44.97	-79.30	07-15-2009 to 12-31-2009 01-01-2010 to 11-30-2010 05-01-2011 to 11-30-2011 06-01-2012 to 06-20-2013	WSPD;WDIR; TA;DEWP;
Ont	YVV	44.75	-81.10	07-15-2009 to 12-31-2009 01-01-2010 to 11-30-2010 05-01-2011 to 11-30-2011 06-01-2012 to 06-20-2013	WSPD;WDIR; TA;DEWP;
Ont	YZE	45.88	-82.57	07-15-2009 to 12-31-2009 01-01-2010 to 11-30-2010 05-01-2011 to 11-30-2011 06-01-2012 to 06-20-2013	WSPD;WDIR; TA;DEWP;
Sarnia Airport	YZR	43.00	-82.32	07-15-2009 to 12-31-2009 01-01-2010 to 11-30-2010 05-01-2011 to 11-30-2011 06-01-2012 to 06-20-2013	WSPD;WDIR; TA;DEWP;

Station ID	Location	Latitude	Longitude	Period of data availability	Parameters
				Table 7: NCDC Meteorological station locations	
711720	Parry Sound-Canada	45.333	-80.033	01-01-2009 to 06-20-2013	DEWP;CC
712600	Sault Ste Marie - Canada	46.483	-84.517	01-01-2009 to 06-20-2013	DEWP;CC
712610	Goderich - Canada	43.767	-81.717	01-01-2009 to 06-20-2013	DEWP;CC
712680	Elliott Lake - Canada	46.350	-82.567	01-01-2009 to 06-20-2013	DEWP;CC
712700	Colling Wood - Canada	44.500	-80.217	01-01-2009 to 06-20-2013	DEWP;CC
712960	Egbert – Canada	44.233	-79.783	01-01-2009 to 06-20-2013	DEWP;CC
713140	Barrie-Oro - Canada	44.483	-79.550	01-01-2009 to 06-20-2013	DEWP;CC
714390	Cove Island - Canada	45.333	-81.733	01-01-2009 to 06-20-2013	DEWP;CC
714600	Killarney - Canada	45.967	-81.483	01-01-2009 to 06-20-2013	DEWP;CC
714620	Great Duck Island - Canada	45.633	-82.967	01-01-2009 to 06-20-2013	DEWP;CC
715320	Muskoka Awos - Canada	44.967	-79.300	01-01-2009 to 06-20-2013	DEWP;CC
715340	Borden - Canada	44.250	-79.917	01-01-2009 to 06-20-2013	DEWP;CC
716300	Muskoka - Canada	44.967	-79.300	01-01-2009 to 06-20-2013	DEWP;CC
716310	Mount Forest - Canada	43.983	-80.750	01-01-2009 to 06-20-2013	DEWP;CC
716330	Wiarton Arpt - Canada	44.750	-81.100	01-01-2009 to 06-20-2013	DEWP;CC
716940	Beatrice Climate - Canada	45.133	-79.400	01-01-2009 to 06-20-2013	DEWP;CC
717040	Sarnia - Canada	43.000	-82.317	01-01-2009 to 06-20-2013	DEWP;CC

Table 7 (cont'd)

Station ID	Location	Latitude	Longitude	Period of data availability	Parameters
717300	Sudbury - Canada	46.617	-80.800	01-01-2009 to 06-20-2013	DEWP;CC
717310	North Bay - Canada	46.350	-79.433	01-01-2009 to 06-20-2013	DEWP;CC
717330	Gore Bay Airport - Canada	45.883	-82.567	01-01-2009 to 06-20-2013	DEWP;CC
717334	Elliot Lake Muni - Canada	46.350	-82.567	01-01-2009 to 06-20-2013	DEWP;CC
717460	Sarnia Climate - Canada	43.000	-82.300	01-01-2009 to 06-20-2013	DEWP;CC
717670	Tobermory Rcs - Canada	45.233	-081.633	01-01-2009 to 06-20-2013	DEWP;CC
719560	Gore Bay Climate - Canada	45.883	-82.567	01-01-2009 to 06-20-2013	DEWP;CC
720321	Cheboygan Co – United States	45.654	-84.519	01-01-2009 to 06-20-2013	DEWP;CC
720375	Drummond Island - United States	46.007	-83.743	01-01-2009 to 06-20-2013	DEWP;CC
720629	Jack Barstow - United States	43.663	-84.261	01-01-2009 to 06-20-2013	DEWP;CC
722007	Tuscola Area - United States	43.459	-83.446	01-01-2009 to 06-20-2013	DEWP;CC
722125	Saginaw Co HW Brown - United States	43.433	-83.867	01-01-2009 to 06-20-2013	DEWP;CC
725384	St Clair Co Intl - United States	42.911	-82.529	01-01-2009 to 06-20-2013	DEWP;CC

Table 7 (cont'd)

Station ID	Location	Latitude	Longitude	Period of data availability	Parameters
725386	Port Hope - United States	44.022	-82.793	01-01-2009 to 06-20-2013	DEWP;CC
725406	Huron Co Mem - United States	43.780	-82.986	01-01-2009 to 06-20-2013	DEWP;CC
726379	MBS Intl - United States	43.533	-84.080	01-01-2009 to 06-20-2013	DEWP;CC
726390	Alpena/Phelps Colli - United States	45.072	-83.564	01-01-2009 to 06-20-2013	DEWP;CC
726395	Oscoda Wurtsmith - United States	44.450	-83.40	01-01-2009 to 06-20-2013	DEWP;CC
727340	Sault Ste Marie - United States	46.479	-84.357	01-01-2009 to 06-20-2013	DEWP;CC
727344	Chippewa Co Intl - United States	46.250	-84.467	01-01-2009 to 06-20-2013	DEWP;CC
727347	Pellston Rgnl Arpt - United States	45.564	-84.793	01-01-2009 to 06-20-2013	DEWP;CC
727417	Presque Isle Co - United States	45.407	-83.813	01-01-2009 to 06-20-2013	DEWP;CC
727435	Mackinack Island - United States	45.865	-84.637	01-01-2009 to 06-20-2013	DEWP;CC
994063	Presque Isle Light - United States	45.356	-83.492	01-01-2009 to 06-20-2013	DEWP;CC

Table 7 (cont'd)

Station ID	Location	Latitude	Longitude	Period of data availability	Parameters
994064	Sturgeon Pt Light GL - United States	44.713	-83.273	01-01-2009 to 06-20-2013	DEWP;CC
994065	Tawas City Glos Weat - United States	44.256	-83.443	01-01-2009 to 06-20-2013	DEWP;CC
994979	Gravelly Shoals - United States	44.017	-83.533	01-01-2009 to 06-20-2013	DEWP;CC
995980	Georgian Bay - Canada	45.533	-81.017	01-01-2009 to 06-20-2013	DEWP;CC
997257	De Tour Village - United States	45.983	-83.900	01-01-2009 to 06-20-2013	DEWP;CC
997258	Ft Gratoit - United States	43.017	-82.417	01-01-2009 to 06-20-2013	DEWP;CC
997260	Harbor Beach - United States	43.850	-82.633	01-01-2009 to 06-20-2013	DEWP;CC
997265	Point Iroquois - United States	46.483	-84.633	01-01-2009 to 06-20-2013	DEWP;CC
997266	Rock Cut - United States	46.267	-84.183	01-01-2009 to 06-20-2013	DEWP;CC
997268	SW Pier - United States	46.500	-84.367	01-01-2009 to 06-20-2013	DEWP;CC
997359	Alpena - United States	45.067	-83.417	01-01-2009 to 06-20-2013	DEWP;CC

Table 7 (cont'd)

Station ID	Location	Latitude	Longitude	Period of data availability	Parameters
997697	Little Rapids - United States	46.483	-84.300	01-01-2009 to 06-20-2013	DEWP;CC
998203	West Neebish - United States	46.283	-84.20	01-01-2009 to 06-20-2013	DEWP;CC
998242	Saginaw Bay Light 1 - United States	43.800	-83.717	01-01-2009 to 06-20-2013	DEWP;CC
998255	Mackinaw City - United States	45.783	-84.717	01-01-2009 to 06-20-2013	DEWP;CC
998339	Mouth of Black River - United States	42.975	-82.419	01-01-2009 to 06-20-2013	DEWP;CC

3.3   Results and Discussions

Lake-wide summer circulation for three years (2009, 2010, and 2011) was simulated using the large scale hydrodynamic model (LWM). In order to avoid problems with initialization of the stratified temperature, the model simulations were started in May with zero velocity and uniform vertical temperature profile determined from observations at 4 NDBC buoys (45003, 45008, 45137, and 45143). As noted by *Beletsky and Schwab* [2001], the spin-up time for the hydrodynamic model was very short and the effect of the initial conditions on velocity was negligible after about a week of simulation time.

In order to quantify model performance and the agreement between data and the model, we used the root-mean-square error (RMSE) index:

$$RMSE = \sqrt{\frac{\sum_{i=1}^{i=n}(x_i - X_i)^2}{n}} \qquad (17)$$

where x_i denotes the observed data and X_i is the simulation results; and n is the number of data points.

3.3.1   Results

3.3.1.1   Currents

Figures 10 and 11 show typical comparisons between the observed and simulated vertically-averaged velocities (east-west velocity *u* and north-south velocity *v*) for all three years based on the Saginaw Bay Model. The RMSE and standard deviation values for the hydrodynamic model

comparisons are summarized in Table 8. The comparisons indicate that model performance was relatively poor for the year 2009. The main reason is due to the missing data for the GLOS stations from May to July in the year 2009 while we started the model at the beginning of May in order to avoid problems with initialization of the stratified temperature. Therefore, the model used only data from the NDBC stations between May and July. This was not an issue for the remaining two years (2010 and 2011). In all cases, considering the fact that the ADCPs were deployed in very shallow areas of the bay (2 to 3 m depth) where the effects from waves and boat traffic might be significant, we conclude that the model was able to describe the vertically-averaged velocities reasonably well.

Table 8: RMSE and standard deviations between ADCP observed current values and results

from the Saginaw Bay model (SBM)

Deployment Date	Location	RMSE (cm/s) (Eastward, Northward velocity)	Standard Deviation (Eastward, Northward velocity)	
			Observed	Modeled
08/04/09-08/18/09	216	2.53, 2.68	1.00,2.00	3.4,4.7
08/20/09-09/02/09	232	3.82,3.9	1.49,2.33	3.51,4.83
07/13/10-07/27/10	194	3.6, 5.7	1.0,0.90	2.78,5.72
07/30/10-08/12/10	211	2.67,3.09	2.07, 2.89	3.8,5.2
07/27/11-08/28/11	8119	3.24, 2.23	2.43,2.36	3.10,2.47
07/27/11-08/28/11	8126	4.6,8.9	3.31,6.36	5.89,4.17
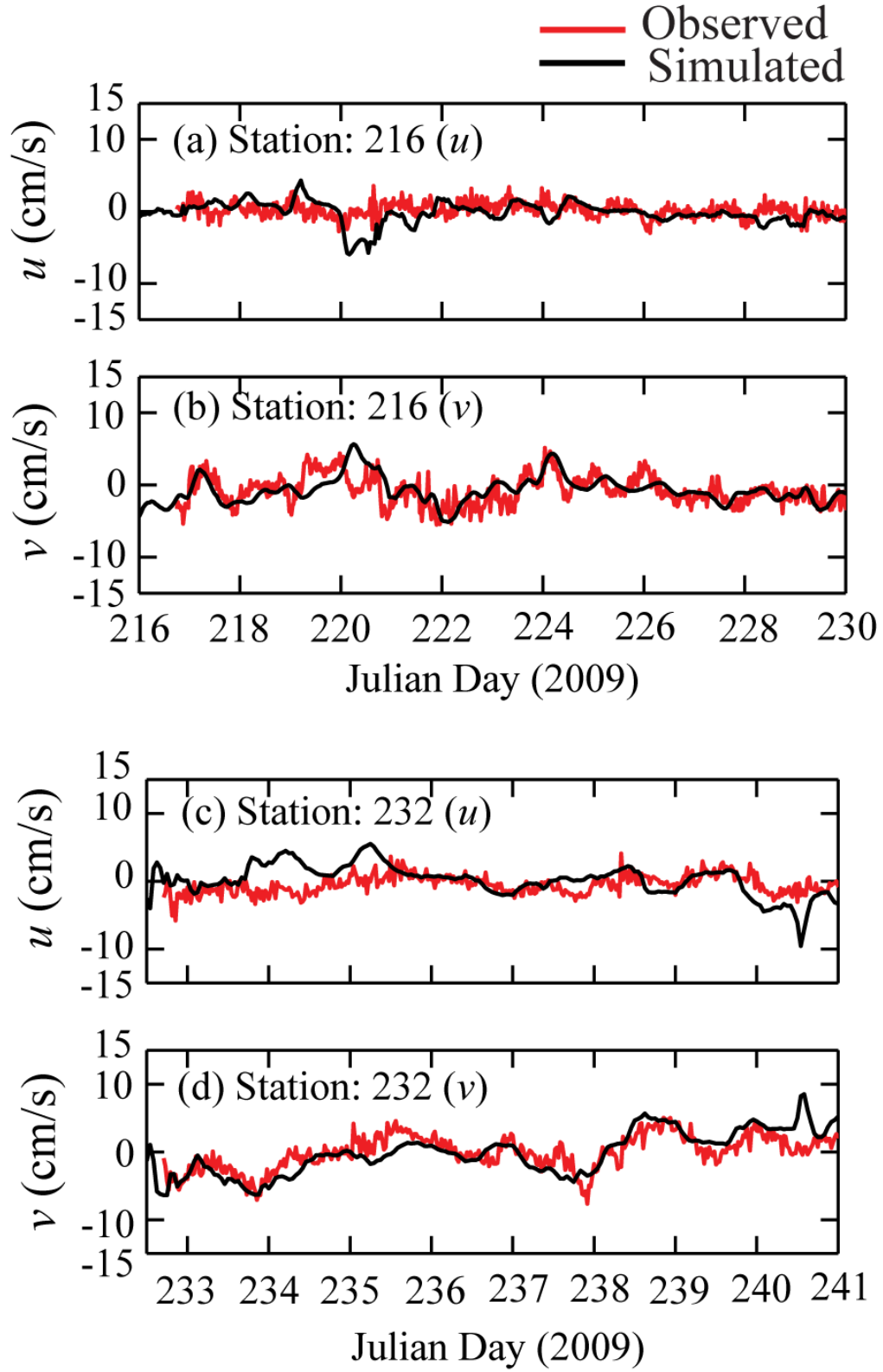
Figure 10: Comparisons between vertically-averaged currents from ADCP observations and simulations for the year 2009 at the station 216 (a, b) and the station 232 (c, d).
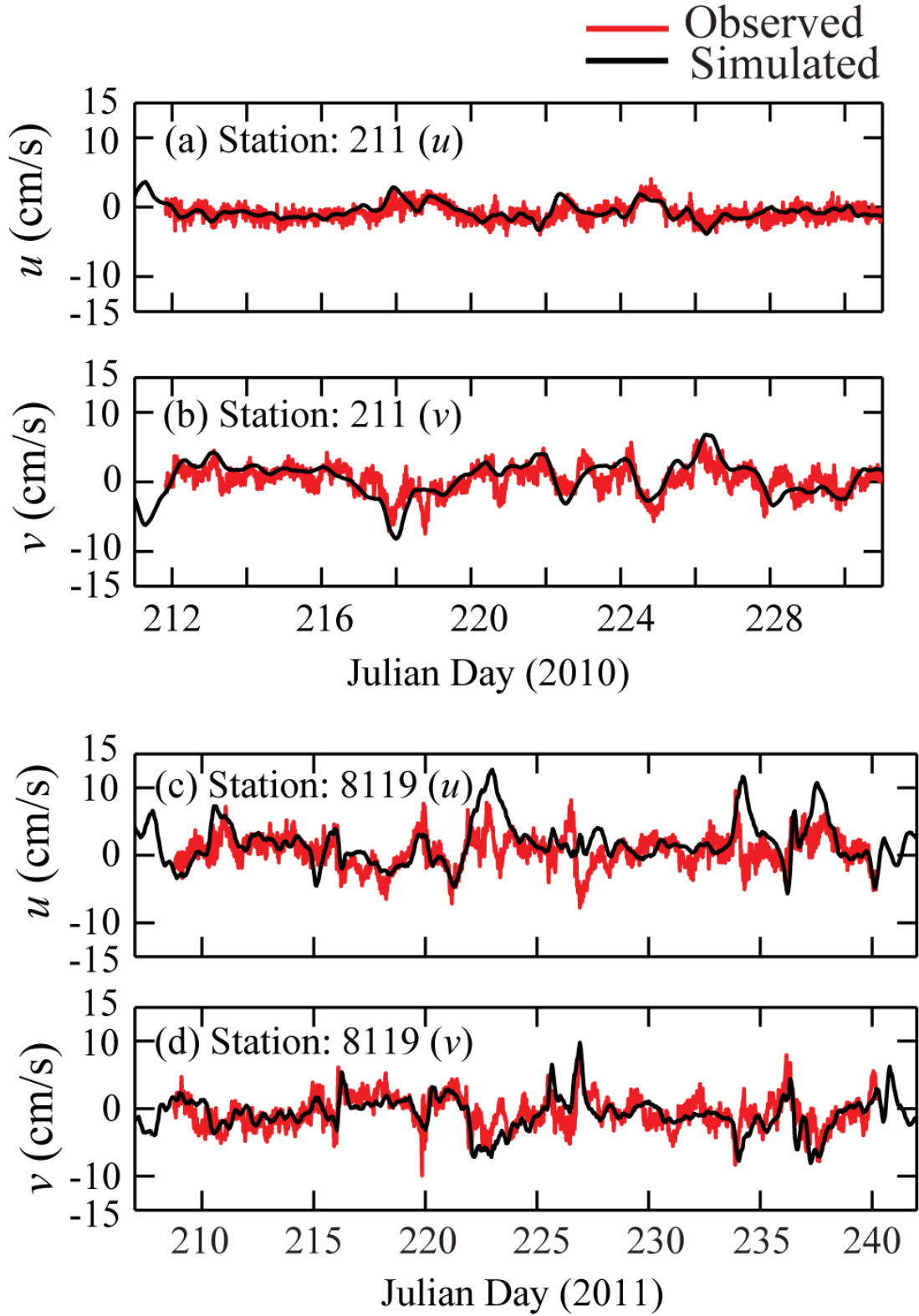
Figure 11: Comparisons between vertically-averaged currents from ADCP observations and simulations for years 2010 at the station 211 (a,b) and 2011 at the station 8119 (c,d).

In addition to the vertically-averaged currents, the numerical model was able to simulate the water levels. The comparisons showed very good agreement between the observed and simulated water level fluctuation at station 5035 (Figure 12).
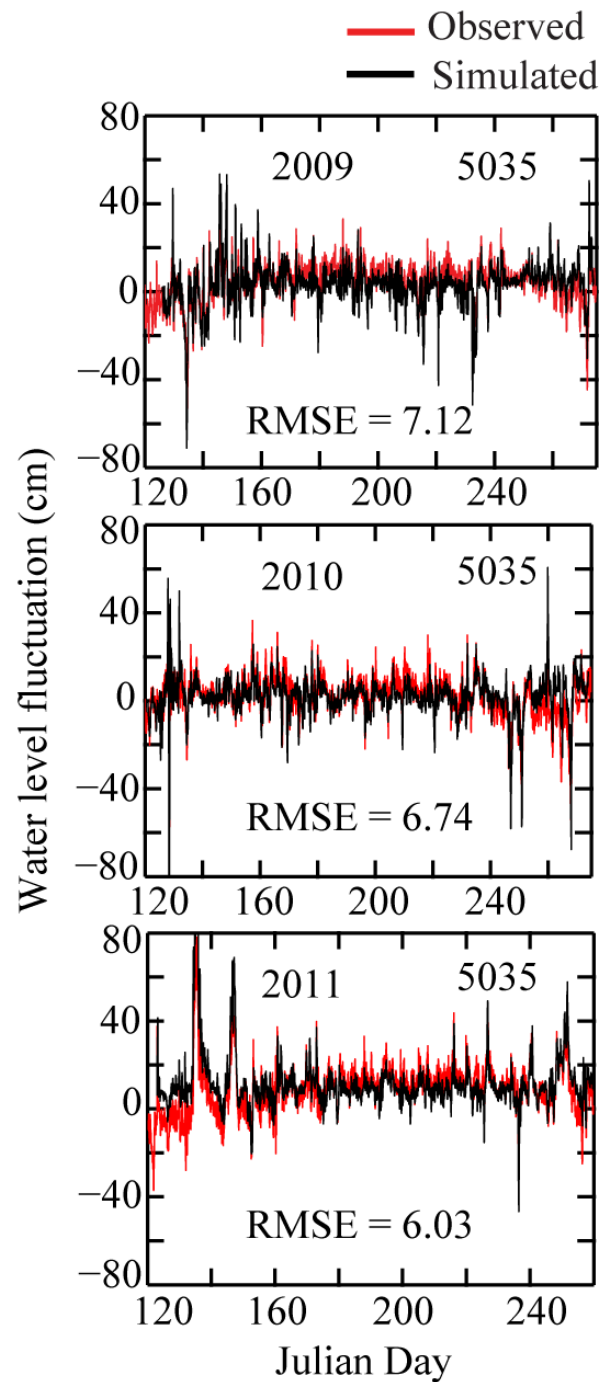
Figure 12: Comparisons between observed and simulated water level fluctuations at station 5035 (Essexville, Michigan) for the years 2009, 2010 and 2011.

48

3.3.1.2 Temperature

The numerical model was also able to simulate the evolution of surface temperatures accurately (RMSE values less than 1.7^{o}C), as shown by the comparisons between model results and observations at NDBC buoys and by ADCP presented in Figure 13 and 14, respectively.
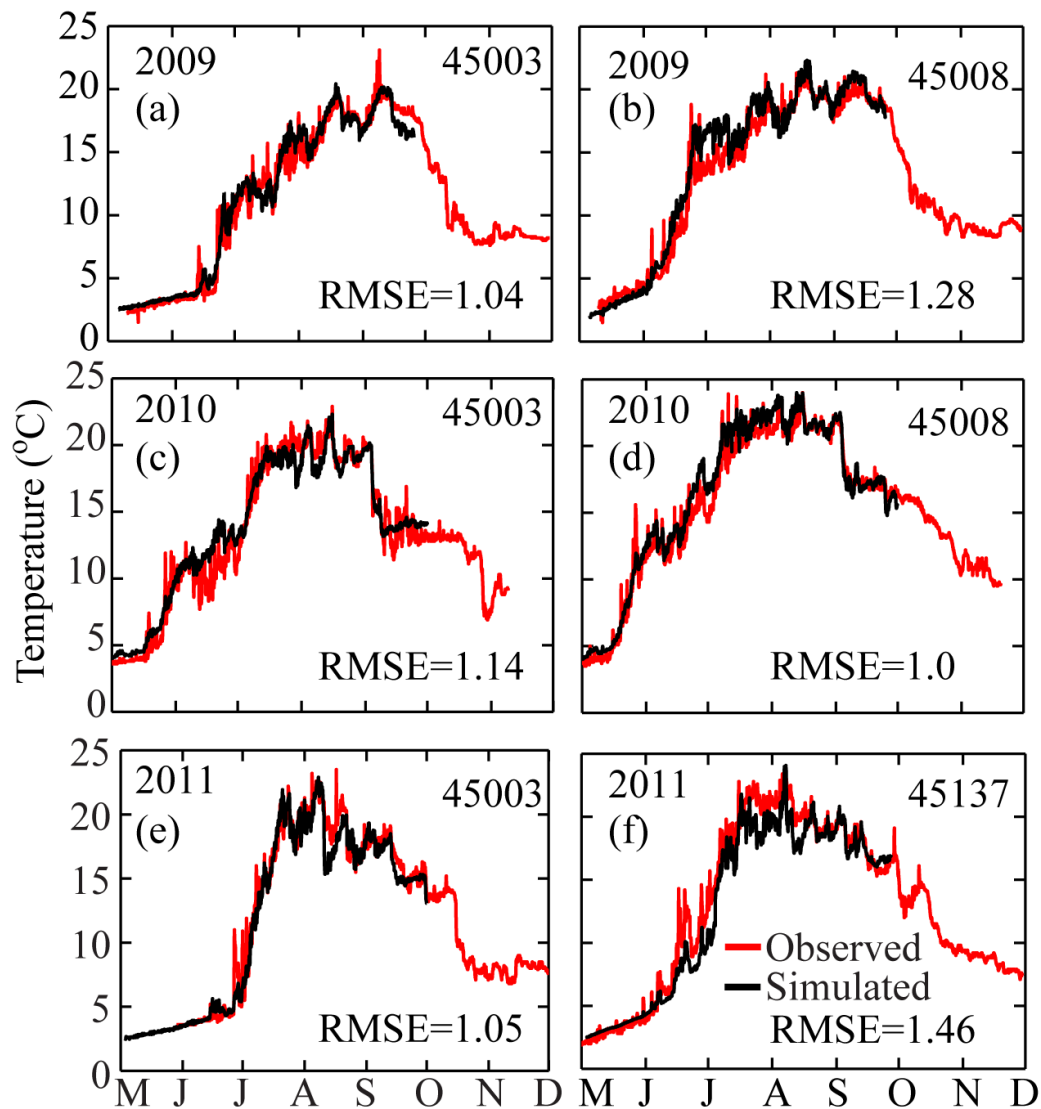
Figure 13: Comparisons between simulated surface temperatures and observations at the NDBC buoys from May to September for the years 2009, 2010, and 2011.
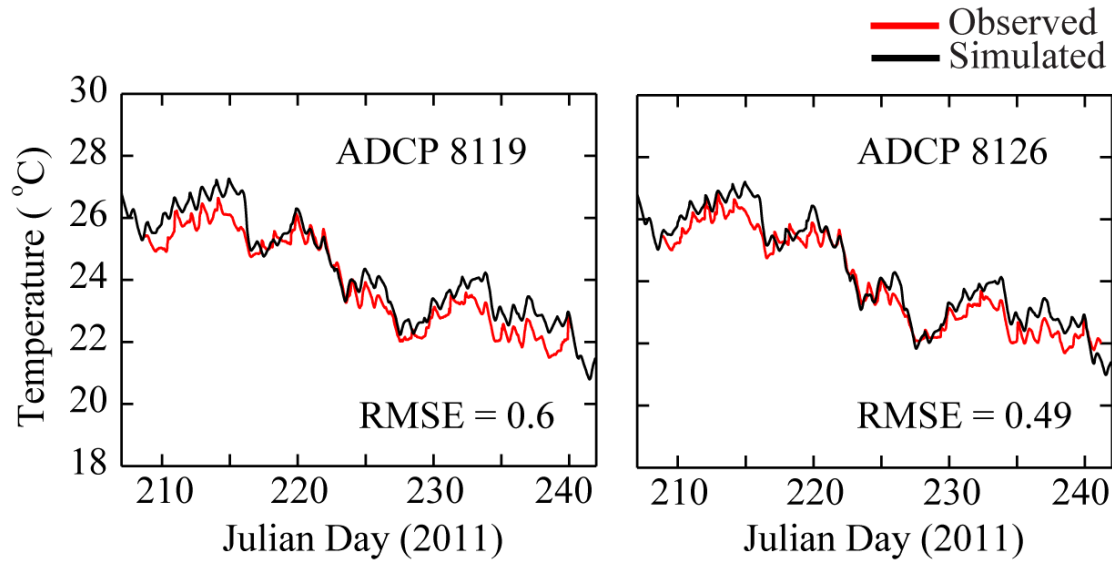
Figure 14: Comparisons between simulated surface temperatures and observations from ADCPs for the year 2011.

While comparisons with observations made at a point can be used to quantify model accuracy, dynamic lake-wide processes can be understood by examining the spatial variability in temperature and currents are more clearly shown in the contour plots presented in Figure 15, and 18. Vertically-integrated currents based on the original unstructured grid, averaged over each summer month for the three year simulation period, were interpolated to a uniform Cartesian grid with a step size of 5 km and shown as vector plots in Figure 18. The dominant current patterns are marked using red lines with arrows showing the direction of flow. The lake-wide circulation became progressively more pronounced and complex with more gyres appearing as time progressed from July to September while circulation in the Saginaw Bay was strong during the month of August in which the direction of maximum wind velocity (Figure 53) is along the axis of the bay. Details of summer circulation in the Saginaw Bay are shown in Figure 19 by interpolating the vertically-integrated currents from the unstructured grid (averaged over the 3

year period) to a uniform Cartesian grid with a resolution of 2 km. We notice the presence of an anticyclonic (that is, clockwise-rotating) gyre at the mouth of the outer Saginaw Bay for all three summer months. As noted by others [*Sheng and Rao*, 2006; *Beletsky et al.*, 1999], mean circulation in Lake Huron is predominantly cyclonic (counterclockwise) during the summer months (Figure 18). Generally, current speeds are higher closer to the shore and dominated by the alongshore component. Currents in the offshore regions of the lake are smaller and organized into gyres strongly influenced by topographical features (e.g., the Manitoulin Basin (MB) and the Alpena-Amberley Ridge (AAR) in Figure 1). As expected, vertically-averaged currents in the shallower parts of the lake (south and south-west) are higher than values in the deeper parts of the lake (north and north-east). Exchange between Lake Huron and the two main bays (Saginaw Bay and Georgian Bay) is complex and influenced by a number of factors, including topography, stratification as well as orientation of the shoreline. For example, Figure 21 shows that mean surface flow is into the Georgian Bay which is associated with a return flow in the deeper layers out of Georgian Bay.

As in the other Great Lakes, Lake Huron shows a significant seasonal variation in the thermal structure. The contour plots of surface temperature presented in Figure15 show the gradual warming of the surface layers as the summer progresses. As expected, the shallower parts of the lake warm more quickly and reach the peak of about 25°C in August. However, the shallower Saginaw Bay reaches this value early by July. The dramatic inter-annual variability in surface temperature is also clear from the results presented in Figure 15, which show the temperature contours for all three summer months and for all three years considered (2009-2011). The vertical variability in temperature is shown more clearly by the temperature profile of the water column along the transects 3-3 and 4-4 in Figures 16 and 17, respectively. The thermal

structure of Lake Huron is affected by the central Alpena-Amberley Ridge (AAR) in the main lake as well as the presence of the numerous islands. The vertical thermal structure is similar and comparable to previous observations [*Saylor and Miller*, 1979; *Boyce et al.*, 1989], and results from the numerical simulations in the Great Lakes [*Beletsky and Schwab*, 2001; *Sheng and Rao*, 2006]. We can also see the presence of Ekman flow-driven coastal upwelling in the northeast of the lake [*Plattner et al.,* 2006] as well as topographically driven upwelling regions associated with sharp changes in bathymetry (e.g. AAR). The impact of these upwelling regions can also be observed in Figure 15 in the form of significantly lower surface water temperatures located north-east of the AAR. These simulated features are also observed in the GLSEA (Great Lakes Surface Environmental Analysis) daily composite temperature images produced from the thermal AVHRR channels of NOAA's polar orbiting weather satellites [*Plattner et al*., 2006; *Leshkevich et al*., 1992].
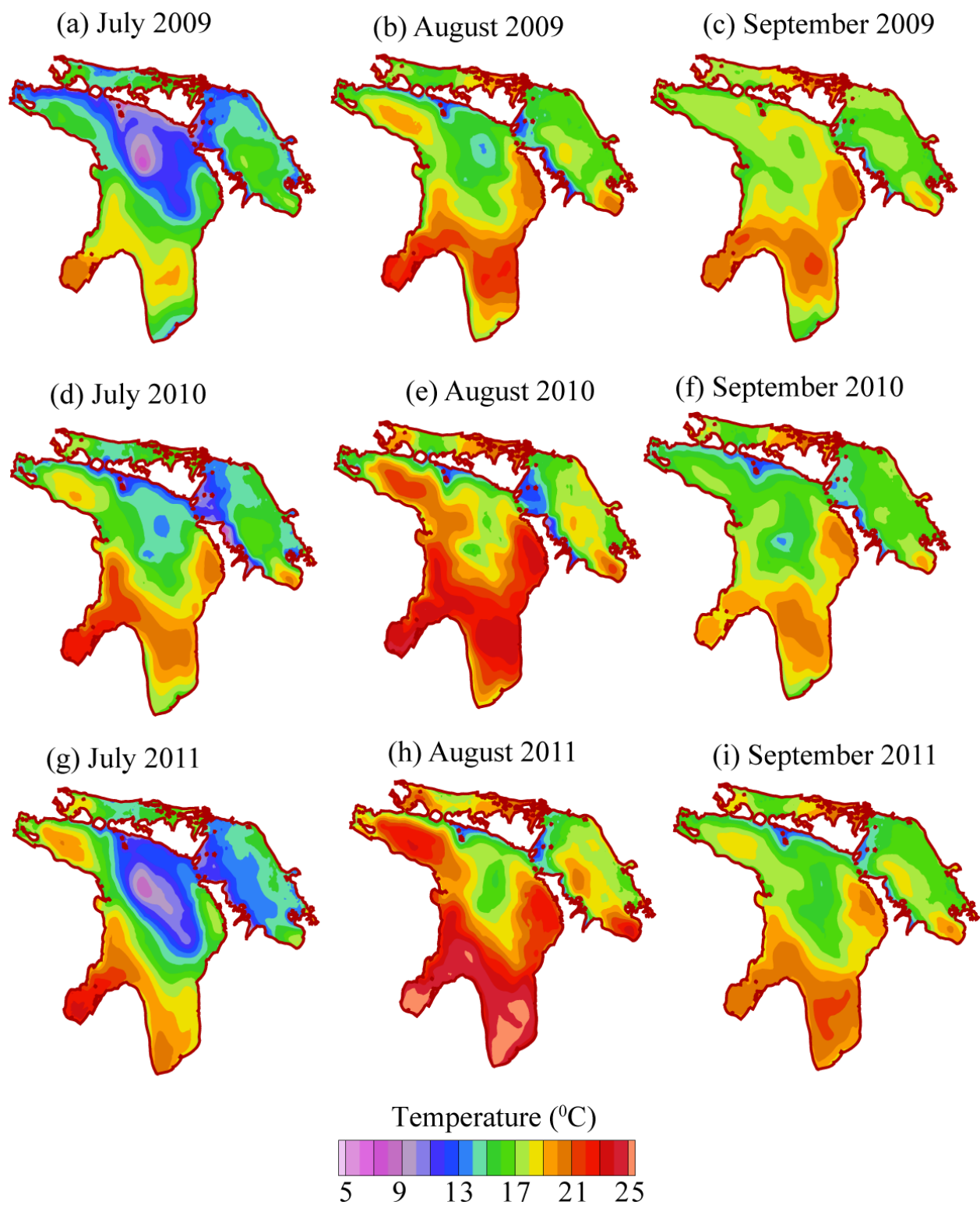
Figure 15: Surface temperature contours for Lake Huron for the summer months July, Aug, and September in 2009, 2010 and 2011.
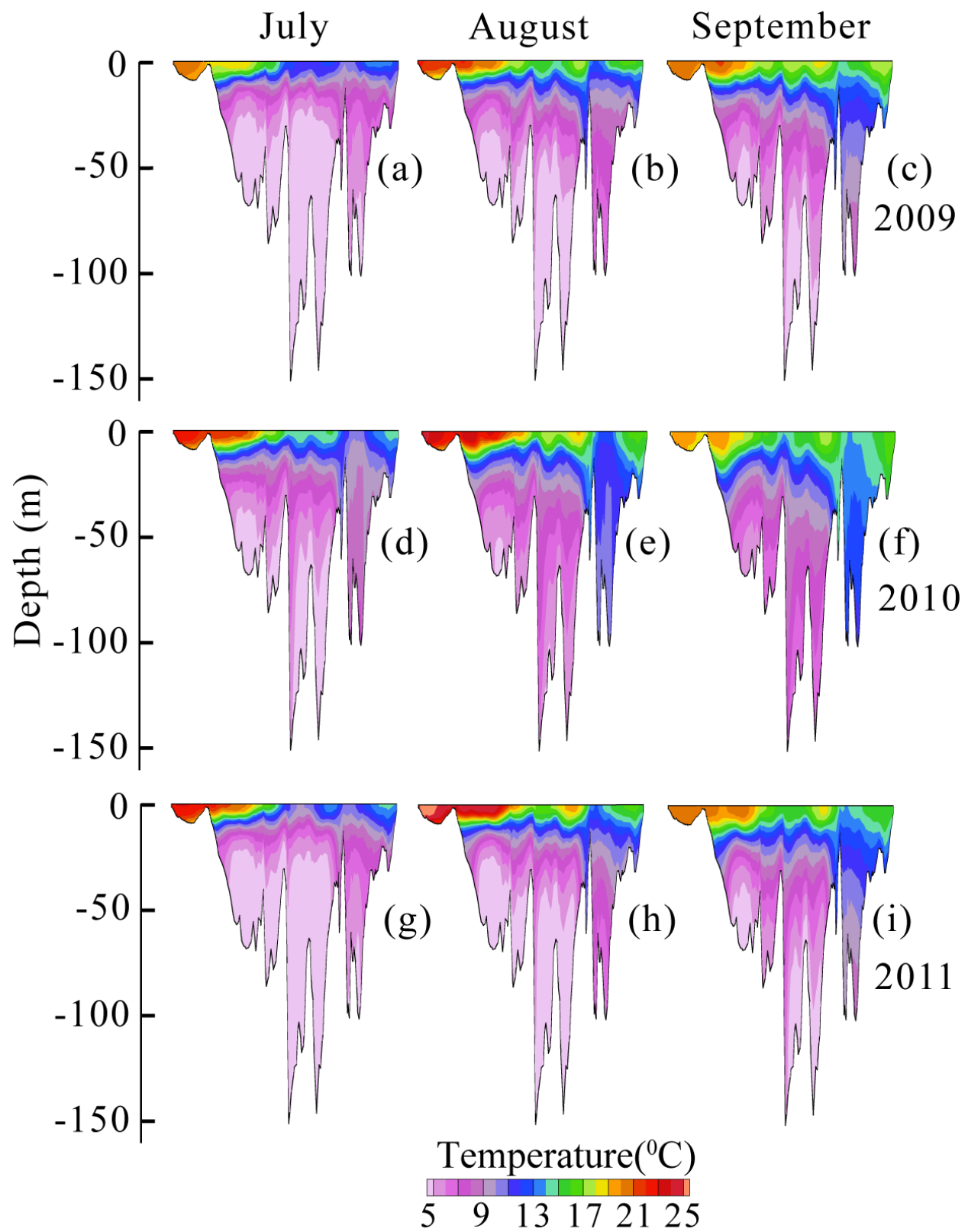
Figure 16: Mean monthly temperature profile along the transect 3-3 in Figure 3.

54
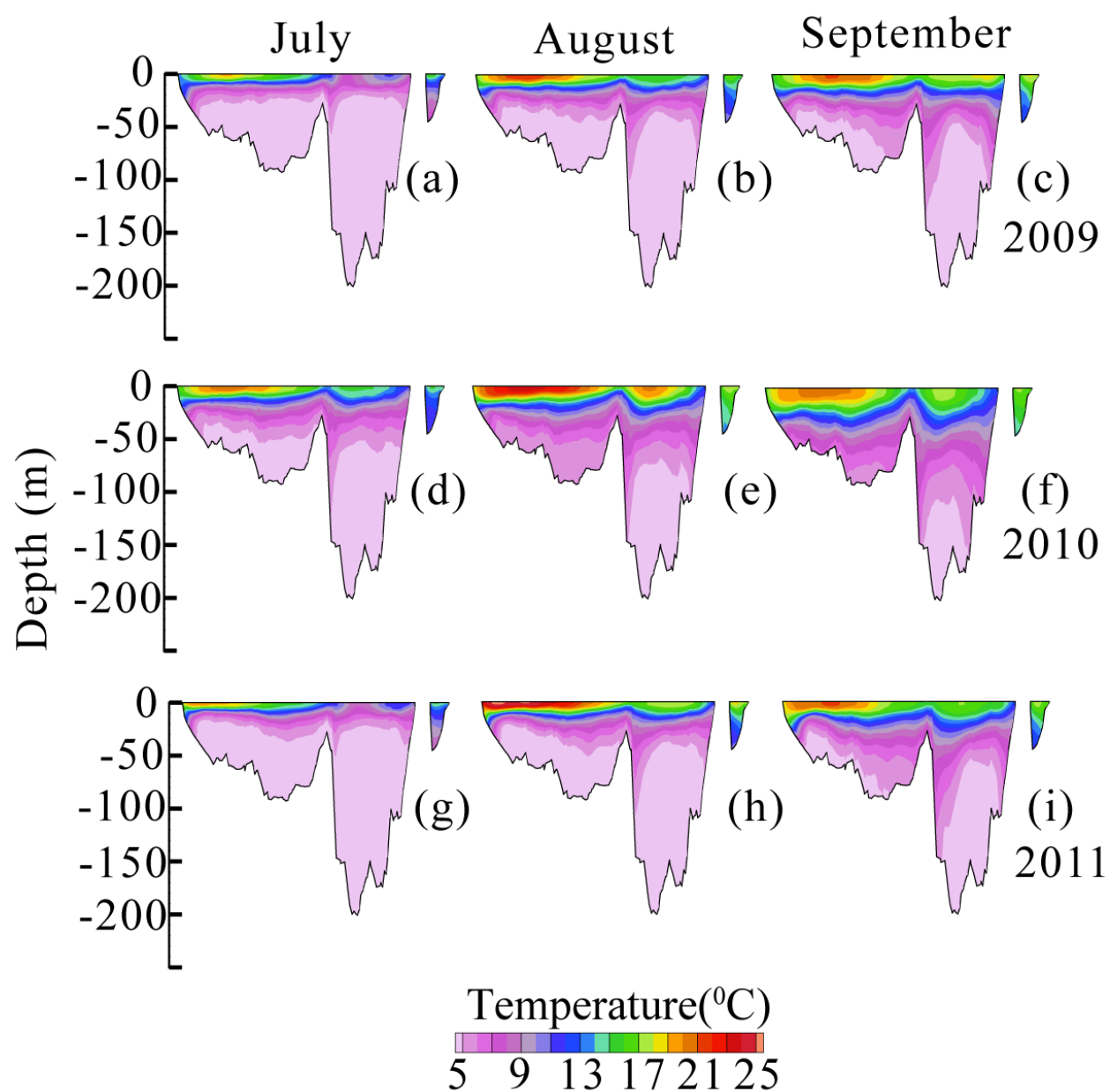
Figure 17: Mean monthly temperature profile along the transect 4-4 in Figure 3.

3.3.2 Discussion

Results from the high-resolution Saginaw Bay hydrodynamic model (SBM) are presented in Figures 10 and 11. Summary statistics for the comparisons between the ADCP observations and model results are provided as RMSE values in Table 8.

Large-scale circulation in Lake Huron is influenced its key physical features (several large islands, exchange with Georgian Bay and Saginaw Bay, and the mid-lake AAR ridge). Field observations and results from numerical models have shown that circulation in the main lake is generally counterclockwise (cyclonic) but not as organized as in Lake Superior due to the presence of the mid-lake ridge. The lake-wide numerical model was able to simulate this feature during the summer months. The mean current speed was around 3 cm/s while currents as high as 20cm/s were found in Eastern Georgian Bay. Exchange with Georgian Bay was uniform over the summer months and the mean surface current speed in the channel connecting Georgian Bay with Lake Huron was about 4cm/s. Surface currents into Georgian Bay during the summer months are associated with a return flow at greater depths as indicated by *Beletsky et al*., [1999]. This feature was confirmed by our numerical model as shown by the vertical profile of mean current velocity at the mouth of Georgian Bay presented in Figure 21. The mean velocity in the deeper layers is about 1 cm/s and generally flows from Georgian Bay into Lake Huron. Here the surface layer coincides with the epilimnion and deeper layer coincides with the hypolimnion. Therefore, it is likely that the direction of flow at a particular depth is influenced by the strength of the stratification and changes from year to year. Inter-annual variability of currents was evaluated using mean current speeds for different months. We found that current speeds were highest during the year 2010, with a mean current speed of about 4 cm/s.
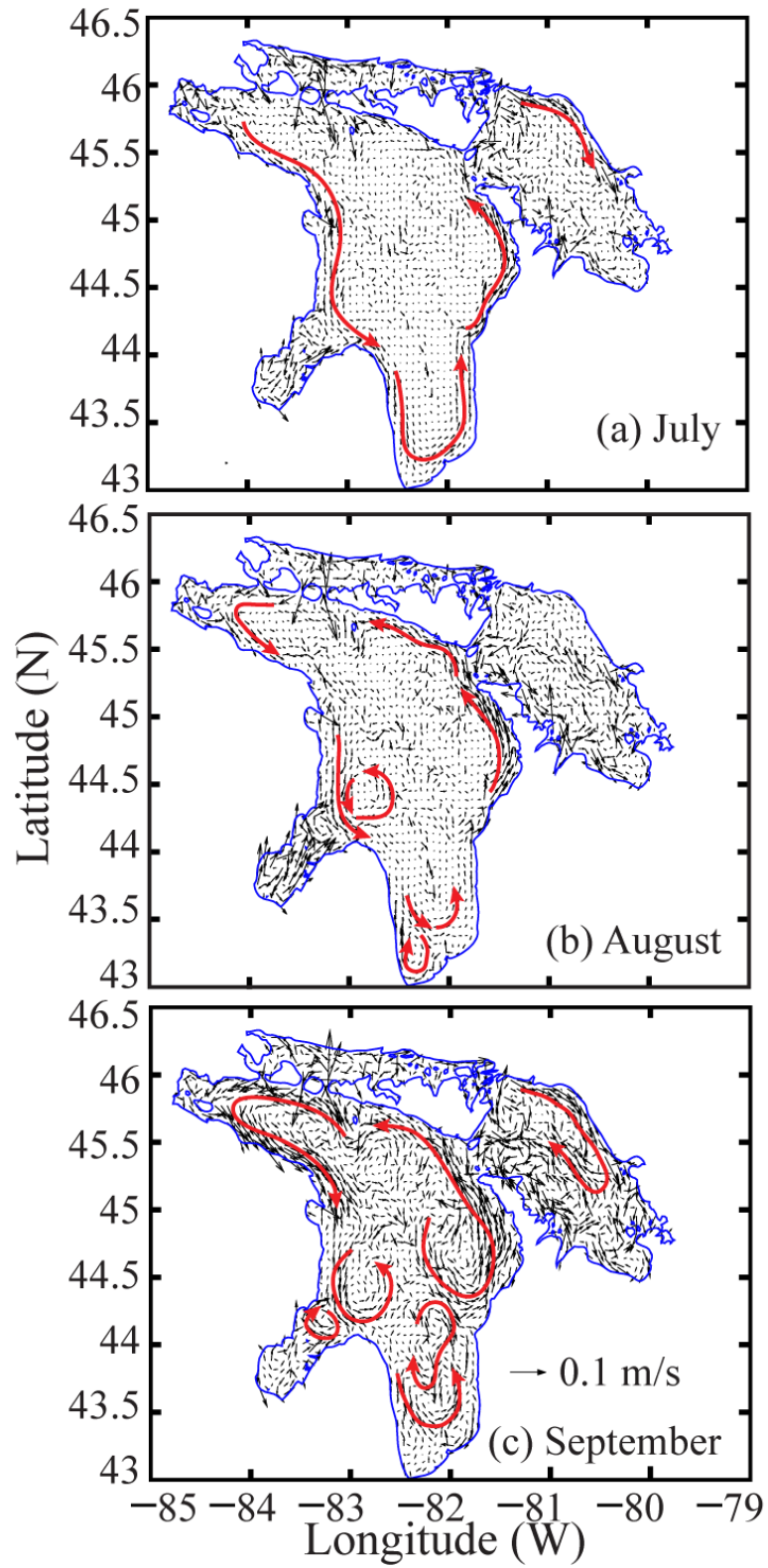
Figure 18: Vertically-averaged currents in Lake Huron averaged over the three year period (2009 – 2011) for each summer month (July, August and September).
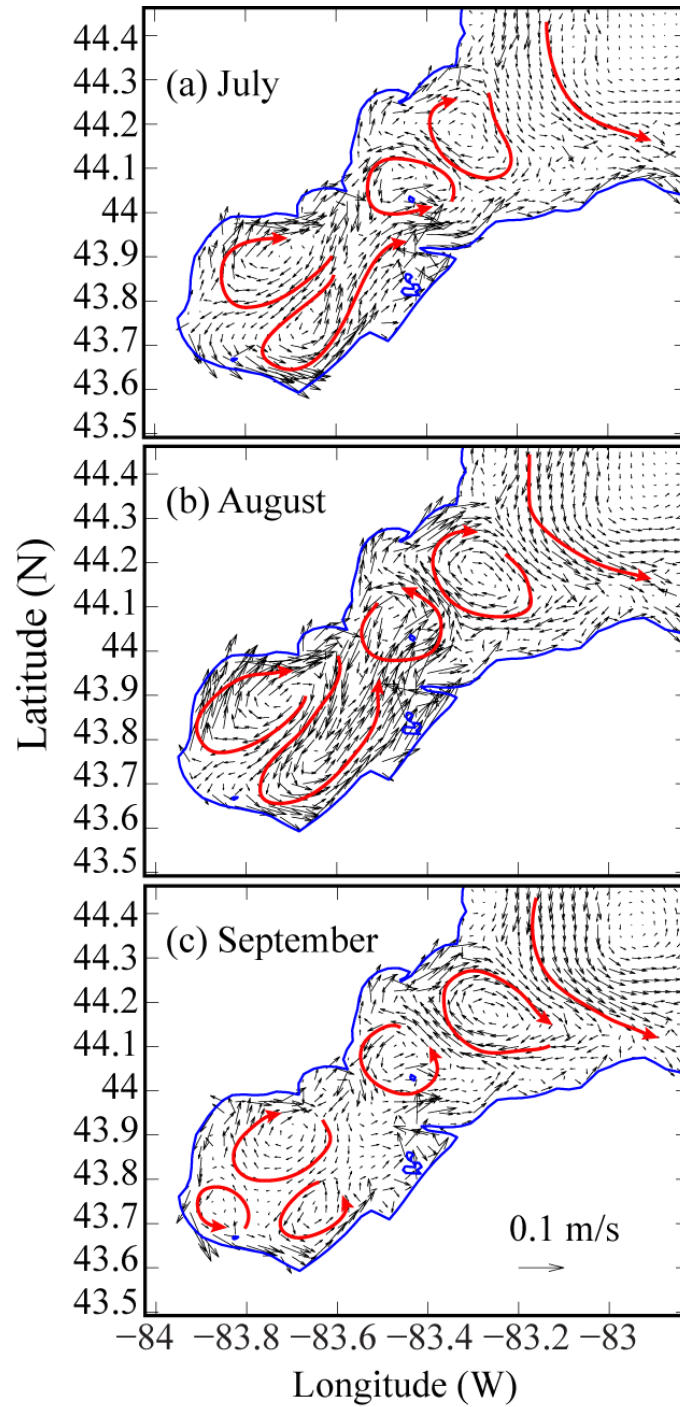
Figure 19: Vertically-averaged currents in Saginaw Bay averaged over the three year period (2009 – 2011) for each summer month (July, August and September).
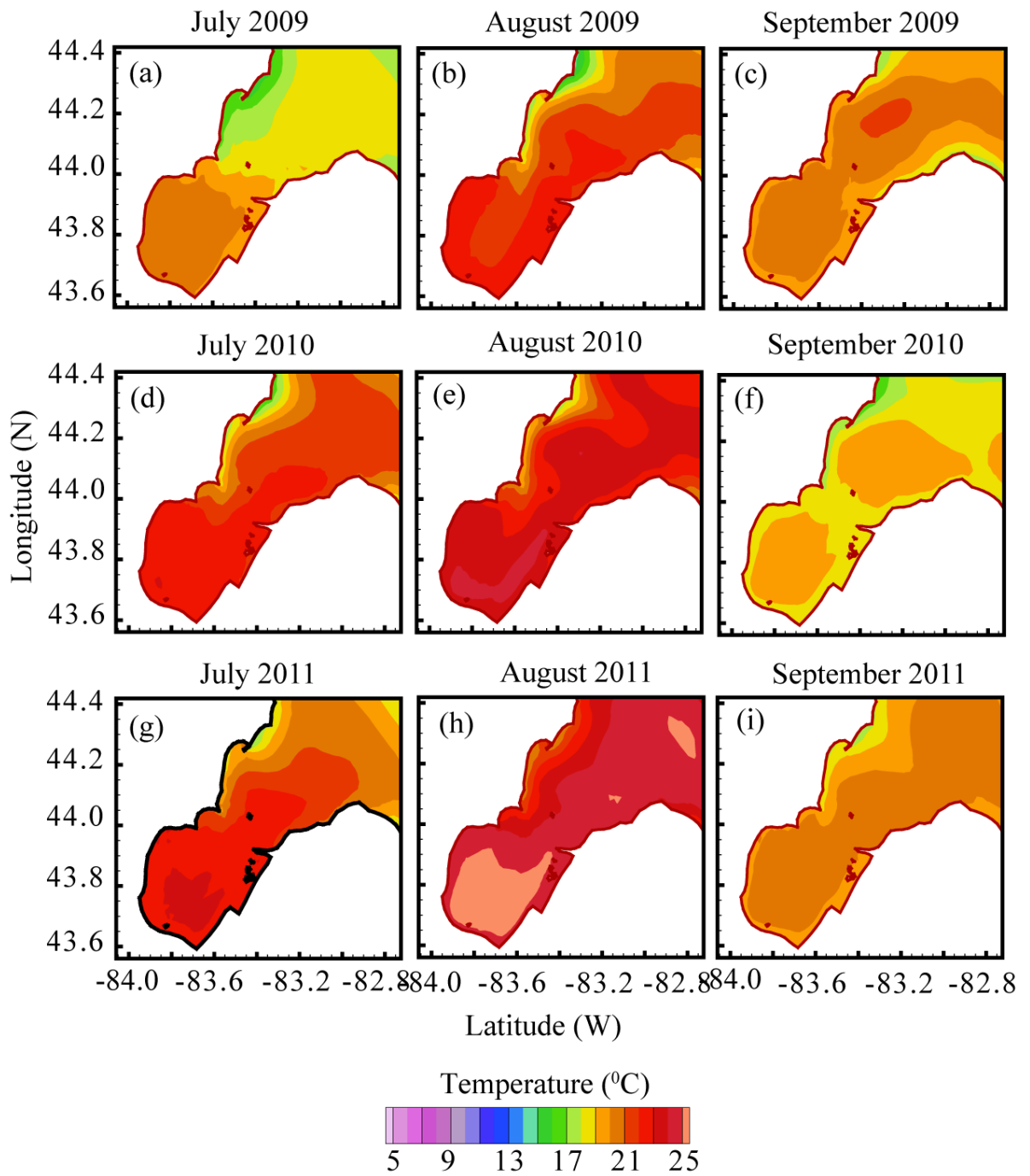
Figure 20: Mean surface temperature contours in Saginaw Bay for the months of July, August, and September in 2009, 2010 and 2011

As a result of differences in area, volume and size of entrance channel, the circulation patterns within Saginaw Bay and Georgian Bay are very different. Mean summer circulation in Georgian Bay was largely counterclockwise with a mean speed of about 3cm/s. However, circulation in Saginaw Bay was much more complex and depended on the wind direction as noted by *Saylor and Danek* [1976] and *Danek and Saylor* [1977]. The circulation at the entrance of Saginaw Bay was either clockwise (for southwest wind direction) or counterclockwise (for northeast wind direction) depending on the wind direction. Winds blowing perpendicular to the axis of the bay did not significantly affect currents within the bay. Current speeds within Saginaw Bay are generally higher than in the lake resulting in higher mixing due to dispersion. Another important feature of circulation within Saginaw Bay was the difference between hydrodynamics in the inner and outer bays and the effect on exchange between the two. We found that currents along the coast are aligned with the prevailing wind direction. Currents in the central (deeper) part of the bay flow in the opposite direction.

Similar to other large, deep lakes, the thermal structure in Lake Huron shows significant seasonal variability. The hydrodynamic model simulations were initialized with constant temperature based on the observed water temperature measured at the buoys. As shown by the vertical temperature profiles presented in Figures16 and 17, the process of stratification is generally completed by August. The thermocline was located at a depth of about 9m with an inter-annual variability of less than 4 m. By including a surface wind-wave mixing scheme, *Bai et al.,* [2013] reproduced a reasonable thermal structure with a sharp thermocline located at a depth of about 15 m in the Great Lakes in August. Since the hydrodynamic models use the σ−coordinate, we expect a marginally diffused thermocline as noted in [*Beletsky and Schwab*, 2001]. Due to the lack of any temperature profile measurements in the vertical during our

simulating period, a quantitative comparison of the accuracy of the thermal model is not presented; however, comparisons of temperatures in deeper parts of the lake measured by ADCPs are shown in Figure 14 which show a good agreement between observations and the model (RMSE values are less than 0.6°C). As shown in Figure 15, the southern (shallower) part of the lake warms more quickly. However, as shown in Figure 13, surface water temperature in the lake has a high inter-annual variability especially in the beginning of summer (June). These variations in monthly mean water temperatures could be due to global climate dynamics. The influence of the mid-lake ridge on thermal structure in the main lake is also clear from Figure 16. The deepening thermocline reaches the mid-lake ridge (~20 m) by around August. At this point exchange between the hypolimnion of the northeastern and southwestern basins is limited and exchange between the two basins is largely in the surface (epilimnion) layers.

Several researchers have observed topography-driven upwelling in the marine environment [e.g., *Figueroa and Moffat*, 2000]. However, such features have not been observed in the Great Lakes to the best of our knowledge. Given the highly variable topography in Lake Huron (compared to the other Laurentian Great Lakes), conditions are favorable for the upwelling and hydraulic jumps at several locations the main lake as well as near Saginaw Bay. Coastal upwelling possibly due to Ekman flow driven by the prevailing wind is observed near the northeastern part of the lake. Figure 16 shows the temperature profile along the transect 3-3 marked in Figure 3a. During the stratified summer period, we can see that colder waters are forced upward near the AAR. This indicates the presence of a topographically-driven upwelling and possible ventilated thermocline in central Lake Huron. Another region of interest for this study is the sill at the mouth of Saginaw Bay (BCB in Figure 3). Since the depth here is about15m and the upper-mixed layer reaches the lake-bottom, no

upwelling regions are evident here. However, it is possible that strong currents as a result of winds from the southwest could setup conditions favorable for a hydraulic jump.
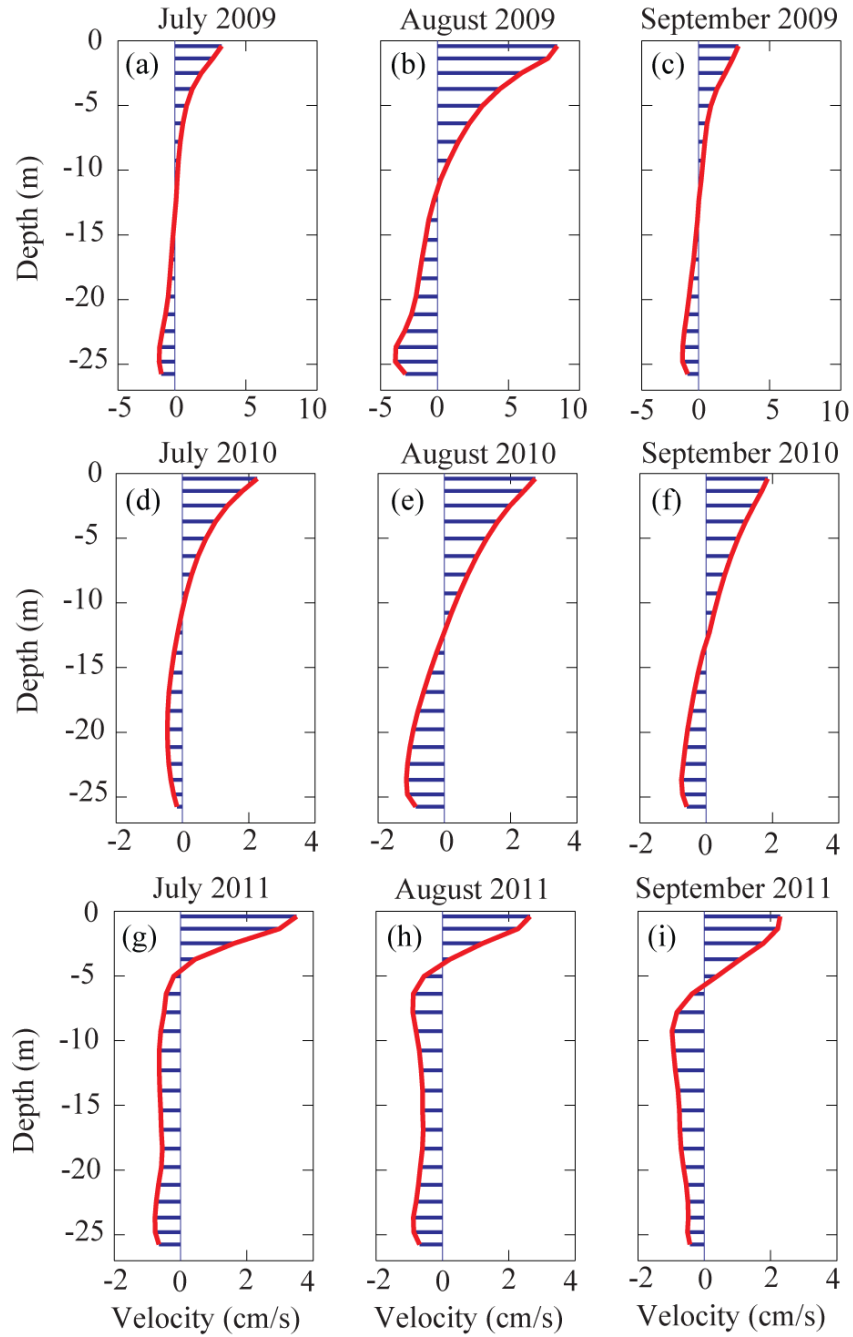
Figure 21: Mean vertical velocity profiles at the inlet of Georgian Bay for different layers confirming the return flow suggested by [*Beletsky, et al.*, 1999].

3.4.3 Particle Tracking Model

The high-resolution Saginaw Bay hydrodynamic model was able to resolve the small-scale bathymetry features and their influence on the circulation within the bay. We used these results to simulate the trajectory of Lagrangian drifters that were released near the mouth of the Saginaw River.

The Lagrangian particle tracking consists of solving a nonlinear system of ordinary differential equations as follows (*Chen et al.,* [2003]):

$$\frac{dx}{dt} = U(x(t), t) \tag{18}$$

where x is the particle position at a time *t*, *dx/dt* is the rate of change of the particle position in time and *U(x,t)* is the 3-D velocity field. FVCOM model used the explicit Runge-Kutta multi step methods to solve the equations in which the particle position at a time *t* is calculated from solving the discrete integral:

$$x(t) = x(t_n) + \int_{t_n}^{t} U(x(t), \tau)d\tau \tag{19}$$

Assume that $x(t_n) = x_n$ is the position of a particle at time $t=t_n$,

$x(t_{n+1}) = x_{n+1}$ is the new position of a particle at time $t_{n+1} = t_n + \Delta t$ and can be determined by the 4th order explicit Runge-Kutta method as follows:

$$\epsilon_1 = x_n \tag{20}$$

$$\epsilon_2 = x_n + \frac{1}{2}\Delta t.\, U(\epsilon_1) \tag{21}$$

$$\epsilon_3 = x_n + \frac{1}{2}\Delta t.\, U(\epsilon_2) \tag{22}$$

$$\epsilon_4 = x_n + \Delta t.\, U(\epsilon_3) \tag{23}$$

$$x_{n+1} = x_n + \Delta t \left[\frac{U(\epsilon_1)}{6} + \frac{U(\epsilon_2)}{3} + \frac{U(\epsilon_3)}{3} + \frac{U(\epsilon_4)}{6}\right] \tag{24}$$

where Δt is the time step. Details of the particle tracking model can be found elsewhere (e.g., *Chen et al.,* [2003]).

Currents from SBM model are used to simulate particles through the Bay. In order to reduce the effects from initial conditions of current we used the "restart mode" in the model. In this mode, the particles were released with the initial conditions based on the current velocity calculated from the hydrodynamic model. This technique allows the particles to move immediately after being released.

The results from the Lagrangian drifter study and comparisons with observed drifter tracks are presented in Figure 22. As shown by the starting points (initial positions of the drifters at time $t = 0$) marked in the figure, the drifters were released at locations close to the mouth of the Saginaw River where the currents are complex due to plume dynamics and the presence of Shelter Island (SI in Figure 3b). As shown in Figure 22, the Lagrangian drifters moved in either an eastward or northward direction after release near the Saginaw River mouth. The general direction of the drifters was affected by the prevailing winds and indicative of the complex plume dynamics near the mouth of a large river. The model simulated particle trajectories

64

compare well with GPS locations of the Lagrangian drifters on all the days. It must be noted that during the field study, it was observed that the drifters would often get in the shallower depths and get entangled in vegetation present close to the shore in this part of the bay. As a result, mean buoy speeds were used to determine the status of the buoy and comparisons with model are presented only till the first grounding event. Long-term drifter trajectories might track the gyres in the inner and outer Saginaw Bay that are predicted by the numerical model.
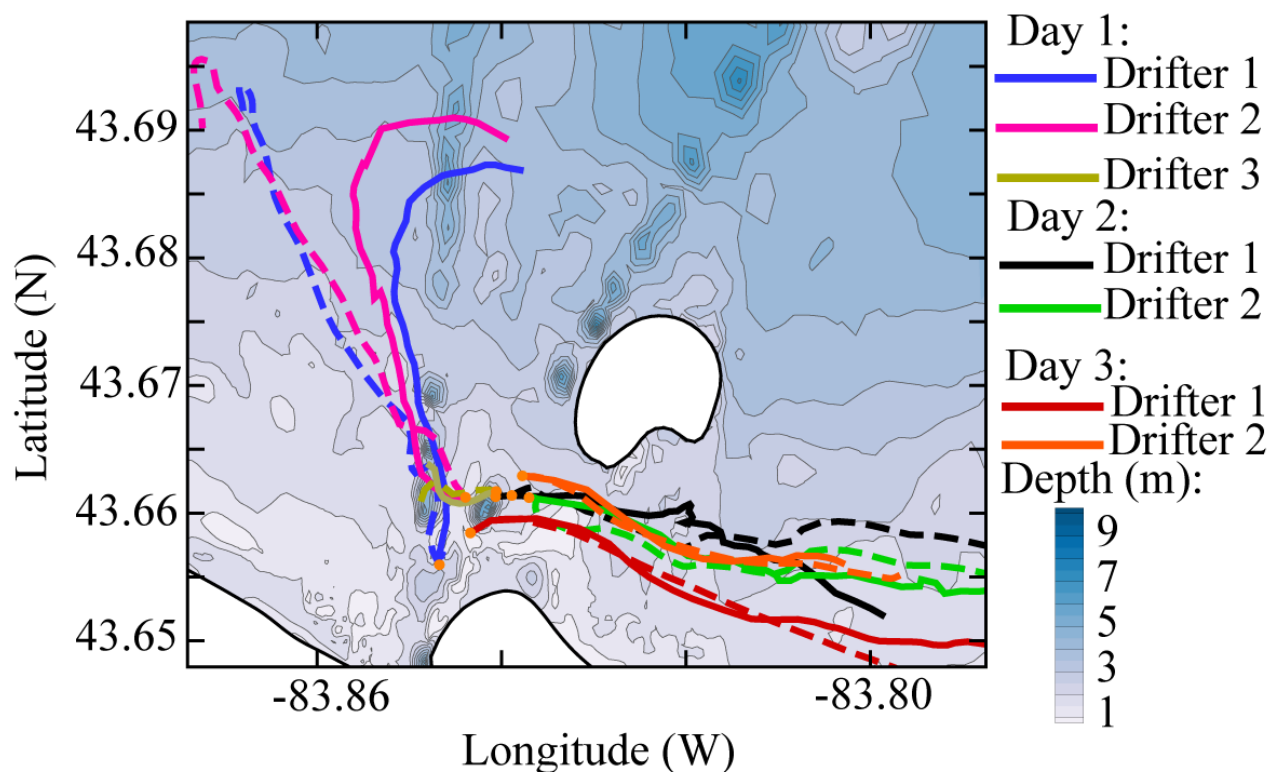
Figure 22: Comparisons between observed positions of GPS-enabled Lagrangian drifters and simulated particle trajectories based on the Saginaw Bay hydrodynamic model. For each drifter, the solid lines (observed) and dashed lines (simulated) are shown in the same color.

3.4.4 Dispersion coefficient in Saginaw Bay

Studies of dye (tracer) diffusion in the open lake and ocean have found that while mixing rates in open waters follow the Okubo 4/3 power-law scaling [*Okubo*, 1971], mixing rates close to shore are higher due to shear effects resulting from lateral and bottom boundaries [*Lawrence et al.*, 1995; *Peeters et al.*, 1996; *Stoket and Imberger,* 2003; *Ojo, et al.*, 2006]. Based on data from a continuous Rhodamine-WT dye release study conducted during summer 2008, [*Thupaki et al.*, 2013] estimated a horizontal dispersion coefficient of about 5.6 m^2/s close to the shore in southern Lake Michigan. Dispersion rates in the near-shore can also be calculated using Lagrangian drifters, which have the additional advantage of higher sampling rate [*Spydell et al.*, 2007; *Nekouee*, 2010]. *Spydell et al.,* [2007] calculated the absolute (one-particle) and relative (two-particle) dispersion rates using statistical analyses of drifter observations. They found that the relative diffusion rate$(D)$for Lagrangian particles followed the scaling $(D \sim l^{2/3})$ in the surf-zone, where l is the particle separation distance. *Brown et al.,* [2009] found that rates are higher in the presence of rip currents with relative diffusion rates following the relation $(D \sim l^{1/5})$ on rip-channel beaches. In the presence of sheared along-shore currents *Spydell et al.,* [2009] found that along-shore diffusivity is greater than cross-shore diffusivity, but still lower than the diffusion rate predicted for 2D inertial sub-range$(D \sim l^{4/3})$. Absolute diffusion rates can also be calculated from single-point Lagrangian drifter statistics by assuming isotropic turbulence. Using particle diffusion trajectories in the surf-zone, *Spydell et al.,* [2007] found that diffusion rates in the along-shore and cross-shore directions varied from 4.5 m^2/s to 0.7 m^2/s over a two-day period.

Data from the Lagrangian drifter study were also used to calculate the absolute dispersion rates near the mouth of Saginaw River. The recorded GPS locations based on the drifter positions were used to calculate the one-point dispersion statistics in Saginaw Bay near the mouth of the Saginaw River. Using the hydrodynamic results from the SBM, a Lagrangian particle-tracking model was used to simulate the drifter trajectories. The simplest case for dispersion in turbulent flow involves the statistical analysis of particles released from a point source in isotropic turbulent flow. Lagrangian statistics provide useful estimates of time and space scales over which flow fields are correlated and are based on the velocity autocorrelation function:

$$\rho(\tau) = \frac{\langle u_i(t)u_i(t+\tau)\rangle}{\langle u_i(t)^2\rangle} \tag{25}$$

where $\rho(\tau)$ is the velocity autocorrelation function as a function of the time lag τ, u_i for $i=1,2$ denote the fluctuations in the along-shore and cross-shore components of the velocities (U_i , $i = 1,2$) respectively defined as $u_i = U_i - \langle U_i\rangle$, where $\langle U\rangle$ denotes the time-average of the velocity over the period T, where T is the total period of integration. *Taylor* [1921] established that one-particle diffusivity in *x*-direction (κ_{xx}) is related to the derivative of the variance in displacement [*Pope*, 2000]:

$$k_{xx} = \frac{1}{2}\frac{d\sigma_{xx}^2(t)}{dt} \tag{26}$$

$$\sigma_{xx}^2 = 2u'^2 \int_0^t (t - \tau)\rho(\tau)\, d\tau \tag{27}$$

where $u' = \langle U_1^2\rangle^{1/2}$ is the root mean squared velocity in the *x*-direction and t and τ denote the time and time-lag respectively. σ_{xx} is the standard deviation of particle displacements and can be

calculated by integrating the Lagrangian auto-correlation (auto-covariance) function $\rho(\tau)$. The equation to calculate one-particle diffusivity in the y-direction $\left(k_{yy}\right)$ is similar to Equation 26. Diffusivity values can be calculated using the zonal and meridional components of the velocity. However, since the Saginaw Bay shoreline is almost perpendicular to the axis of the bay near the mouth of the Saginaw River where the drifters were released, we used the along-shore and cross-shore velocities to compute the diffusivities in those directions. We used a MATLAB (The Mathworks Inc., Natick, MA, 2013) program based on the `autocorr` function to calculate diffusivity values in the alongshore (x) and cross-shore (y) directions for observed and simulated drifter tracks.

Quality controlled data from the Lagrangian drifters were used to calculate the observed dispersion rates in Saginaw Bay near the Saginaw River plume. Results from the drifter model were used to calculate the model predicted dispersion coefficients and are presented in Table 9. Comparisons between the observed and simulated alongshore and cross shore dispersion coefficients are shown in Figure 23 for different drifters. Combined wind and wave processes contribute to the observed drifter tracks and dispersion in the field, therefore some differences can be expected with comparisons based on a purely hydrodynamic model. The comparisons in Figure 23 show that the observed and simulated dispersion coefficients have similar magnitude and trends. For example, equation (26) predicts a linear spreading rate for short times and square-root spreading for the other extreme of very large times. Observed and simulated spreading rates are generally in agreement in describing these limits (Figure 23).

Figure 23 shows a comparison of the model derived Lagrangian single-point (absolute) dispersion rates in the along shore and cross-shore directions (k_{xx}, k_{yy}) with observed values. It is clear from the observed values that dispersion is (a) highly anisotropic and (b) variable with

time. The model is able to predict some of this variability. However, with time the difference between observed and simulated values increases.

Table 9: Maximum values of absolute dispersion rates (in m^2/s) for Lagrangian drifters and simulated particle paths in Saginaw Bay

Day	Cross-shore diffusivity		Along shore diffusivity	
	Observed	Modeled	Observed	Modeled
Day 1-Drifter 2	1.33	7.0	3.9	4.1
Day 2-Drifter 2	0.16	0.44	2.87	3.1
Day 3-Drifter 2	0.66	0.29	12.5	5.7

Closer to the mouth of Saginaw River, we also notice the presence of two additional, smaller recirculating cells behind the Shelter Island (not shown in the figures). These flow features, not resolved by the lake-wide model, play an important role in controlling the transport of contaminants in the Saginaw River plume.
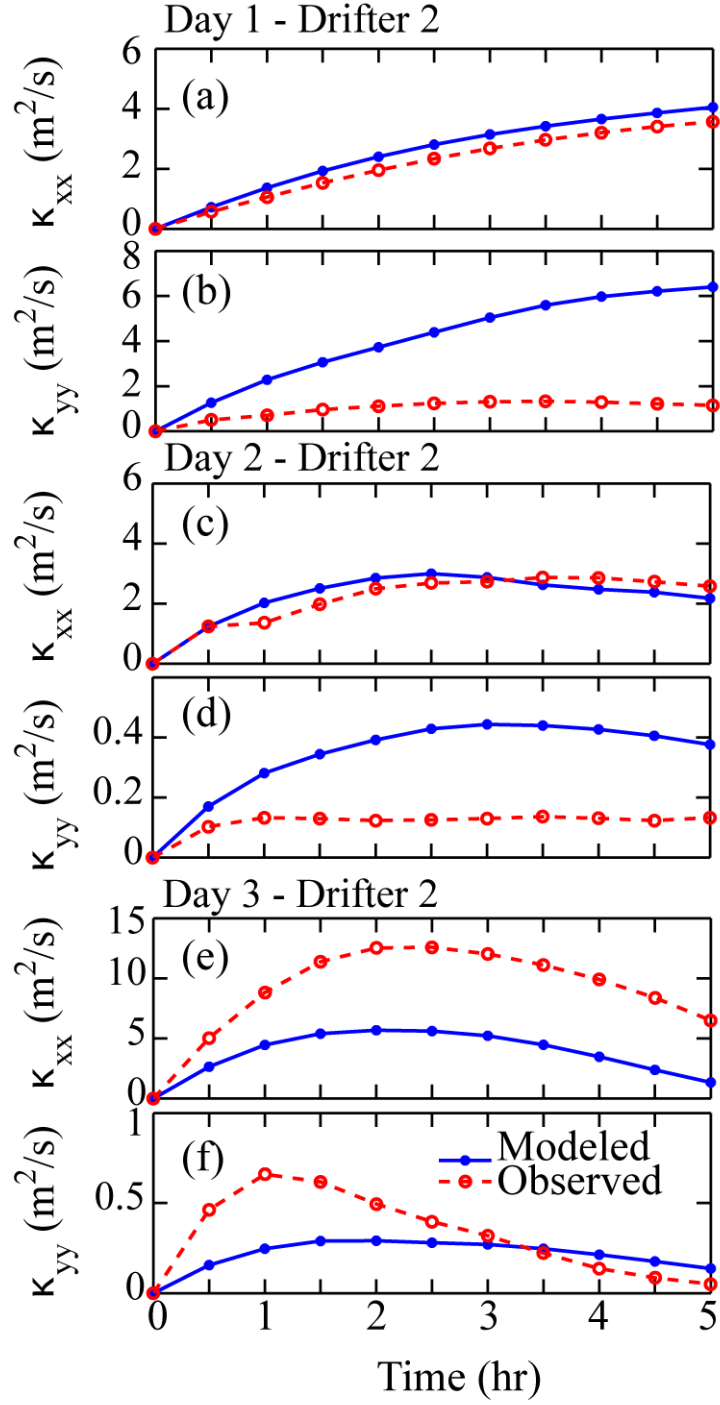
Figure 23: Comparisons between observed and simulated values of single-particle (absolute) horizontal diffusivities in the Saginaw Bay based on data for different drifters.

3.4.5 Lagrangian time-scale and length-scale

The Lagrangian integral time and length scales are useful for estimating the decorrelation scales of the surface water flow. The mean speed ($\bar{S}$), mean alongshore velocity ($\bar{U}$), and mean crossshore velocity ($\bar{V}$) were calculated according to *McCormick et al.,* [2002/2008]:

$$\bar{S} = \frac{1}{n}\sum_{i=1}^{n}\sqrt{(u_i^2 + v_i^2)} \qquad (28)$$

$$\bar{U} = \frac{1}{n}\sum_{i=1}^{n} u_i \qquad (29)$$

$$\bar{V} = \frac{1}{n}\sum_{i=1}^{n} v_i \qquad (30)$$

where u_i, v_i are the East and North components of the velocity for time index i, and n is the total number of time segments for each drifter. The velocity autocorrelation function (equation 25) forms the basis for the computation of the integral length and time scales. The function is evaluated separately in each direction (x and y) to compute the length and time scales in both directions.

The Lagrangian integral time-scale (L^{Time}) is computed as:

$$L^{Time} = \int_0^T \rho(\tau)d\tau \qquad (31)$$

where the upper bound of integration (T) is defined as the first zero crossing of the autocorrelation function $\rho(\tau)$. The Lagrangian integral time-scales are associated with integral length-scales (L^{length}) as follows:

$$L^{length} = \langle u_i'^2 \rangle^{1/2} \int_0^T \rho(\tau) d\tau \qquad (32)$$

where u_i' (i=1,2) denote the fluctuations in the along-shore and cross-shore components of the velocities defined as $u_i' = u_i - \langle u_i \rangle$, where $\langle u_i \rangle$ denotes the time-average of the velocity over the period T.

Details of the drifter deployments in Saginaw Bay including drifters ID, deployment locations and duration of travel for each drifter are shown in the Table 3. Here we present the Lagrangian statistics for drifters in the Table 10.

Drifter ID	Mean Speed ($\bar{S}$) (cm/s)	Mean Alongshore velocity ($\bar{U}$) (cm/s)	Mean Cross-shore velocity ($\bar{V}$) (cm/s)	Lagrangian integral time-scale (hour)		Lagrangian integral length-scale (m)	
				Along-shore	Cross-shore	Along-shore	Cross-shore
Day1-Drifter1	3.15	-1.4	1.88	2.02	1.402	115.48	123.8
	2.54	0	2.02	2.68	0.92	144.15	44.08
Day1-Drifter2	3.07	-1.69	1.76	3.38	2.57	138.14	194.99
	2.83	-0.15	1.82	2.52	0.59	188.59	39.30
Day2-Drifter1	2.68	2.48	0.3	0.927	1.365	31.11	47.39
	2.49	2.16	-0.24	1.47	0.557	110.99	18.70
Day2-Drifter2	2.90	2.69	0.12	1.02	1.15	36.39	42.51
	3.38	3.23	-0.11	0.448	0.538	41.19	17.58
Day3-Drifter1	4.81	4.15	1.14	2.37	5.80	442.13	351.79
	4.04	3.77	0.81	0.065	0.63	16.33	46.76
Day3-Drifter2	4.00	3.90	-0.39	0.958	0.746	38.19	25.82
	4.64	4.46	-0.32	1.088	0.575	136.53	36.35
MEAN	3.44	1.69	0.8	1.77	2.17	133.5	131.1
	3.32	2.24	0.66	1.38	0.64	106.3	33.8

Table 10: Lagrangian Statistics for Drifters in Saginaw Bay

(Note: The simulation and observation data are presented in black and red color respectively).

The Lagrangian statistics for Saginaw Bay are shown in the Table 10 and Figures 24, 25. Examining Table 10, the overall mean observed and simulated speed for all drifters are 3.44 cm/s and 3.32 cm/s, respectively where the means for the velocity components are 1.69 cm/s (along-shore velocity) and 0.8 cm/s (cross-shore velocity) obtained from simulation. The corresponding numbers are 2.24 cm/s and 0.66 from observation data.

In theory, the Lagrangian integral time and length scales will describe correctly the behavior of a water parcel if the drifter perfectly tags the movement of the water parcel (that is, there is no slippage due to wind and wave effects). It should be noted there are no drifters can meet this condition. The decorrelation time calculated from observation datasets ranged from 0.06h to 2.68h in the alongshore direction, and from 0.53h to 0.92h in the cross-shore direction. The corresponding numbers calculated from simulation data are 0.92h to 3.38h in the alongshore direction, and from 0.74h to 5.8h in the cross-shore direction. The Lagrangian integral length-scales were calculated following equation 32. The results of the Lagrangian length-scales are shown in the Table 10 and Figure 25. The results show that the integral length scales based on observations are anisotropic. The anisotropy of the Lagrangian length scales are also observed by *McCormick et al.*,[2002] for Lake Michigan. In comparison, the length scales based on simulation are nearly isotropic. The difference can be attributed to the lack of a wave model that accounts for the combined effects of wind and wave processes on the observed drifter tracks. Future modeling efforts including wave processes may be needed in order to improve the simulation of the Lagrangian drifters.

74
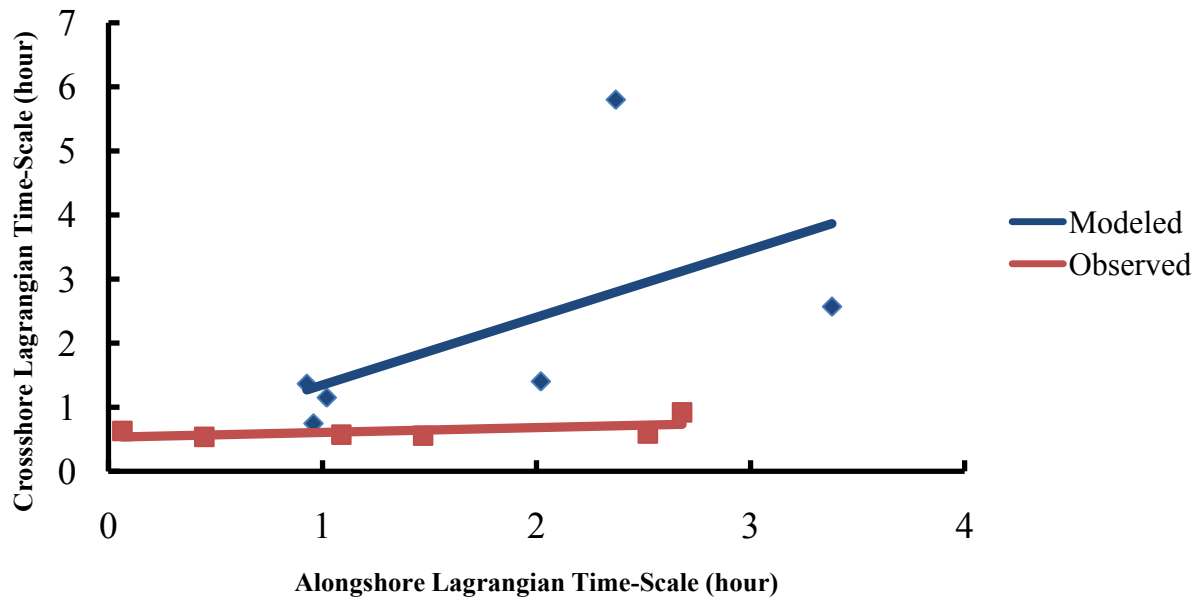
Figure 24: Comparisons of the Crossshore and Alongshore Lagrangian Time-Scale.
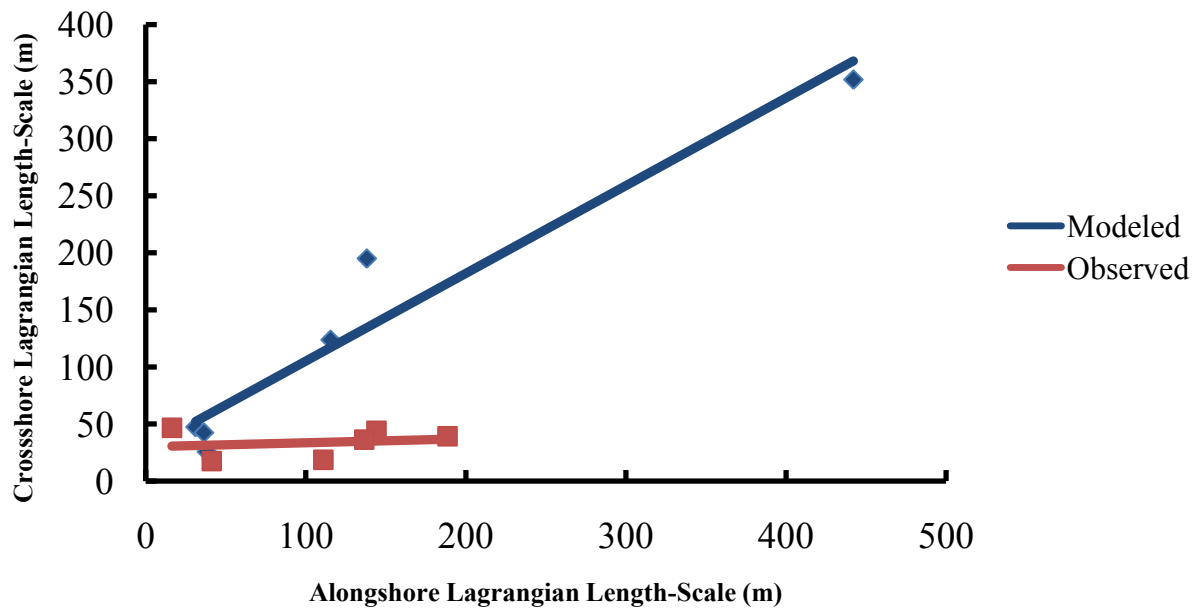
Figure 25: Comparisons of the Crossshore and Alongshore Lagrangian Length-Scale.

3.4   Conclusions

Summer circulation in Lake Huron and Saginaw bay was examined using an unstructured grid hydrodynamic model. The model was tested using ADCP observations in Saginaw Bay, surface temperature measurements at NDBC buoys, and Lagrangian drifter trajectories. Using the unstructured grid model we were able to simulate the small-scale circulation features in Saginaw Bay and Georgian Bay as well as the lake-wide circulation in Lake Huron. The hydrodynamic model was able to reproduce the anti-cyclonic (counterclockwise) lake-wide circulation patterns that have been observed in earlier numerical and field studies on Lake Huron. We found that mean current speeds close to the shore can be as high as 20 cm/s compared with the lake-wide average of 3 cm/s. The complex topography coupled with stratification and rapid warming of the southern part of the lake results in high inter-annual variability in surface temperature values. Several potential upwelling regions have been identified where topographically-driven upwelling brings cold water from the deeper layers to the surface. One such region is in the strait connecting Lake Huron with Georgian Bay. In addition to upwelling, our simulations show that in the surface layer (epilimnion) mean flow during summer is from Lake Huron into Georgian Bay, which sets up a return flow in the deeper layers (hypolimnion) from the bay into the lake. Since the hypolimnion is 3-4 times thicker than the epilimnion in this part of the lake, surface velocities are several times larger in magnitude than the velocities in the deeper layers.

Results from the Lagrangian drifter study in Saginaw Bay showed the highly anisotropic and time-variable nature of dispersion near the mouth of Saginaw River. The numerical model was able to predict the drifter trajectories and dispersion coefficients reasonably well. However, differences between observed and predicted values increased with time.

Chapter 4

Ice Cover, Winter Circulation and Thermal Structure

4.1   Introduction

When simulating hydrodynamics in lakes over the seasonal or annual cycle, most studies avoid simulating for winter time due to the lack of observational datasets. The limitations of instruments (e.g., the ability to measure currents accurately when the water surface is covered with ice) plus adverse weather conditions are the primary reasons for the lack of many studies on winter circulation in the Great Lakes in the past. As a result, most of the evaluation about environmental consequences related to human activities was based on the hydrodynamic results for ice-free conditions. Meanwhile, the hydrodynamic conditions with ice cover are different from those of an ice-free condition. The ice cover significantly influences lake hydrodynamics and water temperature distribution by inhibiting wind stress and heat flux at the surface. Besides their importance in understanding lake hydrodynamics under winter conditions, a knowledge of and the ability to accurately predict ice cover, ice thickness, ice concentration, and the duration of ice in Lake Huron is very useful for icebreaking operations and for managing the lake

ecosystem during winter periods. The winter season is characterized by nearly homogeneous water in Lake Huron as in the other Great Lakes. In a normal year, the Great Lakes have an ice cover partially from December to April.

One of the first attempts to describe winter circulation in Lake Huron was carried out by *Saylor and Miller [1979]*. In the study they used twenty-one current moorings deployed in Lake Huron during the winter of 1974-1975 for approximately 6 months. They concluded that there is a strong cyclonic flow persisting throughout the winter with current speeds that ranged from 1 to 7cm/s and a mean of 3cm/s. The winter currents are barotropic because of isothermal conditions in the water column [*Beletsky et al., 1999*]. It has been known that the Great Lakes have considerable influence on the regional climate *[Bates and Giorgi, 1993; Scott and Huff, 1996]*. In addition, ice cover is also considered an important indicator of regional climate change [*Robertson et al.,* 1992]. More recently, *Bai et al.,* [2012] found that both North Atlantic Oscillation (NAO) and El Nino-Southern Oscillation (ENSO) have impacts on Great Lakes ice cover. *Rao and Murty* [1970] used a homogeneous, vertically integrated numerical model to conclude that winter circulation in Lake Ontario was driven by wind. Understanding the major effects of colder weather on the lake is crucial in predicting water movement patterns and the thermal structure. In a study related to the trends of ice cover in the Great Lakes, *Assel et al.,* [2003] pointed out that the distributions of ice cover among the five Laurentian Great Lakes were influenced by the spatial pattern of water depth on each lake and regional differences in air temperature. More recently, *Fujisaki A.F et al., [2012]* used the Princeton Ocean Model (POM) which included ice processes to investigate the seasonal variation of ice cover on Lake Erie. Their study showed that the packed ice cover slowed down the surface water velocity. To our knowledge, simulation of lake process beneath the ice cover in three dimensions has not been

attempted. Therefore, there are large gaps in our understanding of the lake circulation, temperature structure, the role of ice cover in Lake Huron during the winter time.

In this chapter, we investigate the evolution of ice cover, ice concentration, circulation, and thermal structure over Lake Huron during winter time using a hydrodynamic model that is coupled with an ice model. We used the unstructured grid FVCOM numerical ocean model originally developed by *Chen et al., [2003]* coupled with ice module to describe the winter circulation in Lake Huron during the winters of 2009-2010 and 2012-2013. The main reason for implementing the model for the specified years is based on the available observational data. FVCOM has been successfully applied in many previous studies for lakes or oceans but to date the application of the model coupled with ice model has not been seen from previous studies. In this chapter, the comparisons between the field data during the winter seasons, satellite remote sensing data and model simulations of currents, temperature, and ice cover extent are presented. The observed ice concentration data are downloaded from the Great Lakes Ice Atlas (http://www.glerl.noaa.gov/data/ice/) and used to test with the simulated ice concentration. The winter simulation results are also used to estimate the mean flushing times and residence times for the Saginaw Bay that will be presented in Chapter 5. These novel results are expected to aid in our understanding of how contaminants are flushed out of the bay during winter seasons and how lake processes are changing in this important ecosystem.

4.2 Observations and Numerical Methods

4.2.1 Numerical Model

We use an unstructured-grid, three-dimensional hydrodynamic model of Lake Huron coupled with a two dimensional ice model to understand the nature of circulation and the extent of ice cover over the Lake Huron during winter seasons and to quantify exchange rates between the Saginaw Bay and Lake Huron. The unstructured-grid ICE model was designed in the Cartesian coordinate fully coupled to The Los Alamos Community Ice Code (CICE) [*Hunke et al.,* 2010]. The computational domain to investigate the winter circulation and ice cover is the same as the one that was used in the Chapter 3 which has 9611 nodes and 17619 triangular elements in horizontal (Figure 4). The model has 21 vertical sigma levels. Based on the Courant- Friedrichs - Levy (CFL) numerical stability criteria, the time steps are 4s and 10s for external and internal scheme. The time steps for the ice model are 40s and 20s respectively.

As stated above, the hydrodynamic model is fully coupled with a two-dimensional ice model. The model solves the hydrodynamic primitive equations (Equation 1 to Equation 5) using the hydrostatic assumption in the vertical direction with the Boussinesq simplification for convective flows. Vertical eddy viscosity and diffusivity are modeled using the Mellor-Yamada 2.5 level turbulence closure scheme [*Mellor and Yamada*, 1982; *Galperin et al.,* 1988]. The horizontal diffusion coefficients are calculated using the Smagorinsky turbulence closure model [*Smagorinsky,* 1963].

In the presence of ice, the surface boundary conditions for momentum equations are given as follows:

$$\frac{\partial}{\partial z}\left(K_m \frac{\partial u_w}{\partial z}\right) = \frac{1}{\rho_w}[c\tau_{wx} + (1-c)\tau_{ax}] \qquad (33)$$

$$\frac{\partial}{\partial z}\left(K_m \frac{\partial v_w}{\partial z}\right) = \frac{1}{\rho_w}[c\tau_{wy} + (1-c)\tau_{ay}] \qquad (34)$$

where c is the ice concentration (unit:dimensionless) , τ_{wx}, τ_{wy} are the water stresses in x and y components, respectively. The movement of ice is driven by a combination of water flows and wind as pointed out by *Leppäranta, M.* [2005].
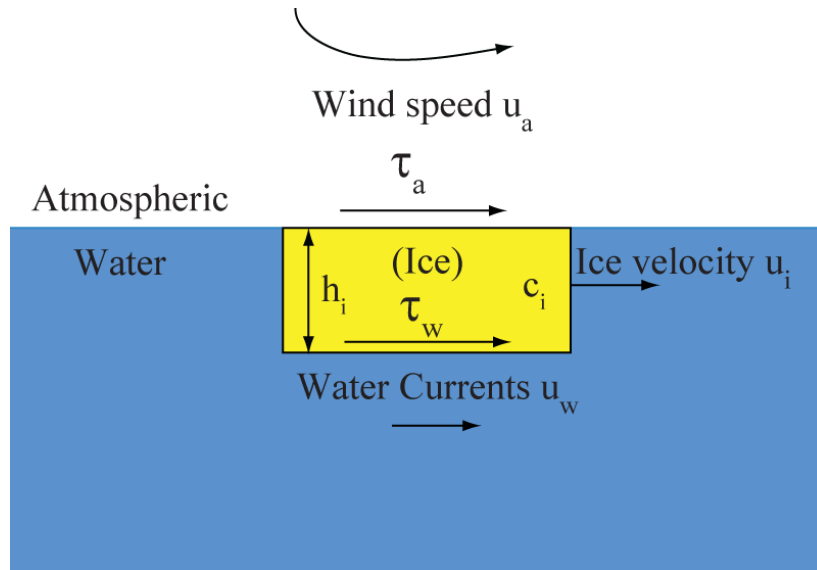
Figure 26: Schematic of Ice Model. c_i is the ice concentration; τ_a is wind stress; τ_w is water stresss; u_w is water current speeds; u_i is the ice velocity; u_a is wind speed; h_i is the ice thickness.

Ice Dynamic Processes Equations

The movements of ice have an important role on lake circulation and thermal process. The drifting of ice will lead to a redistribution of water temperature and it is influenced by a combination of water movement and wind stress. The full nonlinear governing equations of the ice dynamics processes are given as:

$$m\frac{\partial u_i}{\partial t} + m\left(u_i\frac{\partial u_i}{\partial x} + v_i\frac{\partial u_i}{\partial y}\right) - mfv_i = \frac{\partial \sigma_{1j}}{\partial x_j} - mg\frac{\partial H_0}{\partial x} + \tau_{ax} + \tau_{wx} \qquad (35)$$

$$m\frac{\partial v_i}{\partial t} + m\left(u_i\frac{\partial v_i}{\partial x} + v_i\frac{\partial v_i}{\partial y}\right) + mfu_i = \frac{\partial \sigma_{2j}}{\partial x_j} - mg\frac{\partial H_0}{\partial y} + \tau_{ay} + \tau_{wy} \qquad (36)$$

where m is the mass of ice per unit area, u_i, v_i are the x and y components of the ice velocity, respectively. H_0 is the surface elevation σ_{ij} is the internal stress tensor. τ_{ax}, τ_{ay} are the surface wind stresses in x and y components, respectively. τ_{wx}, τ_{wy} are the water stress in x and y components, respectively.

The surface wind and water stresses are formulated as:

$$\tau_a = c_i C_a \rho_a |u_a|(u_a \cos \phi + k u_a \sin \phi) \qquad (37)$$

$$\tau_w = c_i C_w \rho_w |u_w - u_i|[(u_w - u_i)\cos\theta + k(u_w - u_i)\sin\theta] \qquad (38)$$

where c_i is the ice concentration; C_a, C_w are the drag coefficient of air and water, respectively. u_i is the ice velocity. ρ_a, ρ_w are the density of air and water, respectively. ϕ, θ are the air and water turning angles, respectively. k is unit vector.

82

The temperature condition at the water surface is specified as follow:

$$\frac{\partial T}{\partial z} = \frac{1}{\rho_w c_p K_h} \left[(1 - c_i) F_{air} - (1 - c_i) F_{SWa} - c_i F_{swice} + c_i F_{OI} + (1 - c_i) F_{freeze} \right] \quad (39)$$

Where F_{air} is the heat flux from the atmosphere to the lake; F_{SWa} is the shortwave irradiance of the open area; F_{swice} is the shortwave irradiance penetrated through ice; F_{OI} is the net heat flux between the lake and ice; F_{freeze} is the heat gained when ice grows over open water; c_i is ice concentration. Further details of the governing equations, boundary conditions, and thermodynamics can be found in *Chen et al.* [2013]).

The ice transport equation is to describe the evolution of the ice thickness distribution:

$$\frac{\partial g(x,h,t)}{\partial t} = -\nabla \cdot (g u_i) \quad (40)$$

where $g(x,h,t)$ is the thickness distribution function containing the ice area, ice volume. u_i is the horizontal ice velocity. $\nabla = (\frac{\partial}{\partial x}, \frac{\partial}{\partial y})$.

The ice model the distribution of ice thickness is sensitive to the simulation results [*Hunke E.C*, 2010]. In this study, we assumed there are five categories of ice thickness for each grid node which is followed as the linear equation:

$$H_i = i[d_1 + d_2(i - 1)] \quad (41)$$

$$d_1 = {1.0}/{ncat} \quad (42)$$

$$d_2 = {0.5}/{ncat} \quad (43)$$

where H_i is ice thickness of ith category of ice; *ncat* is the number of category of ice thickness. The thicknesses of ice in each category, therefore, are 20cm, 60cm, 120cm, 200cm, and 300cm respectively. With the absence of ice cover, the water temperature of the lake is controlled by exchange of heat flux between the surface water and atmospheric forcing, while with the presence of ice cover, the heat flux is recalculated based on the ice cover conditions.

Winter seasons usually start on 23rd December in previous year and last until 22nd March in the next year. In order to avoid confusion in the winter time definition, we use the next year as the year of winter. The hydrodynamic model simulations were started in May 2009 and 2012 with zero velocity and uniform vertical temperature profile in order to avoid problems with initialization of the stratified temperature. The initial temperature conditions were set up at 2.5 ^{0}C and 3.5 ^{0}C for 2009 and 2012 respectively. The default setting in the model is used to calculate wind stress and net heat flux which were then used in the Ice Model.

4.2.2   Meteorological and observational data

The same meteorological stations and data sources were used to download the atmospheric data as described in the Chapter 2. The model used hourly atmospheric forcing data such as wind speed, wind direction, surface air temperature, relative humidity, and cloud cover fraction for the years 2009-2010, and 2012-2013. It must be noted that due to severe weather conditions the surface water temperature was not observed at National Data Buoy Center (NDBC) stations during winter. Therefore, we used the analysis of surface water temperature from The Great Lakes Surface Environmental Analysis (GLSEA) to evaluate the model results. The GLSEA data is a daily water temperature derived from NOAA polar-orbiting satellite imagery obtained through the Great Lakes Coast Watch program. There are two thermistor

chains (SB32, SB33) deployed in the area of the mouth of Saginaw Bay (Figure 3a). The time series of water temperature was observed through the water column. We also deployed three bottom-mounted, up-looking acoustic Doppler current profilers (ADCPs) during the winter season and collected hydrodynamic data to test the numerical models. The locations of the ADCPs (SB32, SB33, and HM12) are presented on Figure 3. Note that the two years we simulated are the mild winters in Great Lakes area compare to other years within 30 years (Figure 27) where annual maximum ice coverage over Great Lakes are about 30% and 38.4% for 2010 and 2013 respectively. The long-term average is 51.4% as shown in Figure 27.
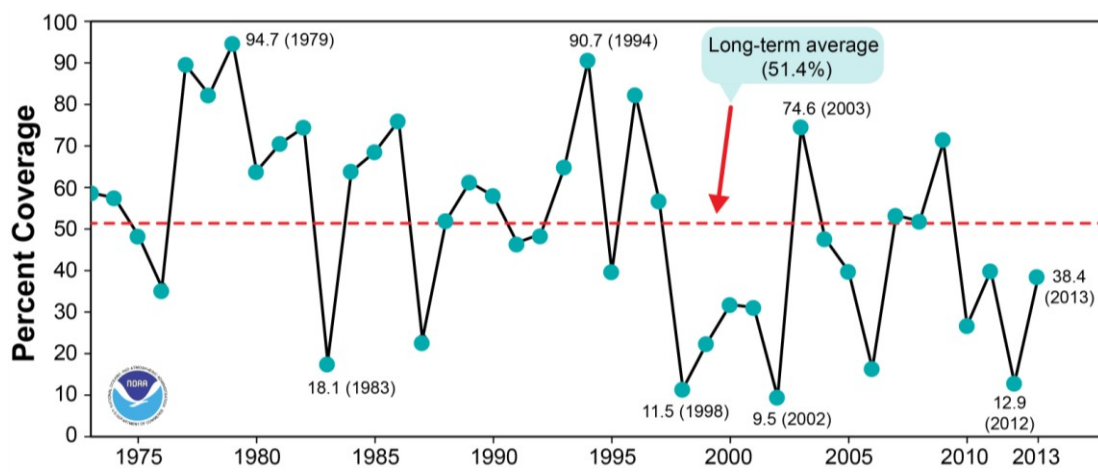
Figure 27: Great Lakes Annual Maximum Ice Coverage (1973-2013)
(http://www.glerl.noaa.gov/data/)

4.3   Results and Discussion

4.3.1   Results

4.3.1.1   Currents

The long time series of current measurements obtained in winters of 2010 and 2013 were used to test the model results. Results from the hydrodynamic model coupled with two dimensional ice model show that the lake-wide model with an average element size of 2.5 km is able to resolve the circulation in the lake. Figures 28 and 29 show the comparisons between the observed and simulated velocities (eastward and northward velocity) for the years 2010 and 2013 during winter time. The model results agree reasonably well with the observed data as shown in Figures 28 and 29.
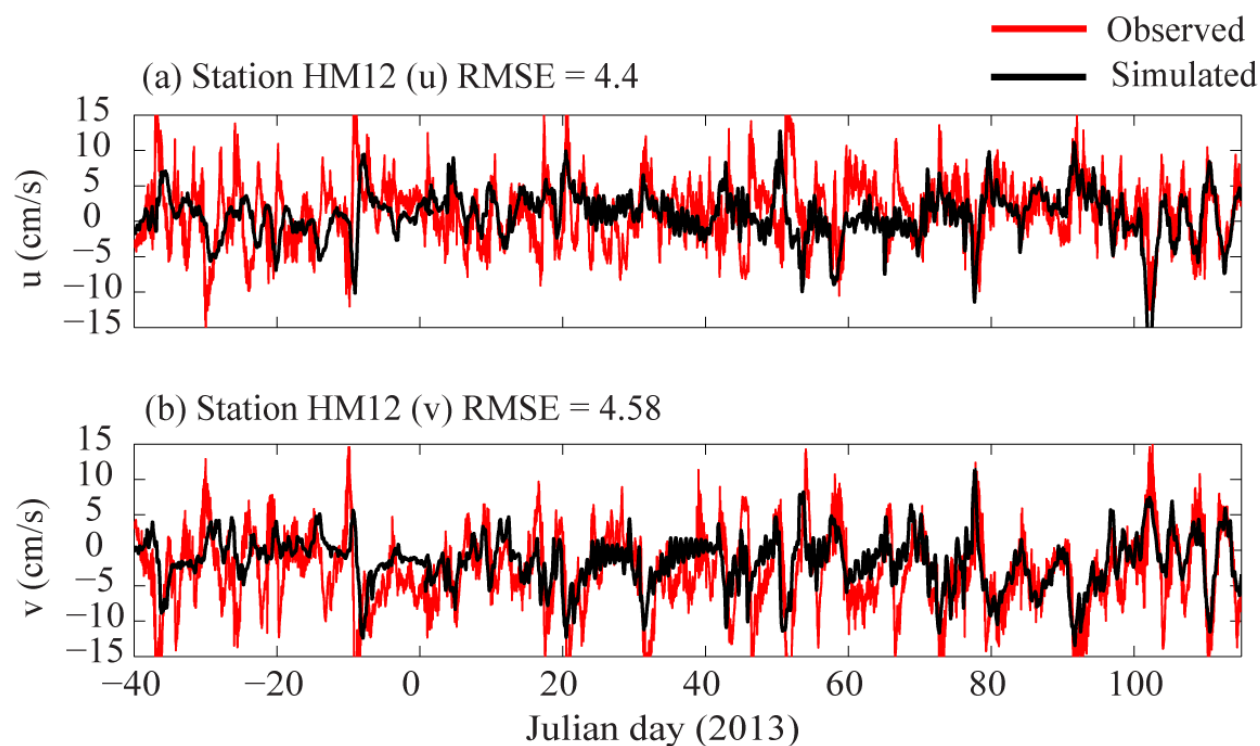
Figure 28: Vertically-Integrated velocity comparison at location HM12 with the model.
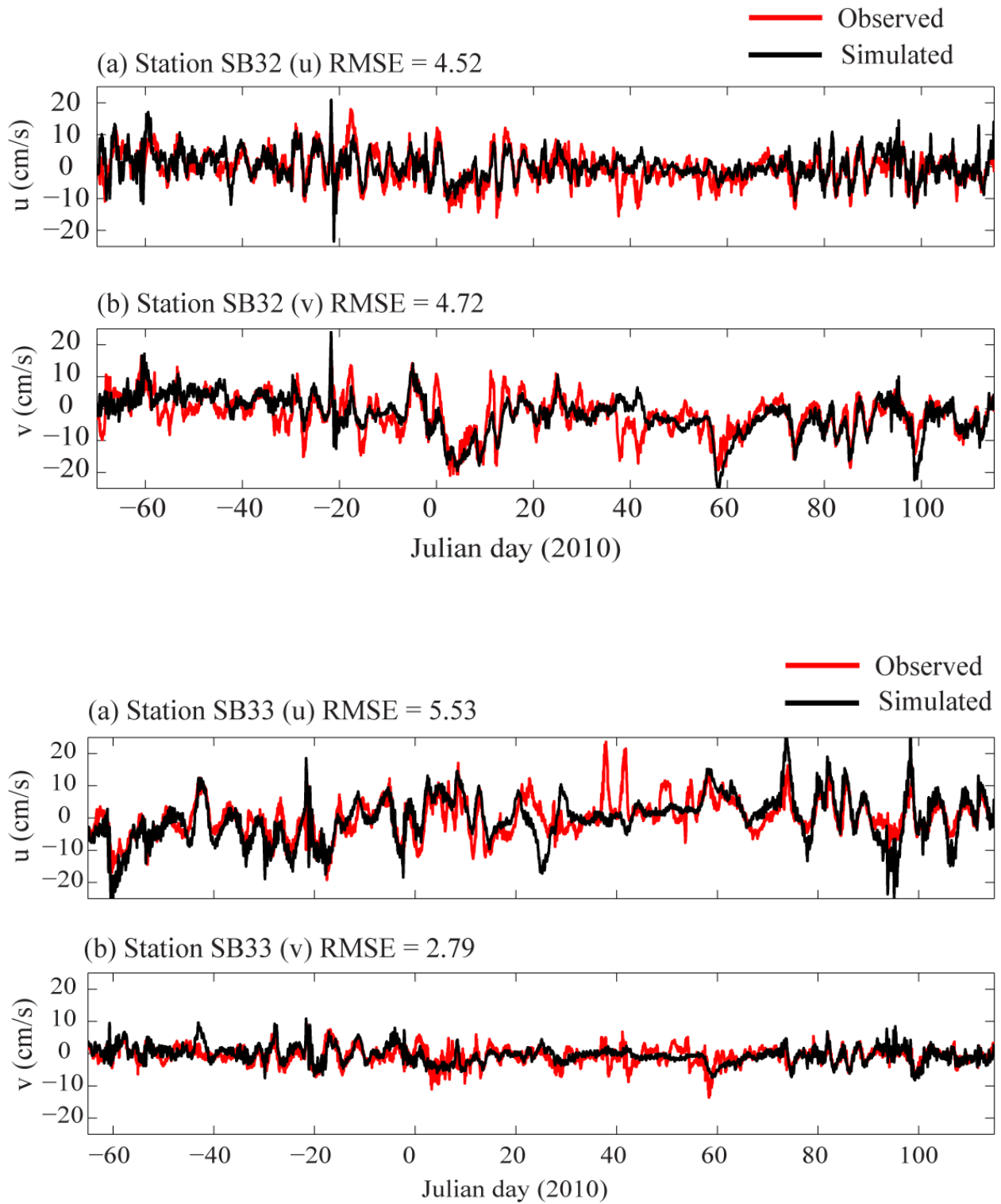
Figure 29: Vertically-Integrated velocity comparison at location SB32 (above) and SB33 (below) with the model.

It should be noted that ADCPs were deployed in difference areas in Lake Huron. For the winter of 2010, ADCPs were deployed in the area near the mouth of Saginaw Bay in the southern part of lake while for the winter of 2013 the ADCP was deployed in the area of Hammond Bay in the northern part of lake. We concluded that the model was able to describe large-scale circulation reasonably well. However, the simulated results for winter 2010 did not capture some peaks of the water velocities at SB32 and SB33 stations during January as shown in Figure 29 but for the long-term simulation the model was able to capture the water velocity relatively well.

4.3.1.2 *Temperature*

Observations of water temperature at the two thermistor chain stations in the area of the Saginaw Bay mouth were used to validate the model during winter 2010. Each temperature mooring measured at every 4 meters vertically from July 2009 to the end of May 2010. In this chapter, we present the comparisons between the simulation results and observations during the winter time only (Figure 30). Accurate modeling of water temperature in vertical direction from surface to bottom is an important test because it shows the accuracy of thermodynamics in the model. In order to test the model, the time series of temperature distribution as a function of depth was presented in Figure 30. The results show that simulated water temperature was in good agreement with observed data. The model produced the evolution of temperature vertically from stratified to homogeneous conditions relatively consistent with thermistor chain measurements at both moorings SB32 and SB33 (Figure 30). The comparisons of vertical profiles of the temperature clearly show that the hydrodynamic model coupled with ice model was able to reproduce the important features of temperature in the water column in the period of transition time from fall season to winter season.
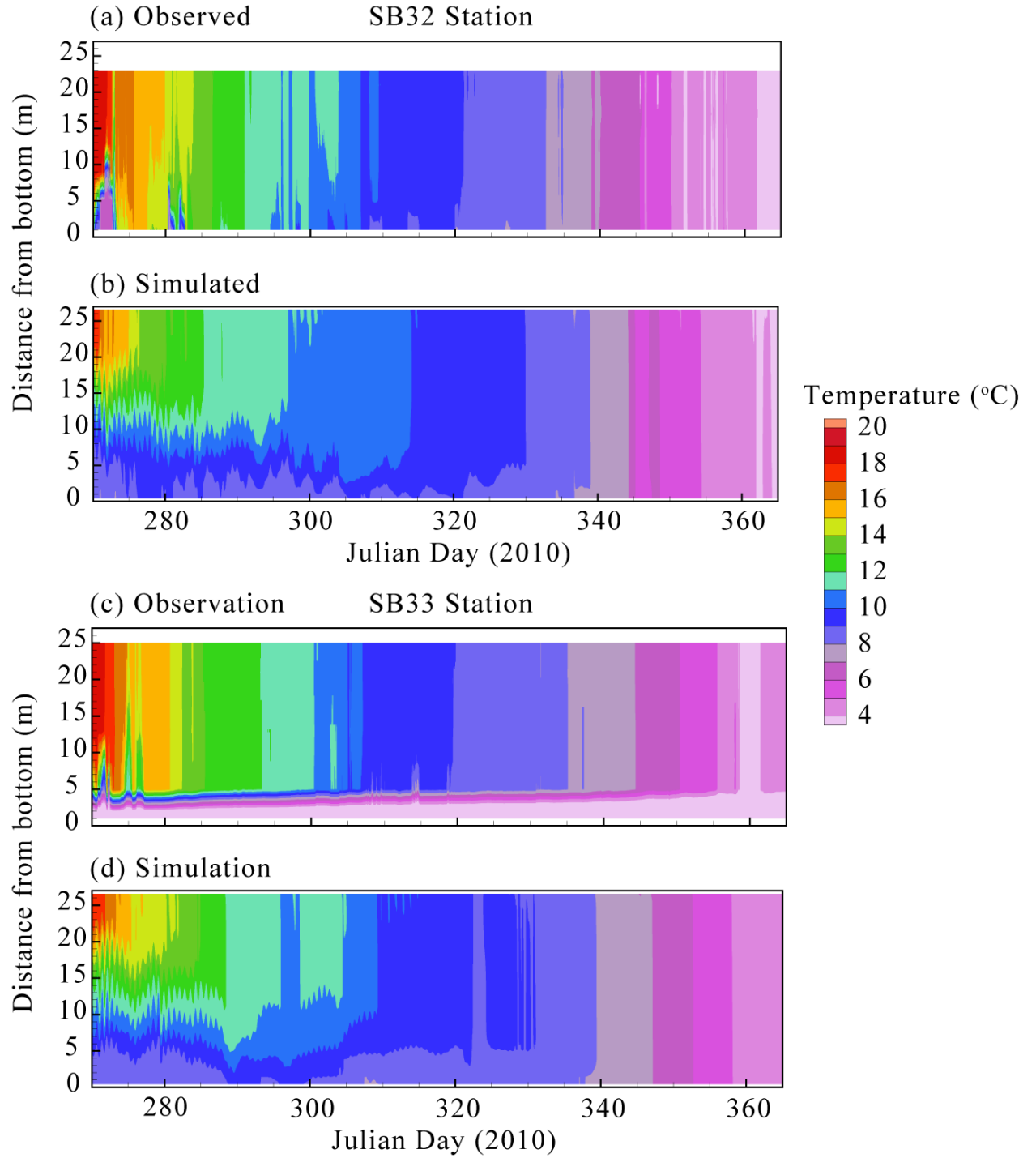
Figure 30: Time series of observed versus simulated temperature in water column at SB32, SB33 station

In addition to the comparisons at thermistor chain moorings, modeled water temperature were also compared to lake-wide averaged surface temperature (GLSEA) derived from NOAA polar-orbiting satellite imagery obtained through the Great Lakes Coast Watch program as shown in Figure 31.
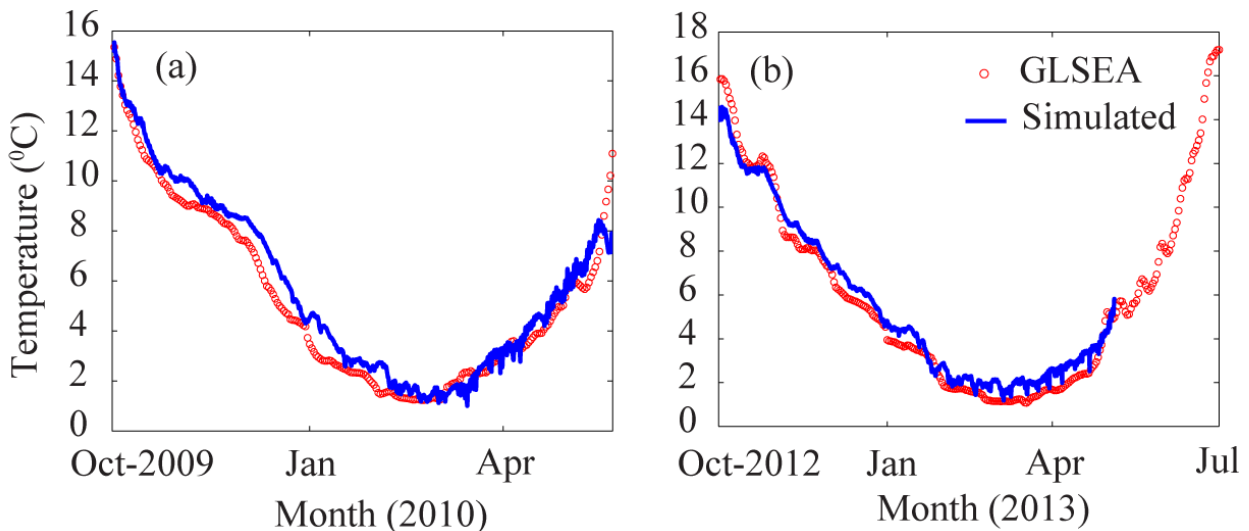
Figure 31: Comparison between lake-wide averaged simulated surface temperatures and observationals data processed by GLSEA for (a) winter 2010 and (b) winter 2013. (The GLSEA data extracted from http://coastwatch.glerl.noaa.gov/).

While comparisons with thermistor chain observations made at a point can be used to quantify model accuracy, evolution of thermal process in Lake Huron and Saginaw Bay in winter season can be understood by examining the spatial variability temperature which is shown in contour plot in Figures 32, 33, 34, 35. At the end of fall (mid-November) the lake is almost homogenous in temperature both vertically and horizontally with temperatures of 8^0C (Figure 30, 32, and 33). As cooling of air continues in late fall, the water temperatures decrease starting in the shallow areas such as the inner Saginaw Bay, some areas located in the Northern Bay and the Georgian

Bay. In March, Lake Huron is almost homogeneous at a temperature of 3^0C. The ice begins to form when the water temperature decreases to freezing point.

The monthly average temperature map in Saginaw Bay was presented in Figures 34, 35. They clearly show that the bay was at a homogeneous temperature in November and April. There is a well-defined "*tthermal boundary*" located near the inner transect 1-1 in December. The difference in temperature between the inner bay and outer bay is about 2.5^0C – 3.0^0C in December. As cooling air continues to decrease in temperature the thermal boundary moves lakeward in winter time until the bay reaches homogeneous temperature conditions.

(a) Nov-2009 (b) Dec-2009 (c) Jan-2010

(d) Feb-2010 (e) Mar-2010 (f) Apr-2010

Temperature (^{0}C)

-2 -1 0 1 2 3 4 5 6 7 8 9 10
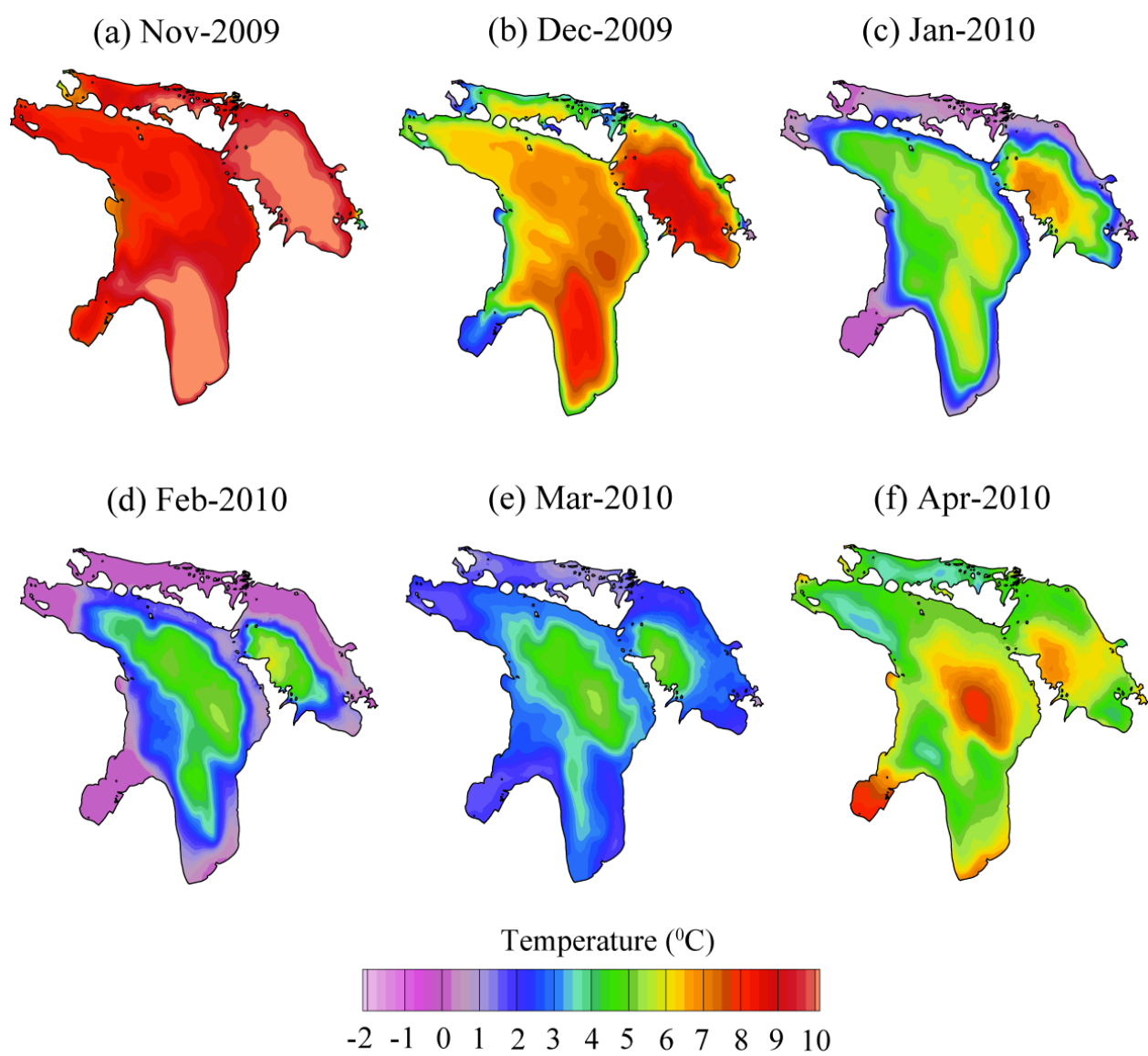
Figure 32: Surface temperature contours for Lake Huron for the winter months 2010.
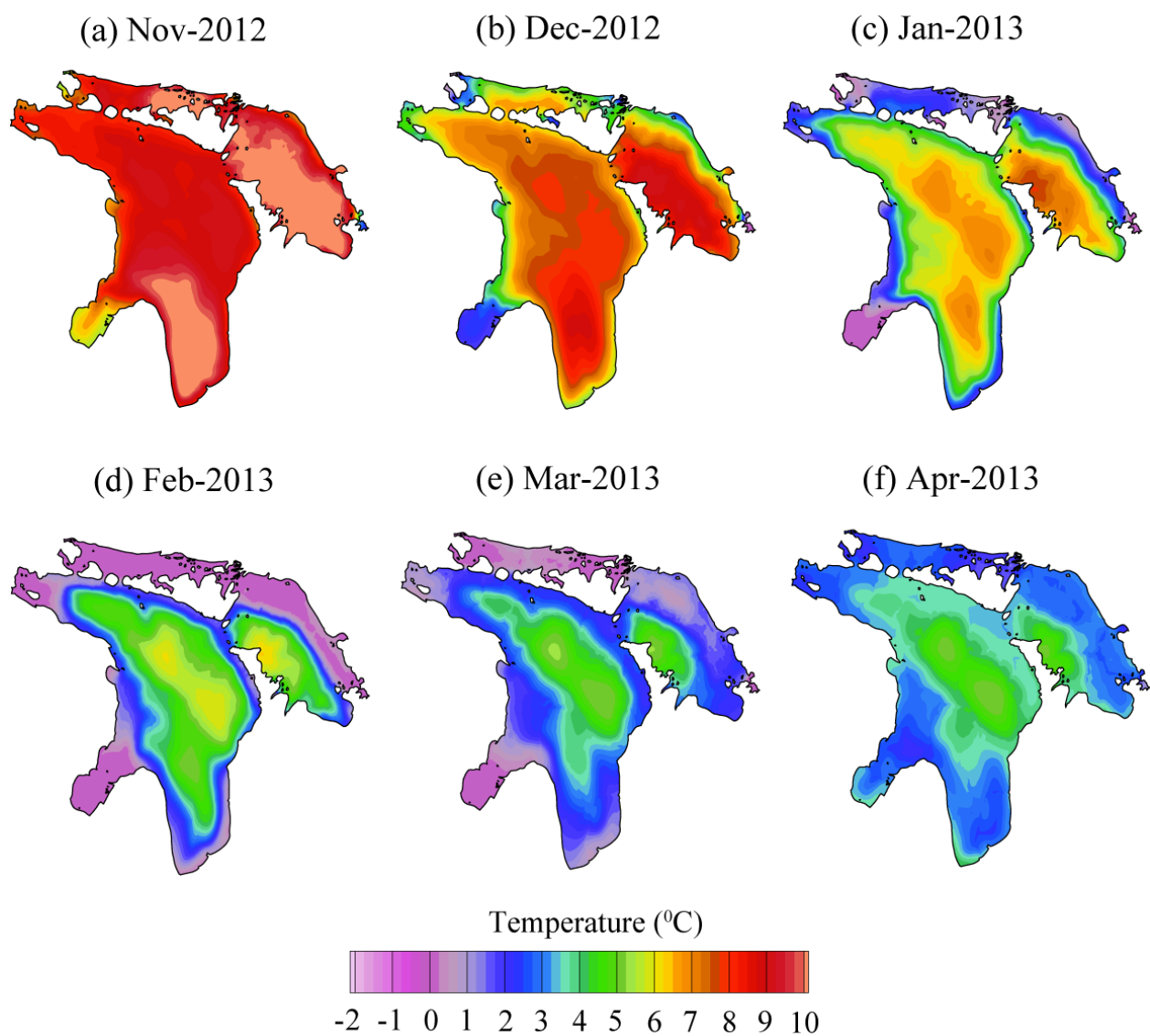
Figure 33: Surface temperature contours for Lake Huron for the winter months 2013.
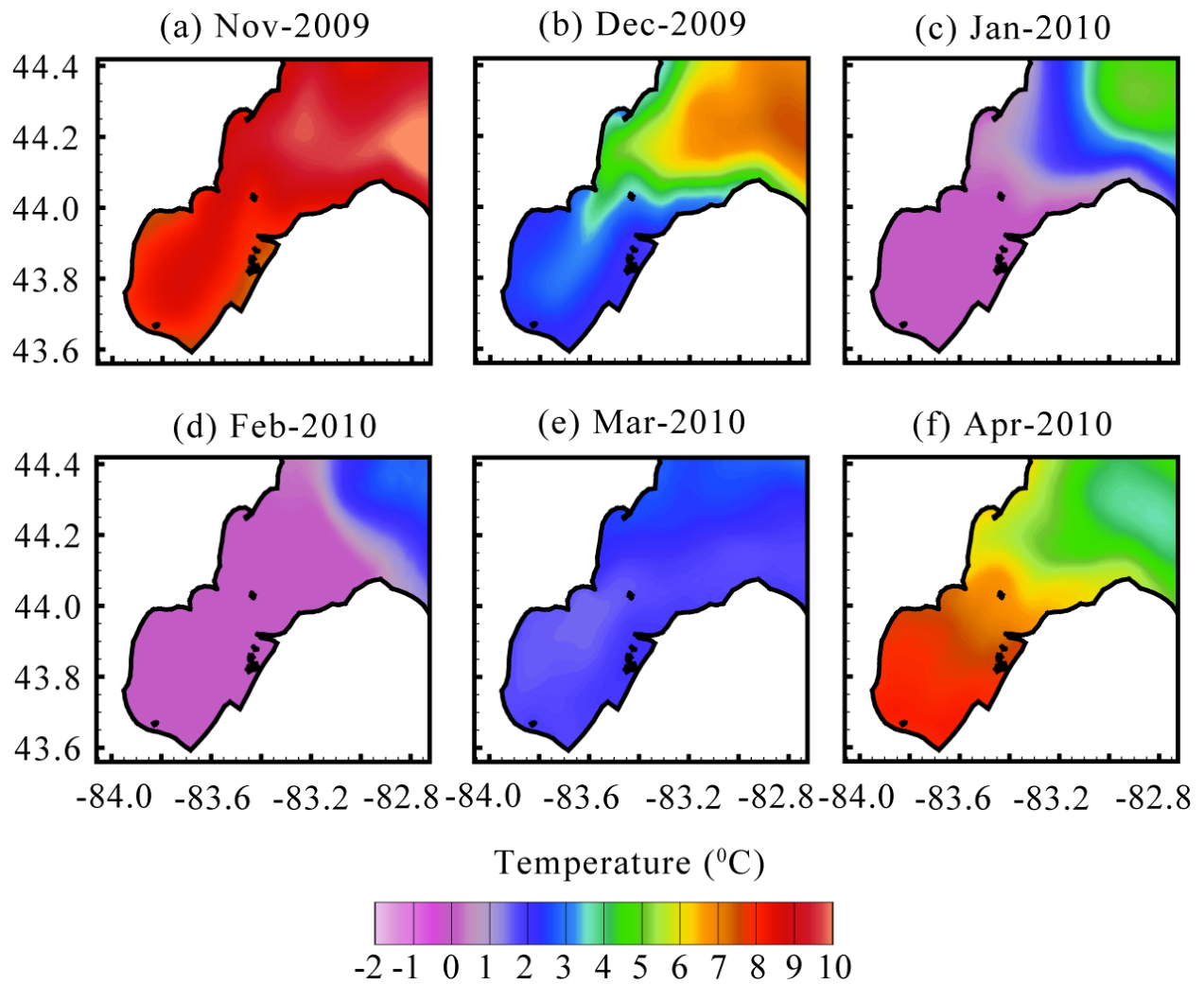
Figure 34: Surface temperature contours for Saginaw Bay for the winter months 2010.
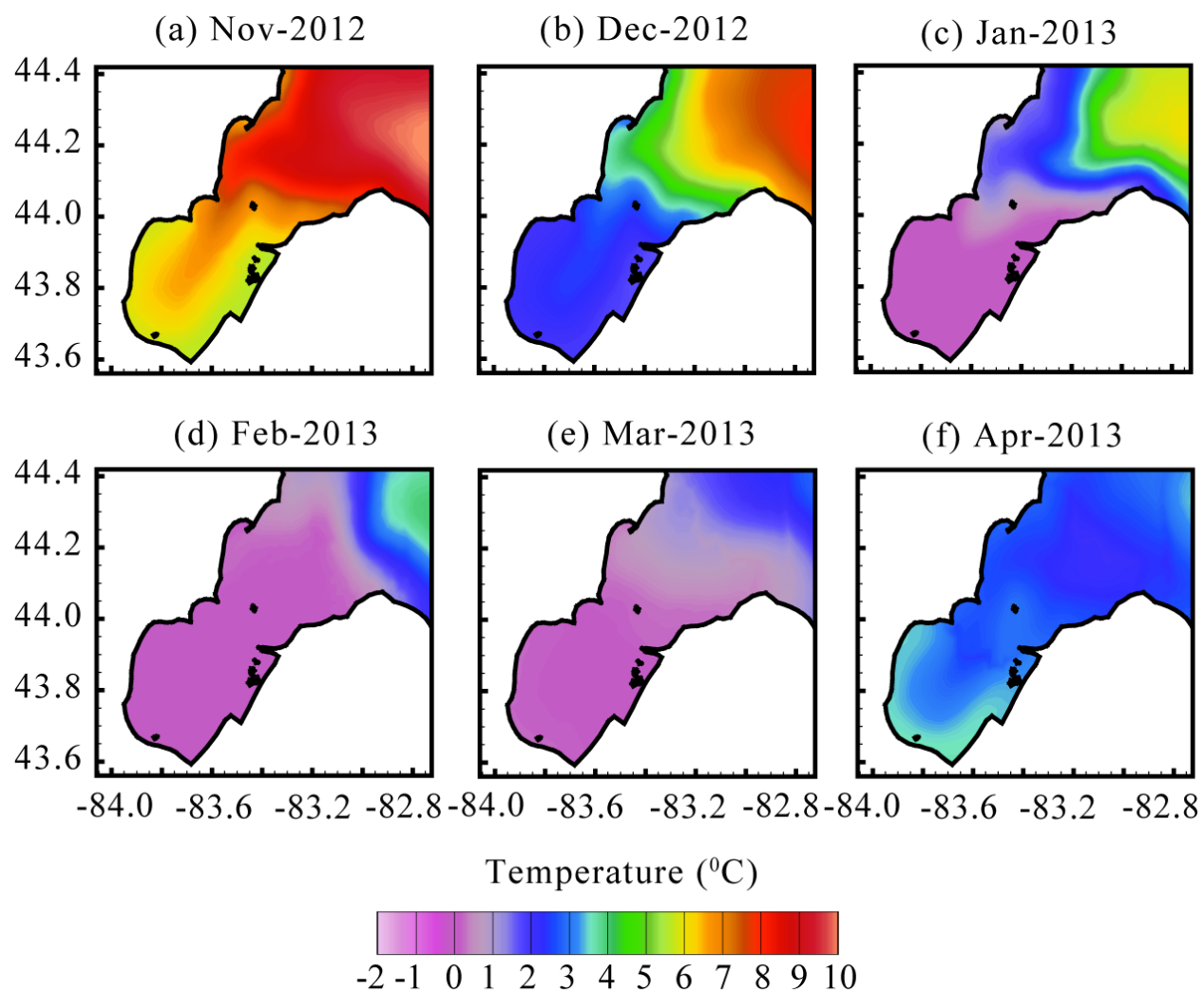
Figure 35: Surface temperature contours for Saginaw Bay for the winter months 2013.

The overturning of temperature in large lakes exhibits a seasonal variation. The lake-wide average of temperatures at surface, mid-depth, and bottom through the winter seasons of 2010, 2013 are shown in Figure 36. The temperature at which the fall overturns is about 5 ^{0}C by mid-December and the spring overturns is about 4 ^{0}C by the end of the next April. The result is consistent with the conclusions of *Saylor and Miller* [1979].
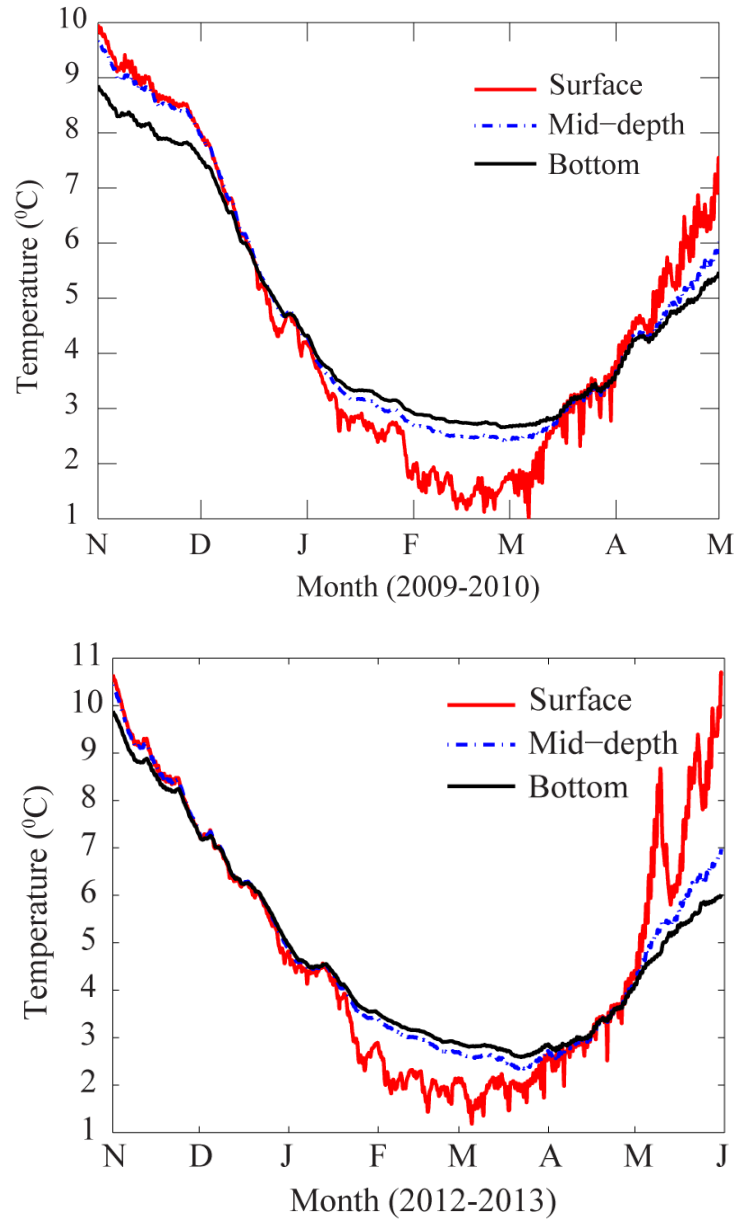
Figure 36: Lake-wide averaged of simulated water temperature at surface, mid-depth, and bottom during winter 2010 (above) and 2013 (below).

4.3.1.3 Ice Cover, Ice Concentration, and Ice Thickness

The comparisons between modeled and observed ice cover are shown in Figures 38, 39. The observed ice concentration data are downloaded from the Great Lakes Ice Atlas (http://www.glerl.noaa.gov/data/ice/). The ice atlas products provide the daily ice concentration data set. The observational ice cover data sets were used to compare with the simulated ice cover extent. The distributions of observed ice concentration are reasonably well represented by the ice model. Because over-lake precipitation and evaporation were not included in the ice model differences between observed and modeled ice cover can be expected. Most of the ice cover in Lake Huron occurred in Saginaw Bay, North Channel, and Georgian Bay during January and February while there are large fractions of open water in the body of Lake Huron during the two winters. The Saginaw Bay is almost entirely ice covered especially in the inner bay area with the maximum ice concentration reaching 100%. The high concentration of ice will influence the flushing rate between the outer and inner bays and between the (entire) bay and the open lake.

In Figure 37 we plot the time series of modeled ice cover in percentage (red and blue lines) compared to observational data (red and blue solid dots) over Lake Huron for the winters of 2010 and 2013. The modeled percentage of ice cover is calculated as in the equation:

$$P_{ICE} = \frac{\sum_{i=1}^{n} A_i}{A_{lake}} \times 100 \ (\%) \qquad\qquad (44)$$

where: P_{ICE} is the total ice cover expressed as a percentage; A_i is the area of cell which has ice; A_{lake} is the total area of Lake Huron and equal 5.88E+04 km^2; n is the total number of cells which have ice. It should be noted that it is assumed ice cover is fully filled at each cell where it has ice formation at the centroid. This assumption may affect to the result of the total area covered by

ice in calculation where the grid size is large. Ice cover on Lake Huron started to form by beginning of December for the years 2009, and 2012. The ice cover increased rapidly on Julian day of 10 (2010) and 20 (2013) and it reached the maximum value of 38.3% and 38.6% in 2010 and 2013, respectively. Maximum values of simulated and observed ice areas are shown in Table 11. With the range of the annual maximum ice cover over Lake Huron varying from 45% to 79% [*Assel et al.,* 2003] the winters of 2010 and 2013 are considered mild winters. It is likely that the model results have overestimated fractional ice cover as shown in Figure 37. The modeled ice areas did not match with the observed data from mid-February to March while the model results agree reasonably well with observations from January to mid-February. The difference between simulations and observations areas covered by ice can be explained by the ice thickness distribution used in the model. Because of the lacking of ice thickness data fields in Lake Huron, therefore, in this study as stated before we assumed the ice thickness have 5 ice categories that are 20cm, 60cm, 120cm, 200cm, and 300cm respectively while the distribution of ice thickness is sensitive to the simulation results [*Hunke E.C*, 2010]. Furthermore, the exclusion of snow cover may affect to the ice growth and melting processes because it is related to surface albedo.

Table 11: Maximum Ice Cover Area over Lake Huron (unit: %)

	Modeled	**Observed**
2010	38.3	38.7
2013	38.6	45.6
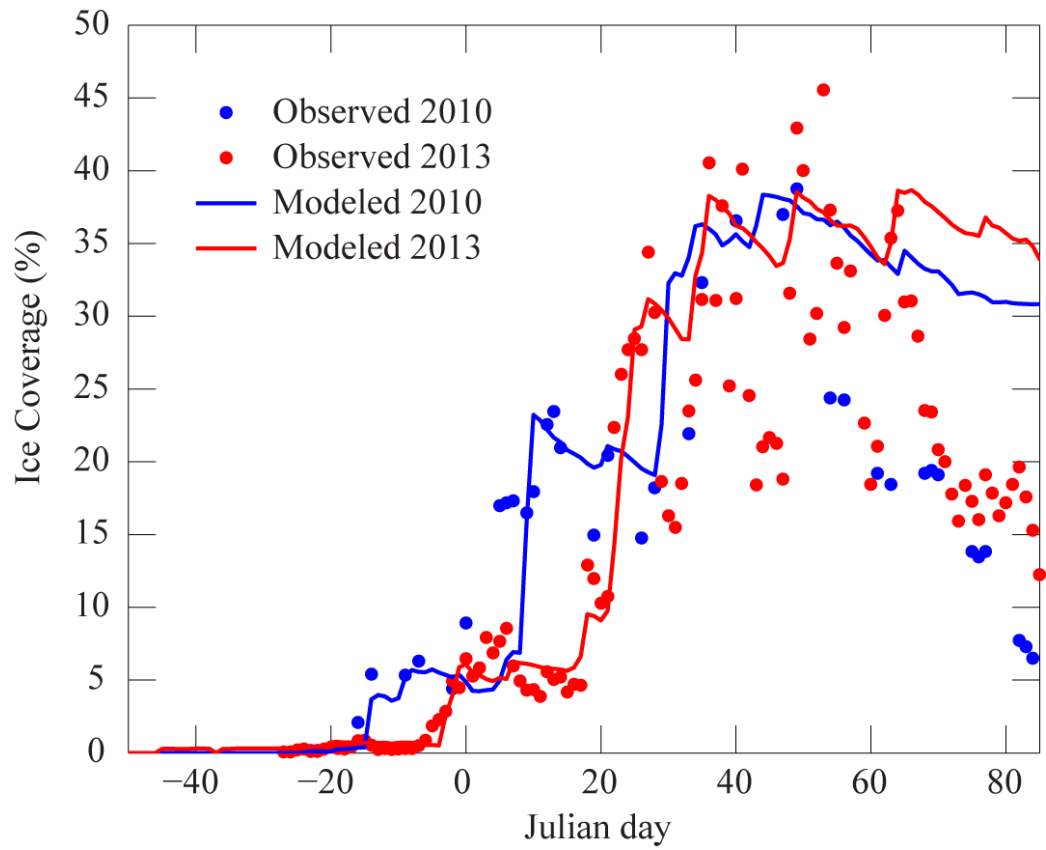
Figure 37: The time series of ice cover in percentage in the winter 2010, 2013
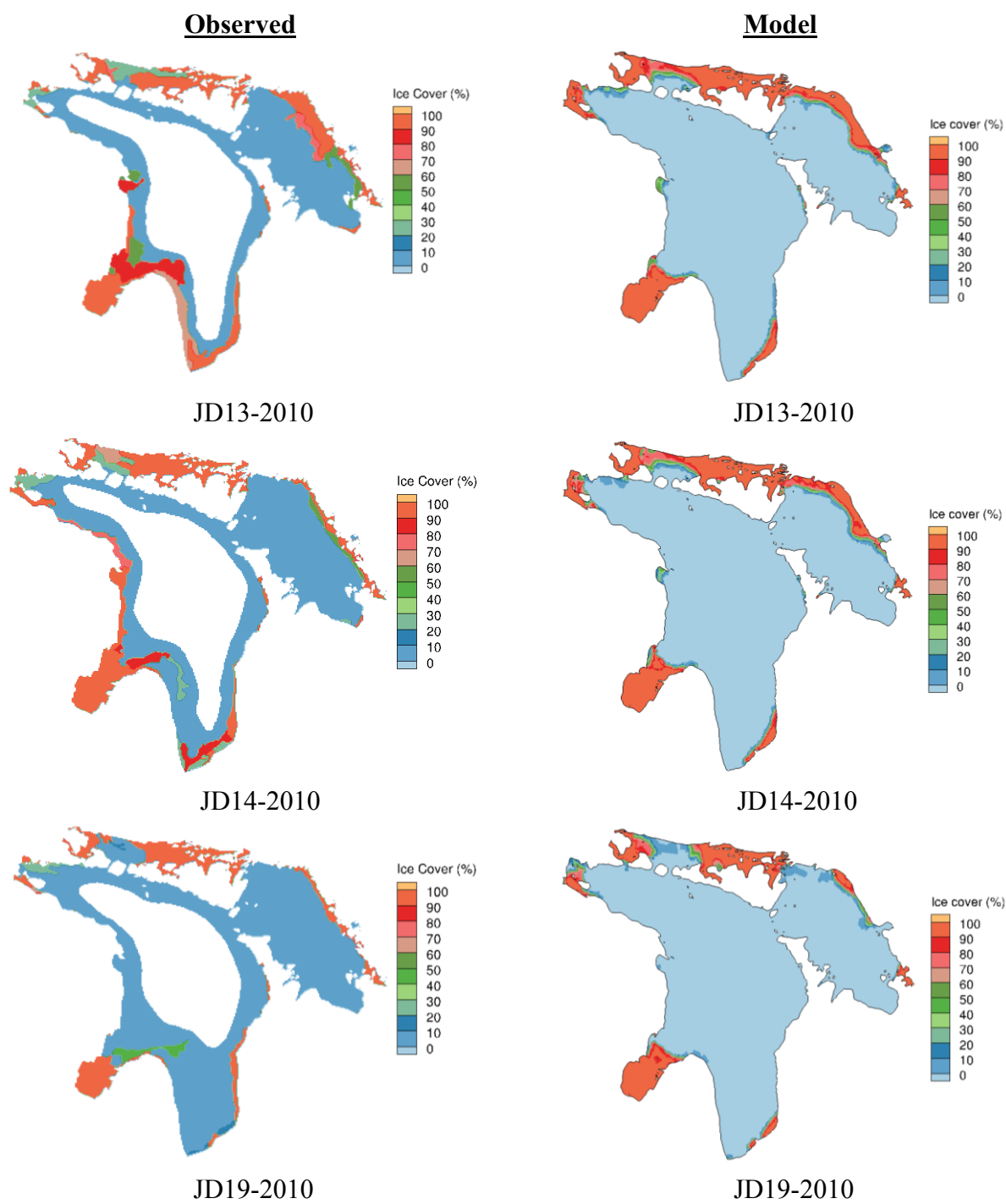
Figure 38: Map of Lake Huron showing observed and simulated ice cover area for winter 2010.

Figure 38 (cont'd)

Observed
JD25-2010

Model
JD25-2010

Observed
JD32-2010

Model
JD32-2010

Observed
JD35-2010

Model
JD35-2010

Figure 38 (cont'd)

Observed   **Model**

JD39-2010   JD39-2010

JD56-2010   JD56-2010

JD68-2010   JD68-2010
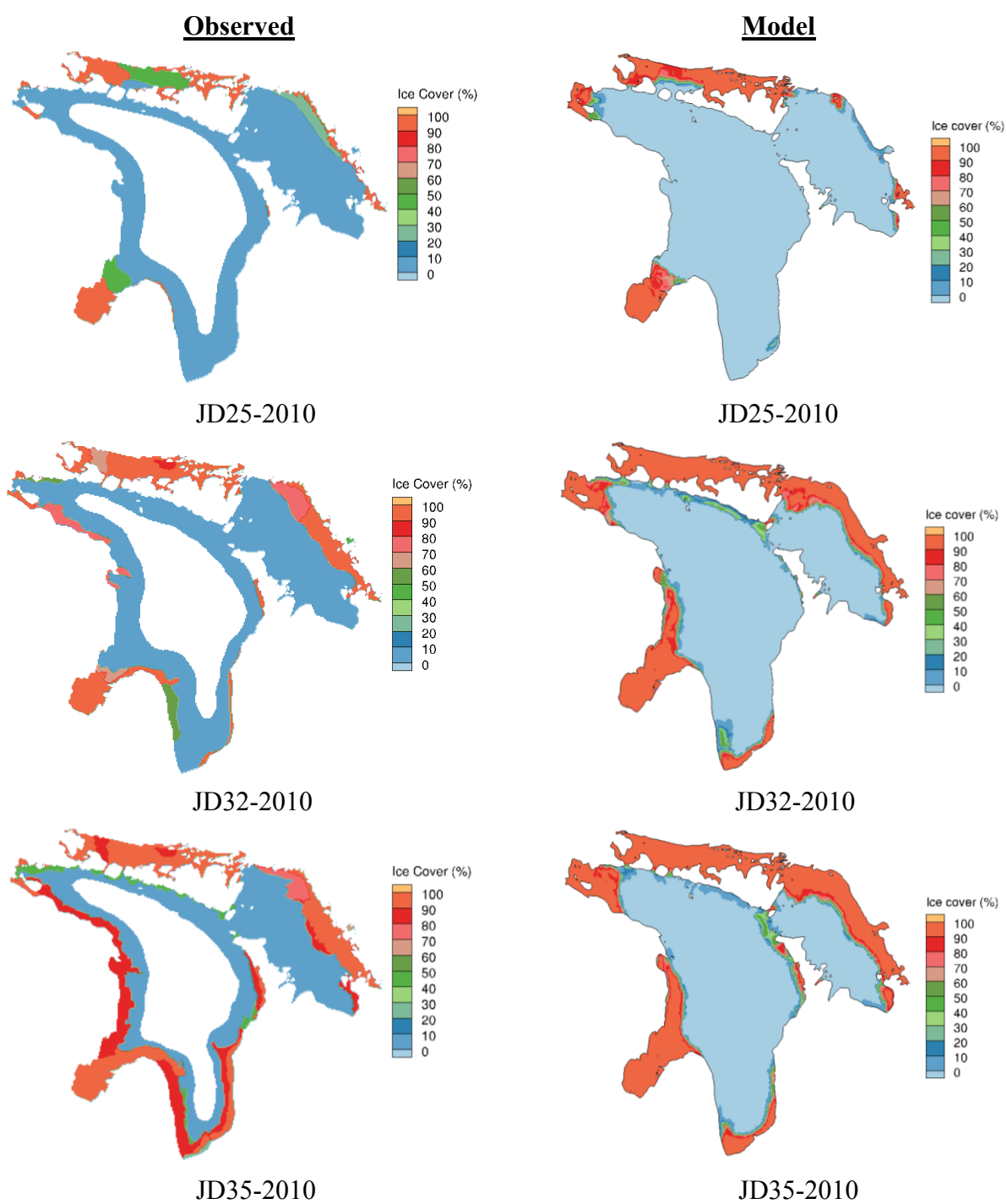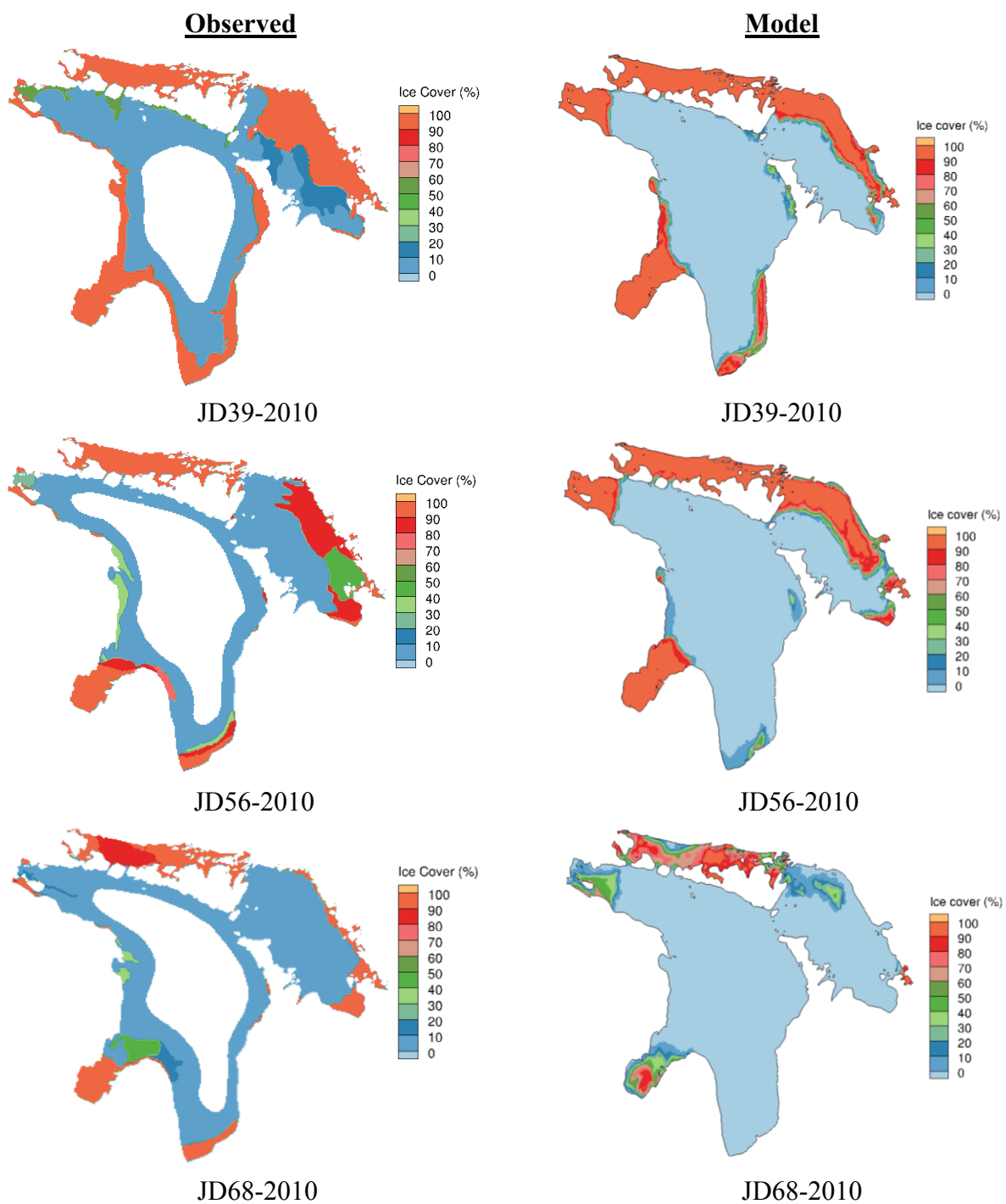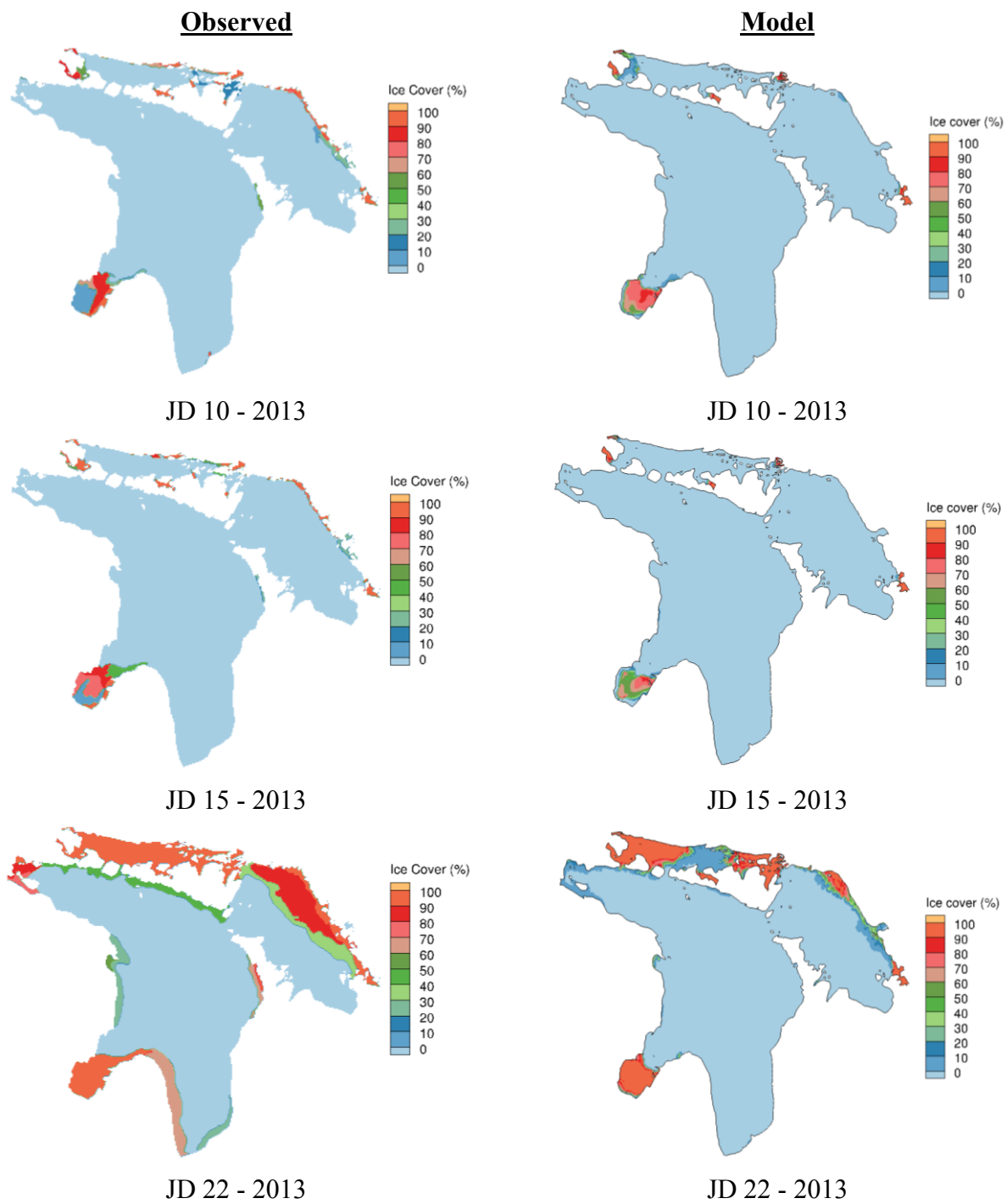
Figure 39: Map of Lake Huron showing observed and simulated ice cover area for winter 2013.

Figure 39 (cont'd)

Observed

Model

JD 24 - 2013

JD 24 - 2013

JD 40 - 2013

JD 40 - 2013

JD 48 - 2013

JD 48 - 2013
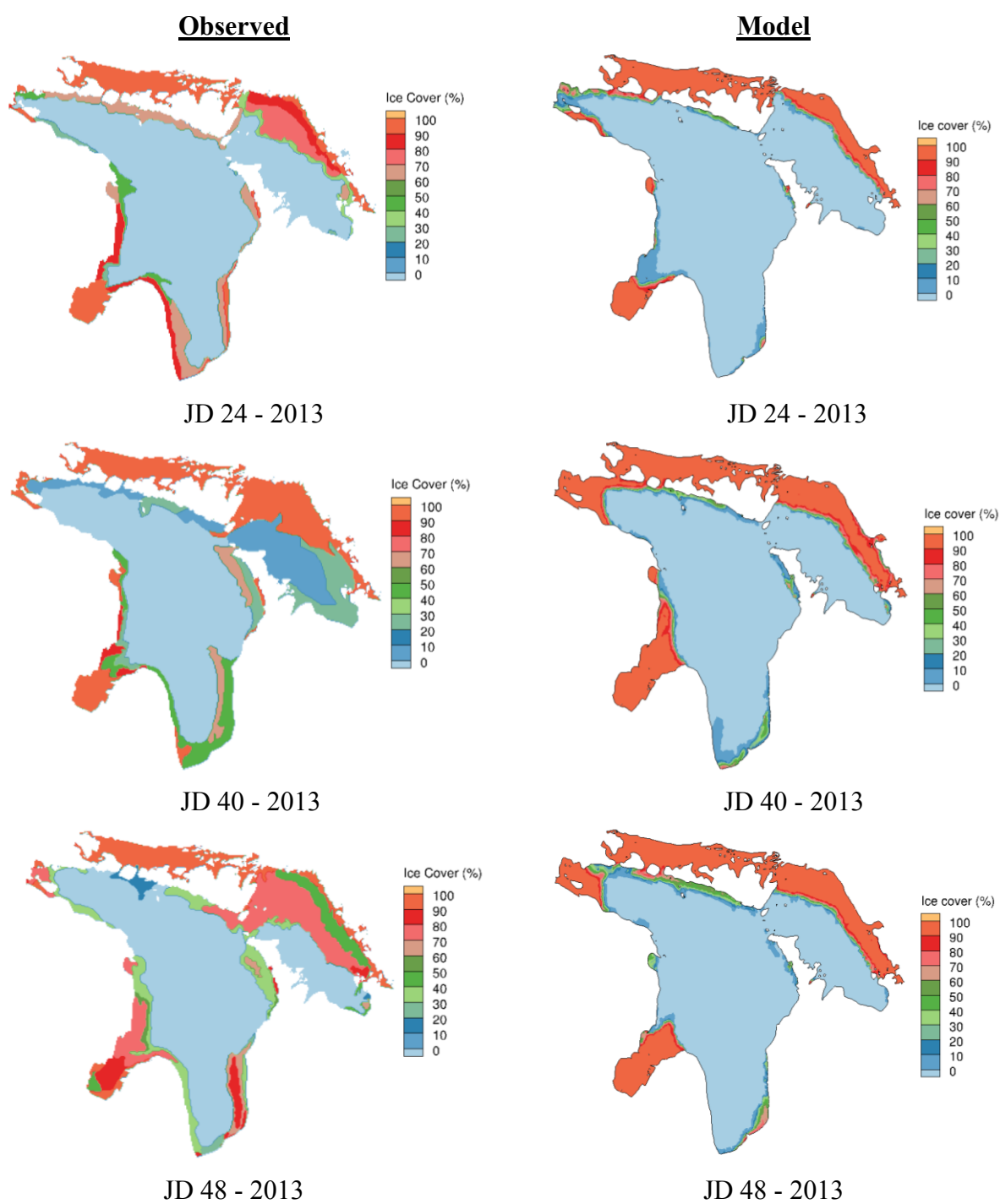
In Figures 40, 41 we plot the contours of modeled ice thickness for some selected days in January, February, and March for winters of 2010, 2013. Mean ice thickness over the three months of winter for the two years was 3.4 cm for Lake Huron and 7.1 cm for the Saginaw Bay. The results of ice thickness in winter months for Lake Huron and Saginaw Bay for the year 2010 and 2013 are presented in Tables 12, 13. The maximum of ice thickness was reached in February with a value of 95.4 cm for Lake Huron. In Saginaw Bay the ice thickness reached the maximum value of 35.4 cm in March 2013.

Table 12: Monthly average ice thickness (in cm) for Lake Huron and Saginaw Bay in winter months

Year	Areas	Jan	Feb	Mar
2010	Lake Huron	1.7	4.8	1.2
	Saginaw Bay	4.5	11.5	2.7
2013	Lake Huron	1.5	6.2	5.0
	Saginaw Bay	3.7	11.8	8.8

Table 13: Maximum ice thickness (in cm) for Lake Huron and Saginaw Bay in winter months

Year	Areas	Jan	Feb	Mar
2010	Lake Huron	60	53.5	36.0
	Saginaw Bay	21.7	22.5	22.4
2013	Lake Huron	42.2	95.4	40.0
	Saginaw Bay	30.4	23.4	35.4
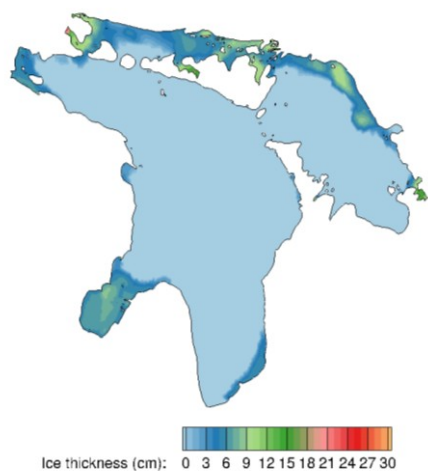
JD13-2010
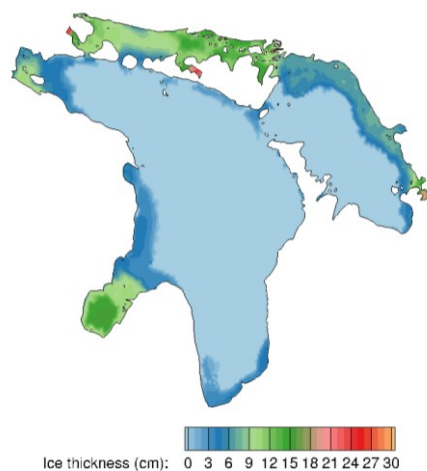
JD32-2010
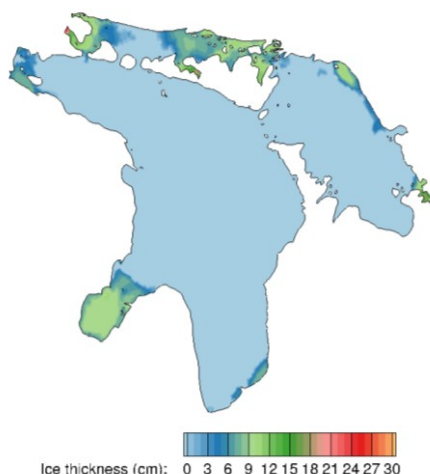
JD19-2010
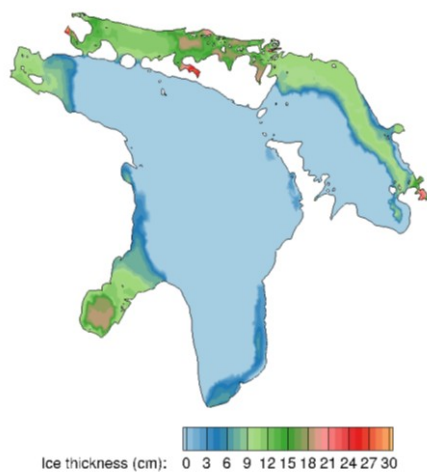
JD39-2010
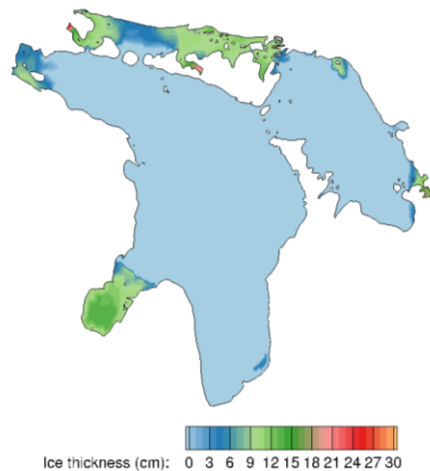
JD25-2010
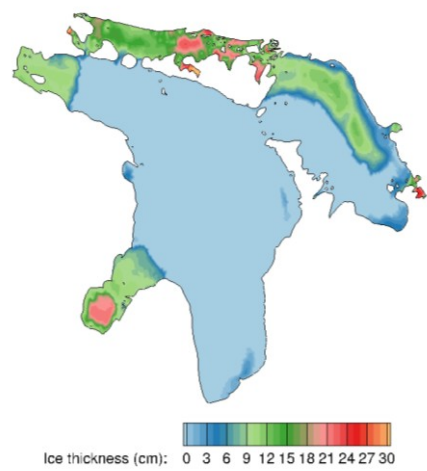
JD56-2010

Figure 40: Modeled Ice thickness contours for Lake Huron for the winter of 2010.

106

Ice thickness (cm): 0 3 6 9 12 15 18 21 24 27 30

JD 22 - 2013

Ice thickness (cm): 0 3 6 9 12 15 18 21 24 27 30

JD 63 - 2013

Ice thickness (cm): 0 3 6 9 12 15 18 21 24 27 30

JD 40 - 2013

Ice thickness (cm): 0 3 6 9 12 15 18 21 24 27 30

JD 67 - 2013

Ice thickness (cm): 0 3 6 9 12 15 18 21 24 27 30

JD 48 - 2013

Ice thickness (cm): 0 3 6 9 12 15 18 21 24 27 30

JD 76 – 2013
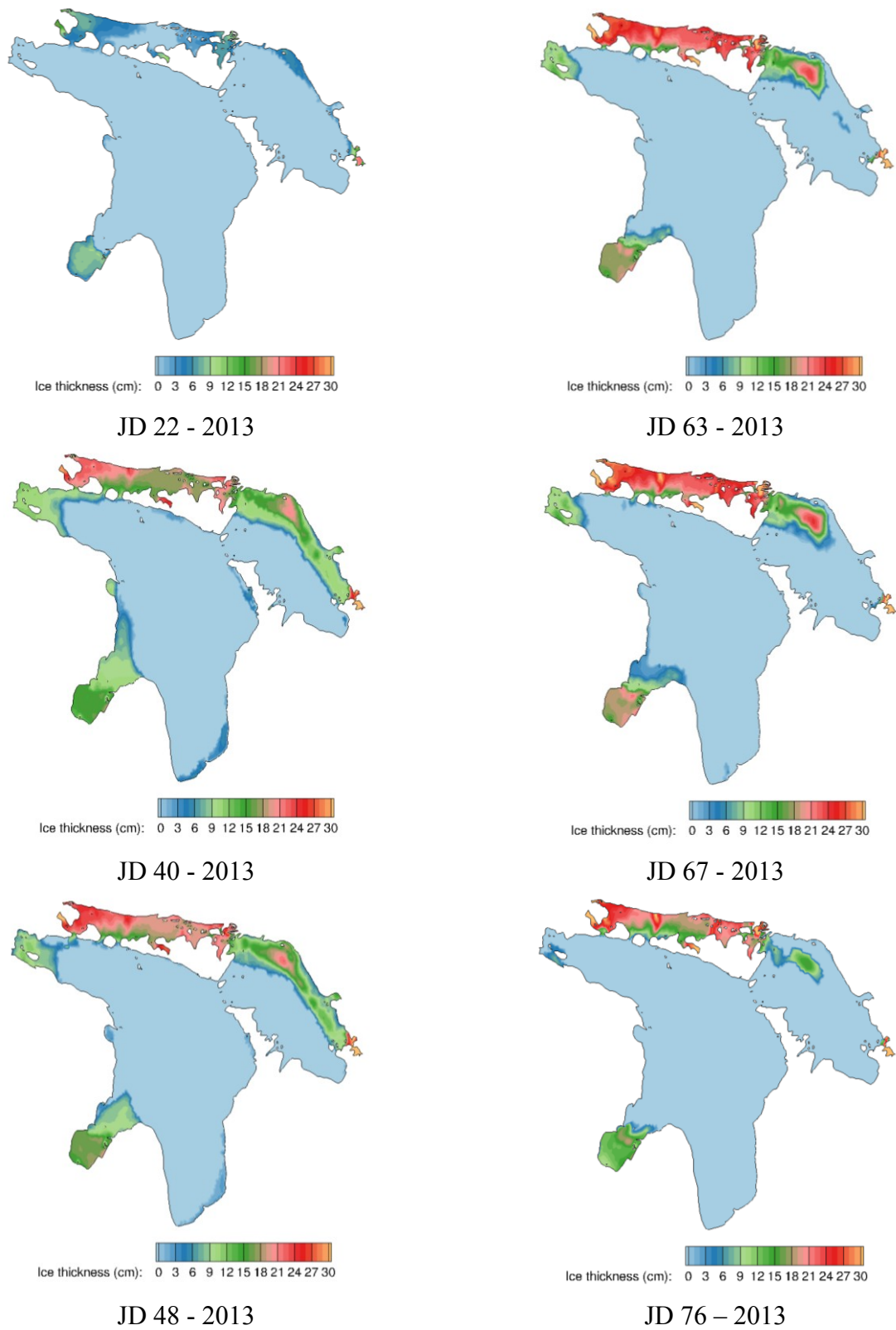
Figure 41: Modeled Ice thickness contours for Lake Huron for the winter of 2013.

4.3.2 Discussion

During the winter season, large-scale circulation in Lake Huron is influenced by a combination of key physical features (islands, exchange with Saginaw Bay and Georgian Bay, and the mid-lake AAR ridge) and the movement of ice. With the presence of ice, the results from numerical model have shown that winter circulation in the main lake is counterclockwise. The mean current speed in Lake Huron was 1.14 cm/s over winter months for the two simulation years. The mean vertical velocity profiles at the inlet of Georgian Bay are illustrated in Figure 42, in which the positive and negative values indicate inflow and outflow currents to and from Georgian Bay, respectively. The velocity profiles in winter time were unusual in February and March in comparison with the earlier reported results by *Beletsky et al.,* [1999]. The results show that there is an outflow at the surface associated with the inflow at the bottom at Georgian Bay mouth. The mean velocity of inflow into Georgian Bay in deeper layers is about 1 cm/s. The presence of flow reversal at Georgian Bay mouth can be explained by the role of dominant wind direction under homogeneous conditions. As shown in Figure 43 the predominant wind directions over Lake Huron in January and February are SW and NE respectively. Furthermore, the circulation can change from year to year or season to season. Circulation in Saginaw Bay was characterized by the presence of a cyclonic gyre at the mouth of the Saginaw bay and two recirculating cells within the inner bay as shown in Figures 44, 45. The role of ice cover on the current velocity was clearly found as presented in Figures 44, 45 with low current velocities in the inner bay especially in February. This finding is supported by the conclusion from *Fujisaki et al.,* [2012] who concluded that the packed ice cover slowed down the water velocity. This finding also has important implications in that it indicates that the flushing time in winter is expected to be longer than the flushing time in summer for the inner bay. The reduction of current velocities in winter

implies lower mixing rates in Saginaw Bay. Another important feature of circulation in winter time that there is a narrow band of flow of about 2km width along the mid-lake ridge from Thunder Bay at Alpena on the west side across to Point Clark on the east side.
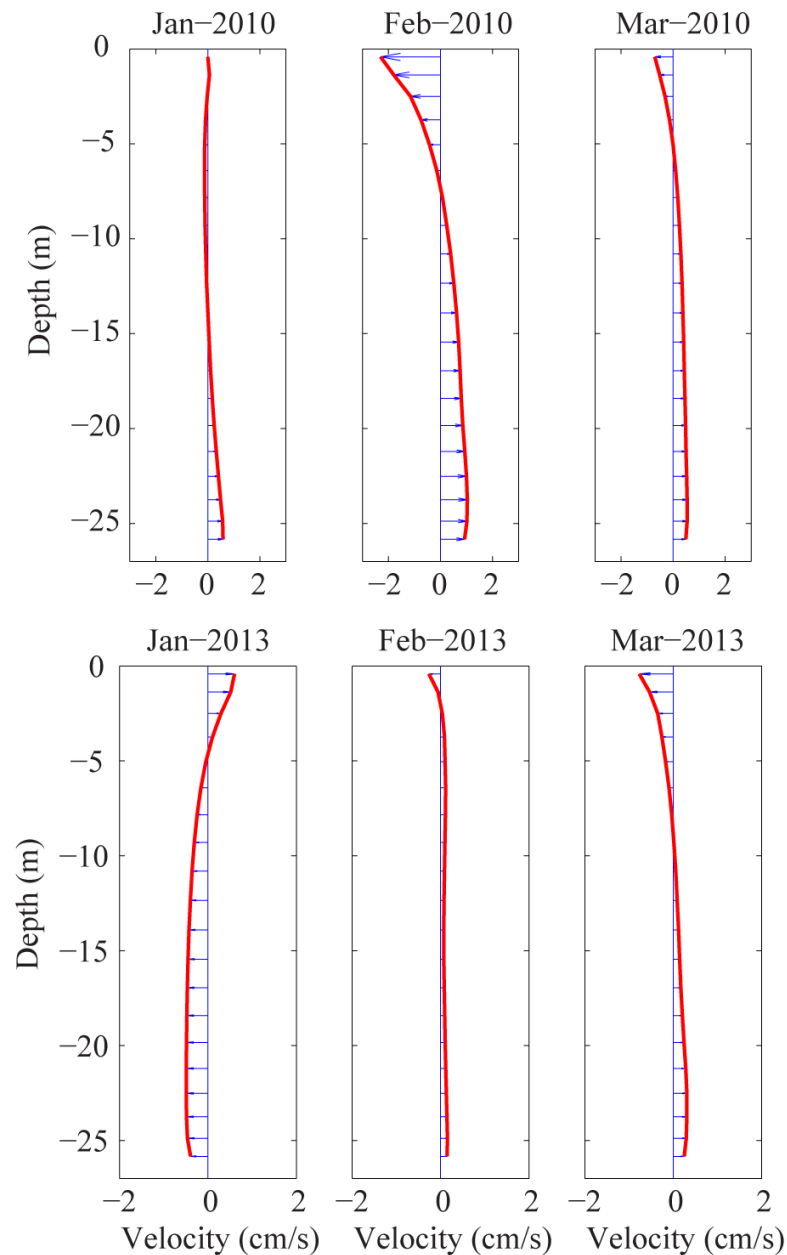
Figure 42: Mean vertical velocity profiles at the inlet of Georgian Bay for different layers in winter months.

Table 14: Maximum and mean currents velocity in Lake Huron in winter months (unit: cm/s)

Year	December		January		February		March	
	Mean	Max	Mean	Max	Mean	Max	Mean	Max
2010	1.2	12.0	1.6	9.7	1.4	15.0	1.3	8.3
2013	0.72	4.5	1.35	10.45	0.6	4.93	1.0	7.4
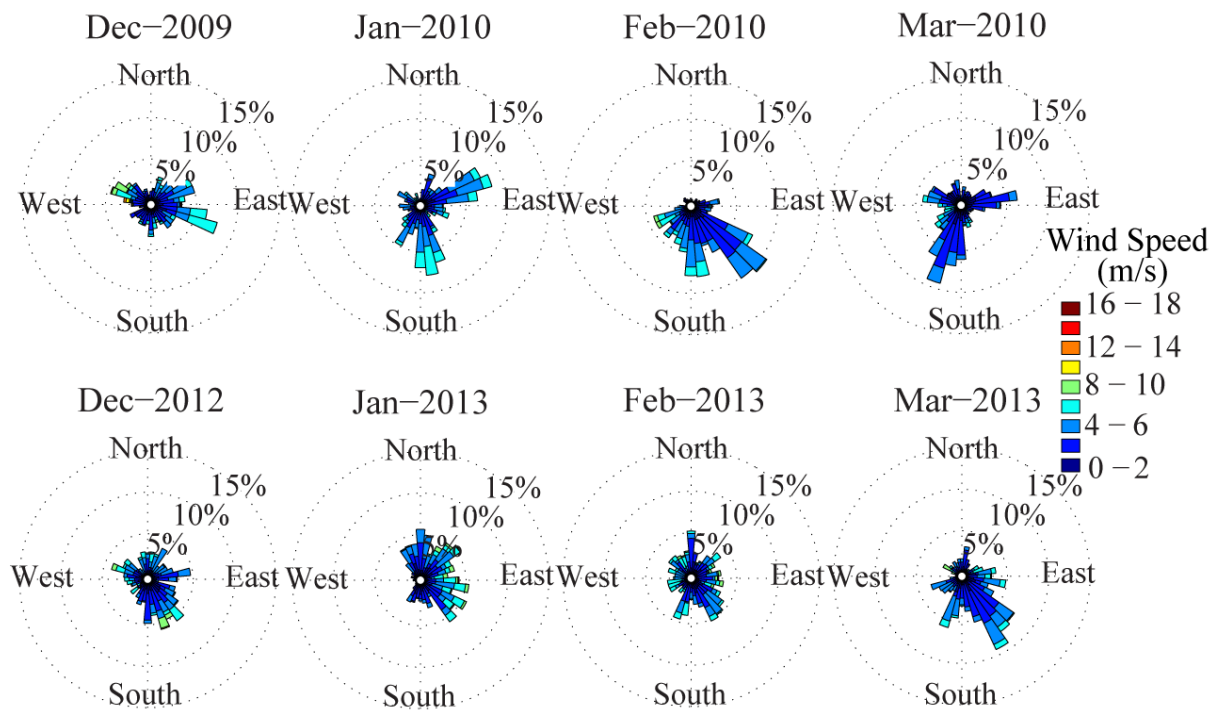
Figure 43: Wind rose plots for winter months over Lake Huron during in the years 2010, 2013.
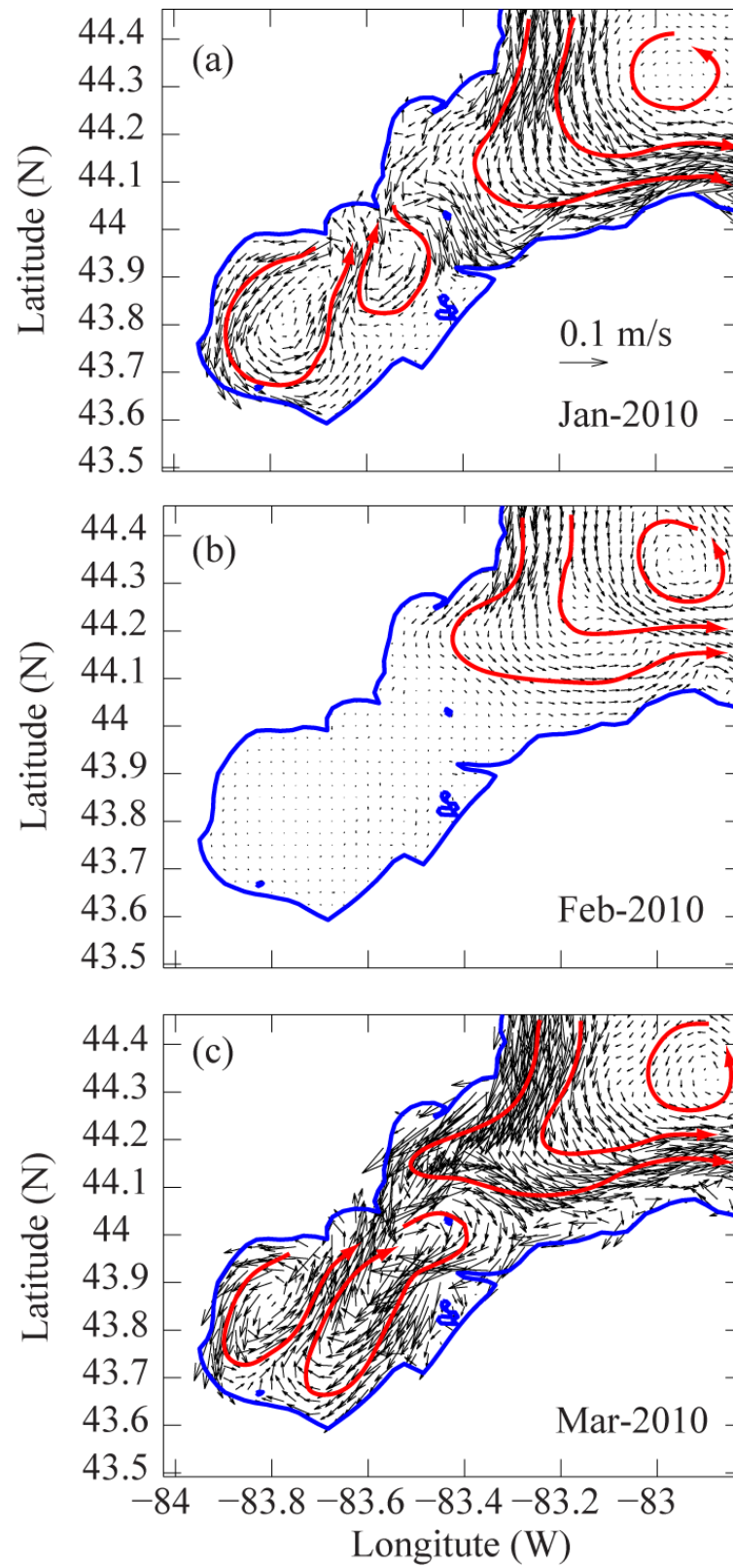
Figure 44: Monthly vertically-averaged currents in Saginaw Bay in winter months 2010
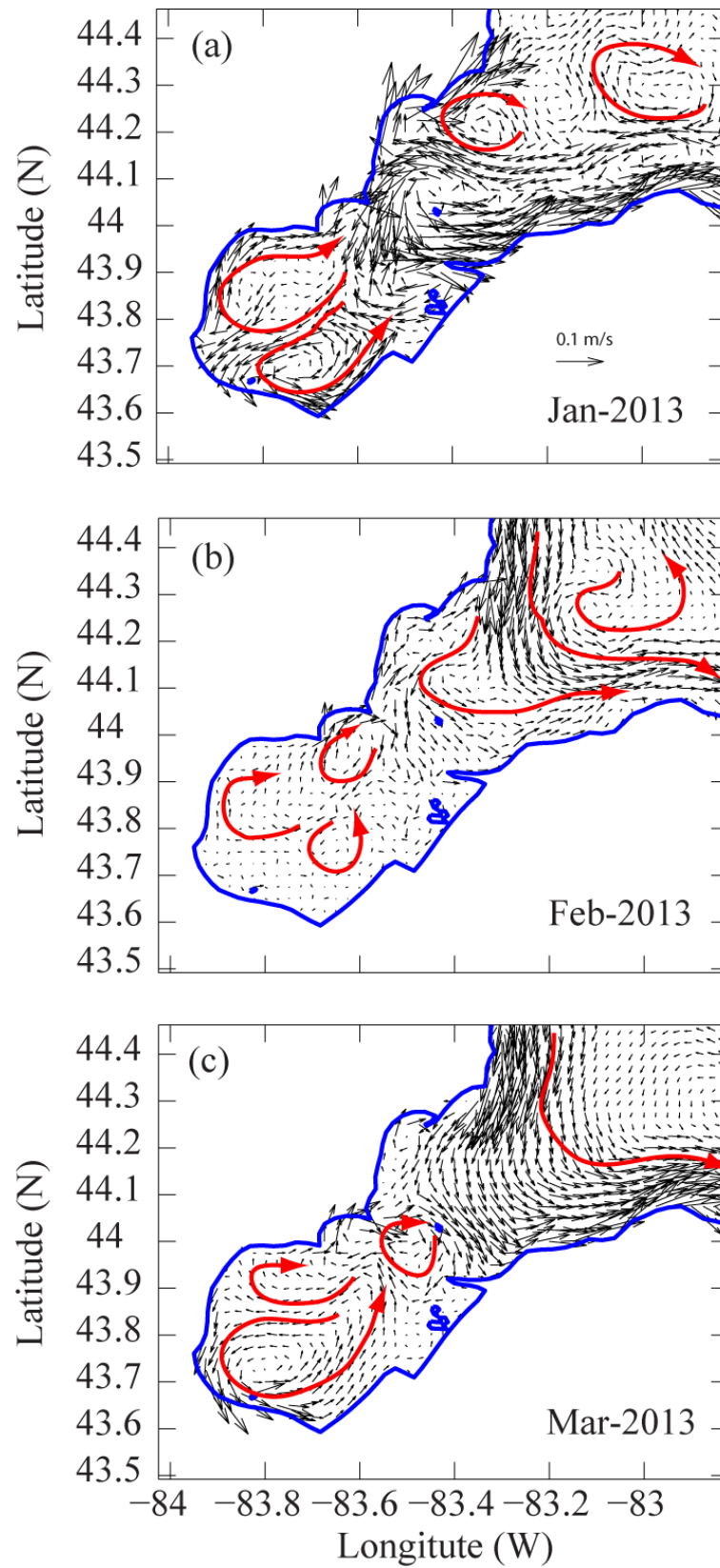
Figure 45: Monthly vertically-averaged currents in Saginaw Bay in winter months 2013
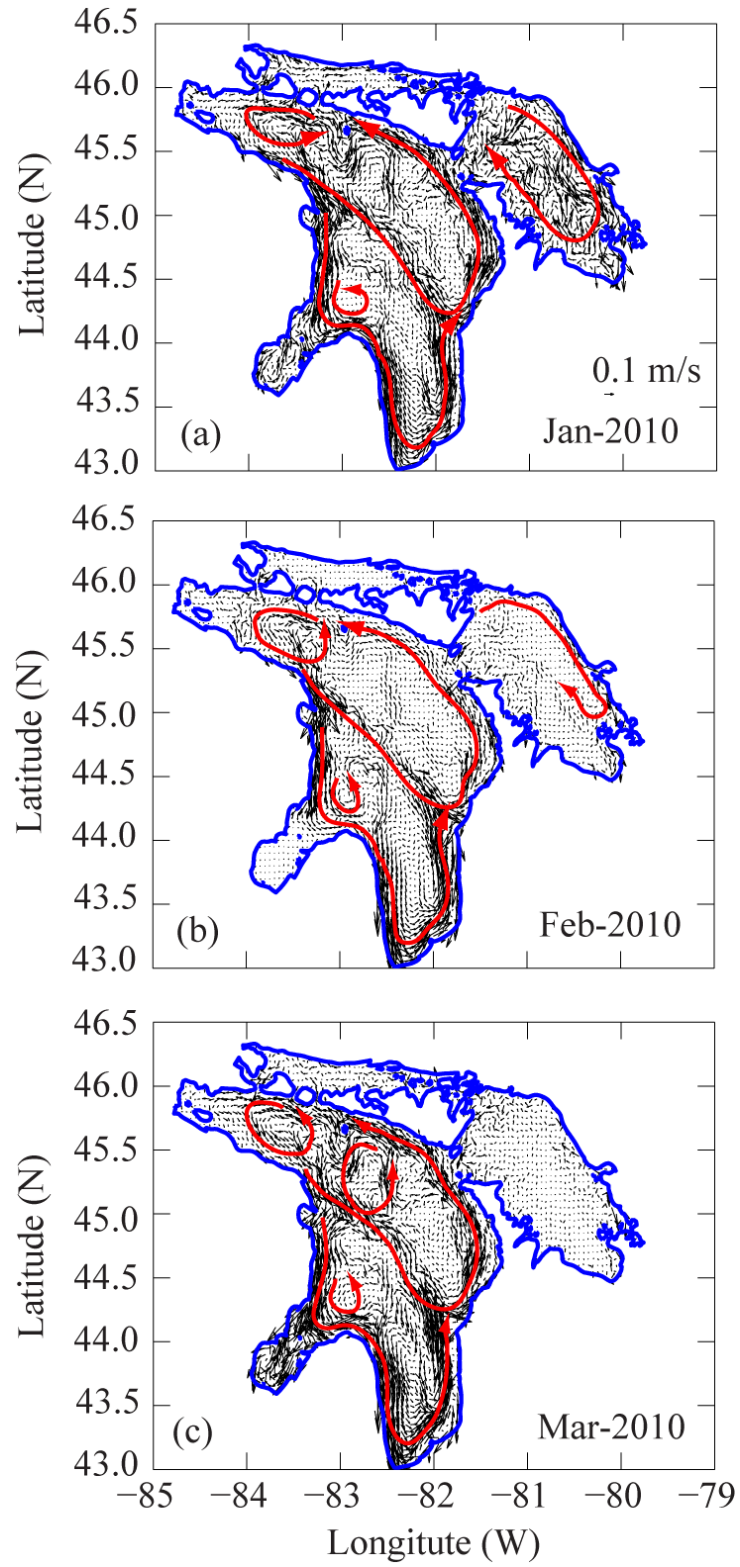
Figure 46: Monthly vertically-averaged currents in Lake Huron in winter months 2010.
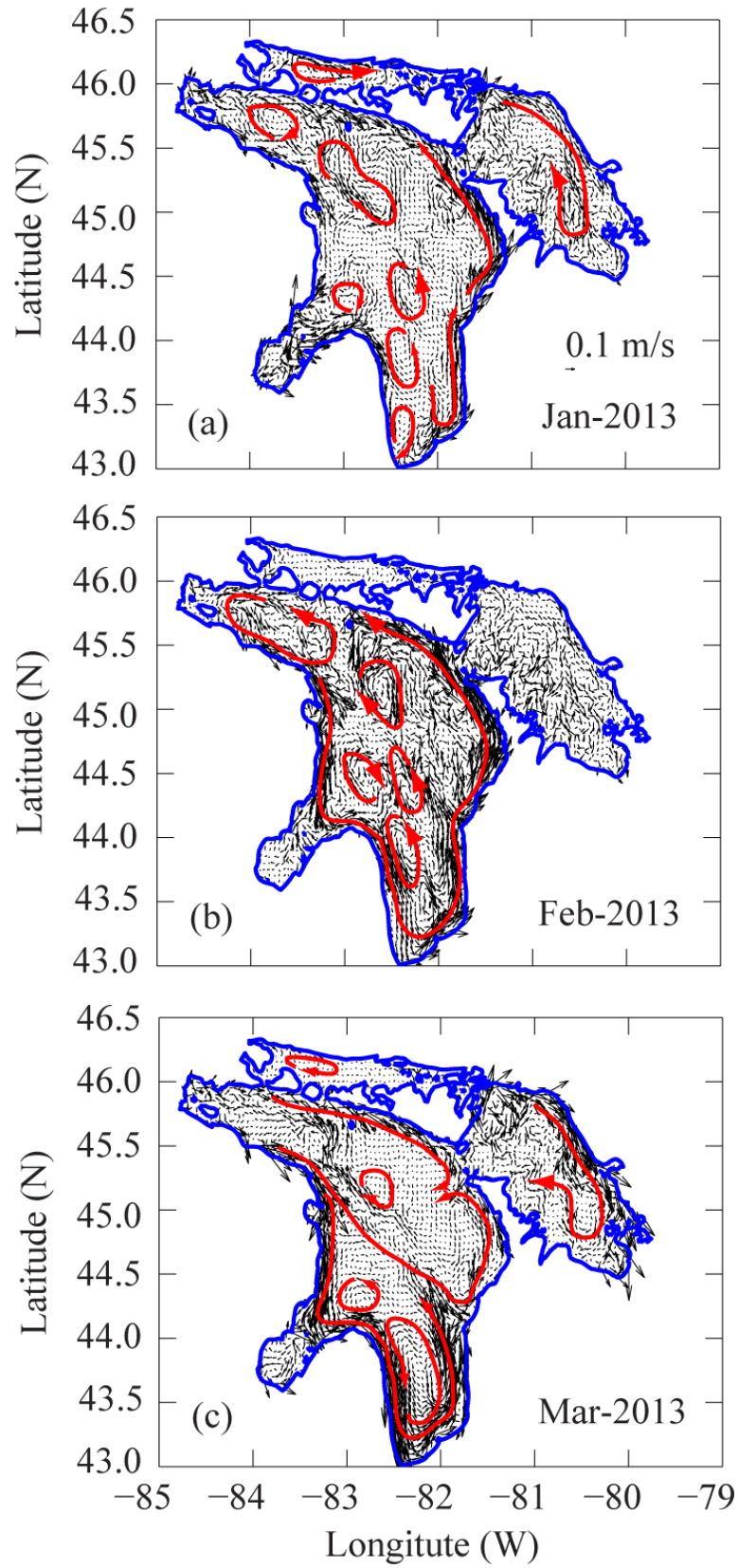
Figure 47: Monthly vertically-averaged currents in Lake Huron in winter months 2013.

As shown by the observed and simulated vertical temperature profiles presented in Figure 30 the lake is almost entirely homogeneous in temperature by mid-November. During the homogeneous period, we can see that the thermal boundary between the inner and outer bays in Saginaw Bay where there is a significant gradient in temperature between the two zones. The presence of this thermal temperature can be associated with the bathymetric features in the bay. Since the mean depth in the inner bay is about 4m, the water temperature decreases relatively quickly than in the deeper layers of the outer bay as cooling of ambient air continues to occur.

The monthly vertically-averaged currents in Figures 44, 45 clearly show the role of ice cover on water movement underneath ice, especially in the inner area in the Saginaw Bay. It is interesting to note that the inner bay almost reached a state of stagnation in February (Figure 44b). The flushing times for inner and entire bay, therefore, are expected to be higher than the flushing times during the summer season. It is likely that the model results have overestimated fractional ice cover over Lake Huron. The ice model needs further improvements in future for more accurate simulation of ice cover. The monthly average ice velocities in Lake Huron for the years 2010 and 2013 are illustrated in Figures 48, 49. In Georgian Bay the ice packs tend to move in the Northeastern direction. It is likely that in Georgian Bay the direction of ice movement is not strongly influenced by the wind direction but the combination of wind stress and water movement. In Saginaw Bay the ice movement is associated with the circulation in the Bay (Figures 50, 51). We can see that the ice movement tends to follow the two re-circulating cells within the inner bay in March 2010 and January 2013.
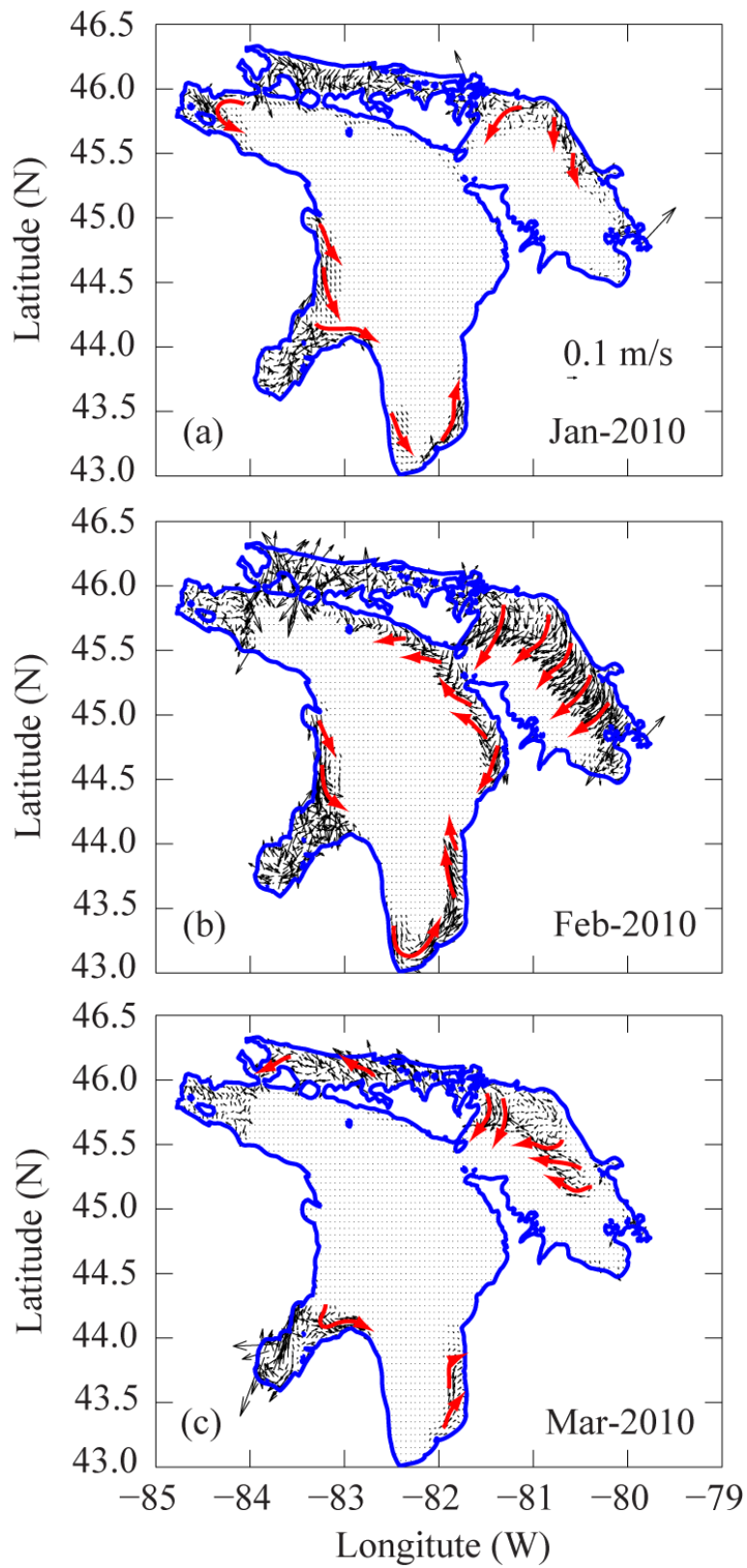
Figure 48: Monthly average Ice velocity in Lake Huron in 2010.

116
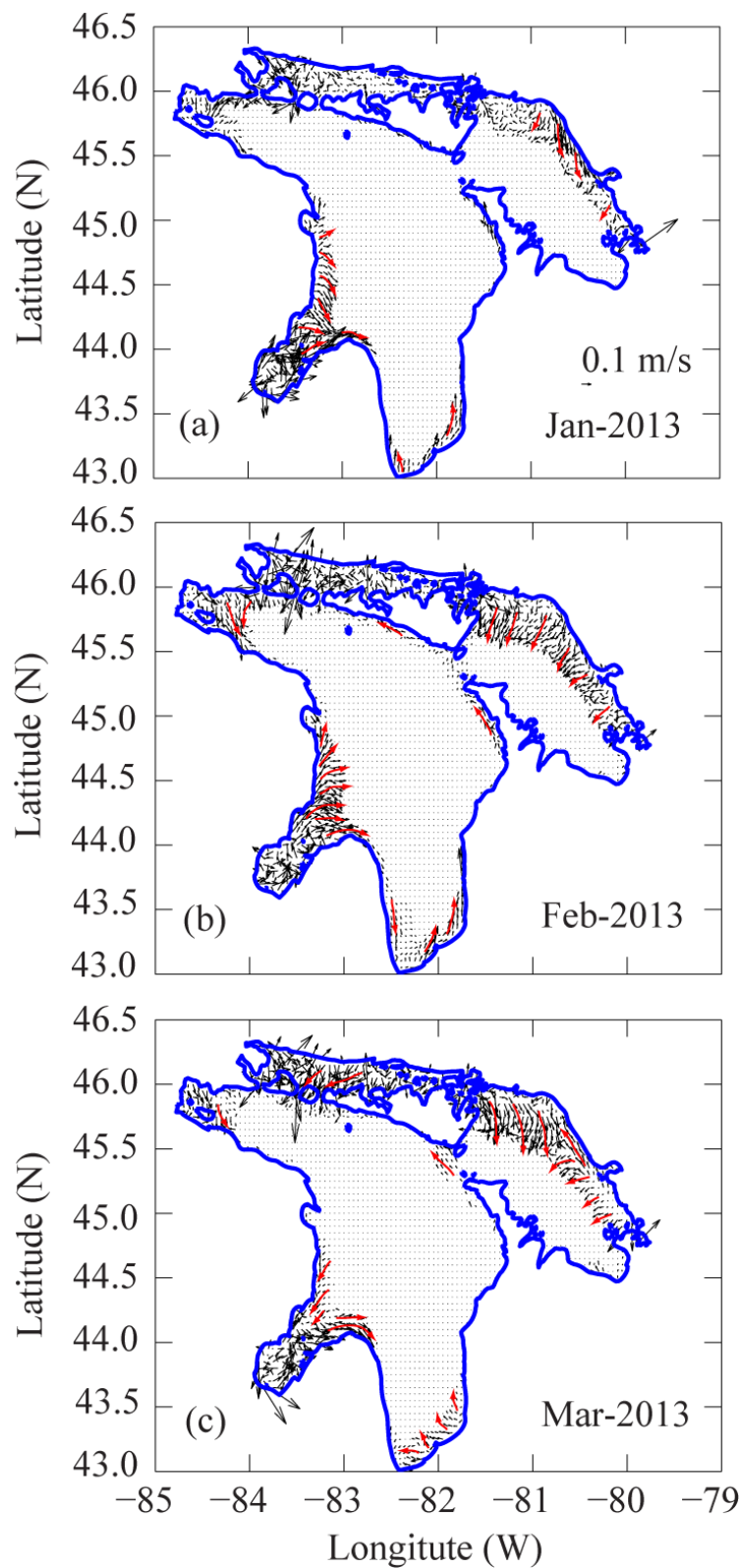
Figure 49: Monthly average Ice velocity in Lake Huron in 2013.
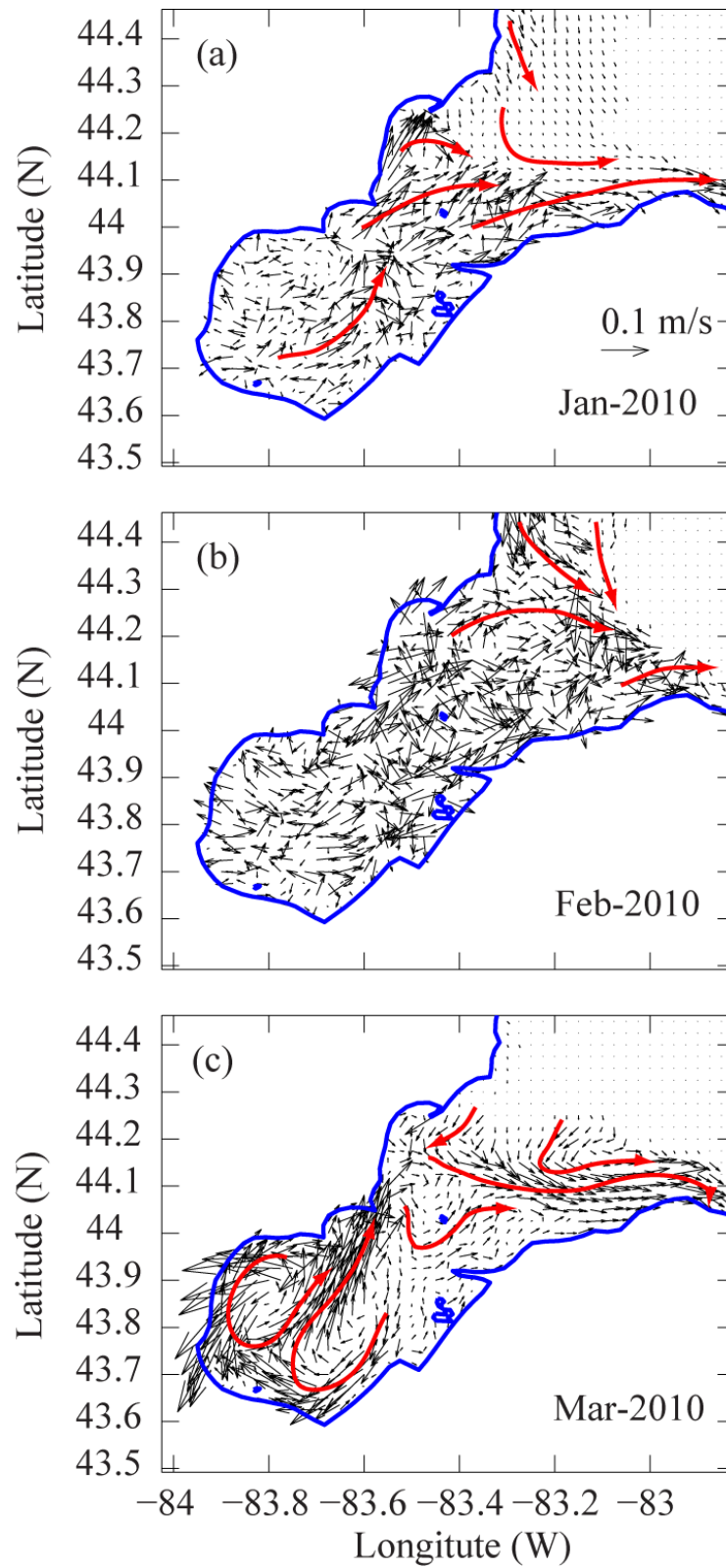
Figure 50: Monthly average Ice velocity in Saginaw Bay in 2010.
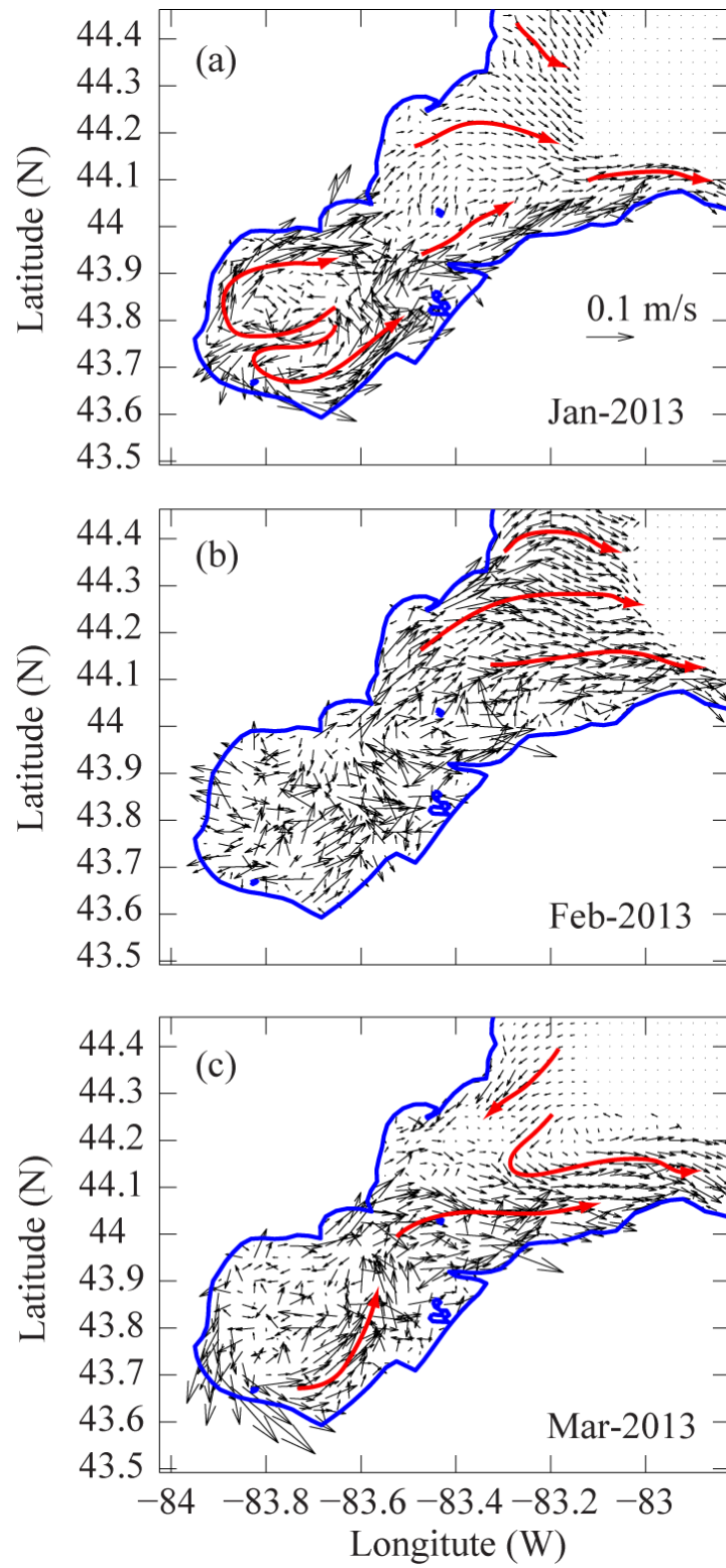
Figure 51: Monthly average Ice velocity in Saginaw Bay in 2013.

4.4   Conclusions

The unstructured grid hydrodynamic model coupled with an ice model is used to investigate the large-scale circulation, thermal structure, and ice cover in Lake Huron and Saginaw Bay. Simulation is carried out for two mild winters of 2010 and 2013. The model included multiple ice categories. The model reproduced reasonably well, the lake surface temperature, circulation, ice cover, ice concentration, and ice thickness in Lake Huron. The model results were tested against ADCP observations of currents, thermistor chain data, and observed ice cover data. Mean circulation in winter time was predominantly cyclonic in the main body of Lake Huron with current speeds being highest in January. Thermal structure in winter was characterized by a homogeneous condition that was found by both observations and simulations in the study. The lake is almost entirely homogeneous in temperature by mid-November. The thermal boundary between the inner and outer bays in Saginaw Bay was found during winter time with a difference in temperature of approximately 2.5^0 to 3.0^0C. The important features of fall and spring overturn were also reproduced by the model. As expected, the model results show that the significant role of ice cover on lake circulation in winter. The inner area in Saginaw Bay was almost in a stagnation state during the ice formation period. As a result, the flushing times are expected to be higher than the corresponding flushing times in summer season (this question will be explored in detail in the next chapter). We found that the mean current speed in Lake Huron in winter time was 1.14 cm/s compared to the summer time average of 3 cm/s found in an earlier chapter. The remarkable feature we found is the unusual nature of currents at the inlet of the Georgian Bay. There is an outflow at the surface layer associated with the inflow at the bottom at the Georgian Bay mouth. The model results show that ice cover reached a maximum of 38.3% and 38.7% in mid-February in 2010 and beginning of March in 2013 respectively. We found that the mean ice

thickness over the three months in winter for 2 years was 3.4 cm for Lake Huron and 7.1 cm for

the Saginaw Bay.

Chapter 5

Residence Time in the Saginaw Bay and Lake Huron System

5.1   Introduction

Agricultural, industrial, and municipal activities, both within the Lake Huron basin and in upstream region of the Saginaw River, have resulted in pollution by a variety contaminants and the subsequent degradation of water quality. Persistent contamination of the water column and bottom sediment has resulted in degraded water quality. The embayed regions tend to accumulate contaminants due to their longer residence times as indicated by *Nixon et al., [1996]*.

Residence time and flushing time of an estuary are important variables used to estimate the rate of removal of pollutants from the bay. Therefore, a spatial map of the residence time and flushing time of the bay can be useful. Understanding the mean residence time and spatial variation in the bay is of critical importance in resolving issues such as contamination, water quality (e.g., harmful algal blooms, bacterial contamination etc.), and for ecosystem analysis; therefore, residence time is an important index that scientists should pay careful attention. *Monsen et al.*, [2002] concluded that first-order transport time scales such as residence times and

flushing times within the bay are useful for understanding, interpreting, and comparing processes and rates across different ecosystems. For example, when attempting to solve issues related to the transport of matter in lakes or a bay, we need to know how the exchange takes place. Recent concerns associated with environmental issues in the Saginaw Bay highlight the need for accurate estimates of transport time scales.

There have been a few studies into the Saginaw Bay and Lake Huron systems that have provided the preliminary description of the mean residence times in these areas. *Quinn [1992]* estimated that the residence time, which is defined as the time it takes to replace the water volume of Lake Huron, is 22 years. *Saylor and Danek*, [1976] calculated the exchange rate between the inner bay and outer bay to be 3700m^3/s, while the mean residence time was 26.5 days for the inner bay. The residence time of any bay may vary with several factors such as wind direction or river inflow. Since the Saginaw bay is shallow, the residence time is strongly influenced by wind. As *Saylor and Danek*, [1976] pointed out, the residence time of water in the bay is much longer when the winds are perpendicular to the axis of the bay. Earlier study by *Dolan [1975]* calculated a residence time of 110 days for the inner bay based on a time-variable chloride model. However, the river discharge was not included in this model.

Until now, there have been no observations and studies on residence times in the Saginaw Bay since the early work cited above. High resolution hydrodynamic models with additional water quality models can be used to estimate the residence times in more detail than with an observational dataset alone. Therefore, the aim of this chapter is to estimate the residence time for Saginaw Bay and to describe the residence time distribution zones using two approaches. Methodologies for computing flushing time and residence time will be presented in the next session. The distribution map will provide "dead-zones" within the Bay that will increase the

capability to solve and manage environmental problems. The contribution of Saginaw River discharge as a source of fresh water to the residence time in the entire and the inner bays will be quantified and the relationship between them will be established.

5.2   Methodology

5.2.1 First-Order Transport Time Scales

The terms, residence time and flushing time, were used in different studies but sometimes there was confusion in the definition [*Sheldon and Alber, 2002*]. One of the simplest and most widely used transport time scales is the flushing time (T_f) defined as "the ratio of the mass of a scalar in a reservoir to the rate of renewal of the scalar" [*Geyer,* 1997; *Monsen et al*., 2002]. Flushing time can be calculated by dividing the volume of the bay (V) by the volumetric flow rate into (Q_{in}) or out of (Q_{out}) the bay (assumed to be equal in this idealized case based on the assumptions of steady-state, and constant-volume):

$$\left(T_f = {V}/{Q_{in}}\right) \tag{45}$$

The volume V can be calculated from bathymetric data over the surface area of the bay. The flushing time as defined here was variously referred to in the past as "residence time" [*Go´mez-Gesteira et al*., 2003; *Chapra* 2008], "turnover time" [*Sheldon and Alber,* 2006; *Takeoka*, 1984], "flushing time" [*Fischer et al.,* 1979; *Monsen et al*., 2002; *Delhez et al*., 2004], "water exchange rate" [*Kraines et al.,* 2001] and "water renewal time" [*Andrefouet et al.,*2001]. The flushing time is an important physical index for determining the capability of the bay itself in term of

flushing out the pollutant. Equation 45 shows that the flushing time is directly proportional to the value of the volume of the bay. In a water body with a long flushing time index it will take long time to flush out the pollutant. In other words, a long flushing time may be a potential condition to increase concentration and accumulate the pollutant within a semi-enclosed water body like Saginaw Bay.

5.2.2 Eulerian Method

Another important transport timescale is the residence time (τ_R), which is a measure of "how long a water parcel, starting at a specified location within the water body, will stay within the boundaries of the water body before exiting" [*Monsen et al.,* 2002]. By treating the bay as a CSTR (continuously stirred tank reactor, [*Chapra,* 2008]), we can calculate the residence time for every grid cell in the domain as the e-folding flushing time [*Monsen et al.,* 2002] – that is, the time at which 36.78% (e^{-1}) of the initial mass still remains within the bay. As pointed out by [*Monsen et al.,* 2002], the flushing time (T_f) is an integrative system measure while the residence time (τ_R) is a local measure that varies from one grid cell to the other.

The dye concentration model was used to define the residence time (τ_R) as the time it takes for the vertically integrated dye concentration at every grid cell to drop below the 1/e value (36.78%).

The dye concentration was solved using the following equations:

$$\frac{\partial DC}{\partial t} + \frac{\partial DuC}{\partial x} + \frac{\partial DvC}{\partial y} + \frac{\partial wC}{\partial \sigma} - \frac{1}{D}\frac{\partial}{\partial \sigma}\left(K_h \frac{\partial C}{\partial \sigma}\right) - DF_c = DC_0(x, y, \sigma, t) \qquad (46)$$

where C is the concentration of the dye, D is the total depth, u,v, and w are the x,y, and σ components of the water velocity, K_h is the vertical diffusion coefficient, F_c is the horizontal diffusion term, and C_0 is the initial dye concentration.

The dye concentration is placed at every grid cell throughout all layers in the water column. The residence time within the bay is then calculated as the time it takes for each element's vertically-integrated concentration to drop as an exponential equation from an initial condition of 100 ppm to 36.78 ppm [*Burwell et al.,* 2000]. A High resolution numerical model is expected to provide accurate estimates of residence time in the bay and that is one of the objectives of this chapter. More details will be presented in the next session.

5.3   Results and Discussion

5.3.1   Results

5.3.1.1 First-Order Transport Time Scales

Due to the recirculating nature of the flow within the bay, if we consider a transect separating the bay from the rest of the lake (as shown in Figure 3), then flow enters the bay over a portion of the transect and exits over the remaining portion (Figure 18, 19). The relative extent of these inflow and outflow regions as well as the magnitude and direction of velocities along the transect exhibit unsteadiness throughout the simulation period. These complexities introduce difficulties in the application of the simple flushing time concept.

The exchanges between the inner and the outer bays and between the outer bay and the open lake fundamentally describe the mean residence time and contaminant flushing rates in Saginaw Bay. The complexity of flows and exchange rates can be seen in Figure 19, Figure 20 which shows the results of vertically-averaged currents from the LWM superimposed on surface temperatures in Saginaw Bay for a three year simulation period. The presence of two large recirculating cells in the inner bay can be clearly noticed (e.g., in July and August for all three years) and the dominant flow features can be related to the predominant wind patterns. Shown as wind rose plots in Figure 51 the length of the histogram denotes the frequency of winds coming from a certain direction while the color denotes the magnitude of the wind velocity.

Equation 47 was used to calculate the mean volumetric inflow into Saginaw Bay at the inner (1-1) and outer (2-2) transects shown in Figure 3a to facilitate the application of the flushing time concept. Horizontal velocities from the lake-wide model were interpolated to points on the Saginaw Bay transects and used in Equation 47 to calculate the mean inflow (Q_{in}) volume during the summer and winter months. The inflow volume at inner and outer transects were used to estimate the flushing rates for the inner and outer bay [*Saylor et al.*, 1976]. The flushing time (T_f) for the inner (and entire) bay are presented in Table 15 for summer months.

$$Q_{in} = \frac{1}{(t_2 - t_1)} \int_{t_1}^{t_2} \left[\int_0^B \left[\int_0^H v_{in}\, dh \right] db \right] dt \quad (47)$$

$$v_{in} = \begin{cases} v.\hat{n} & \text{if } v.\hat{n} > 0 \\ 0 & \text{if } v.\hat{n} \le 0 \end{cases}$$

Where $\vec{v}$ is the velocity (m/s) from the hydrodynamic model, B is the length of the inner (or outer) transect, H is the depth, t_1, t_2 are the start and end times for the calculations, and $\hat{n}$ is a unit

vector normal to the transect pointing into the bay (towards southwest). V is the volume of the inner (or entire) bay.

Figure 52 shows the vertically averaged volumetric influx as a function of time at the inner (and outer) transects for the summer months of 2009-2011. A significant difference between exchange at the outer transect 2-2 and at the inner transect 1-1 was found. Another notable feature is that the exchange at the outer transect has higher fluctuation compared to the one at the inner transect.
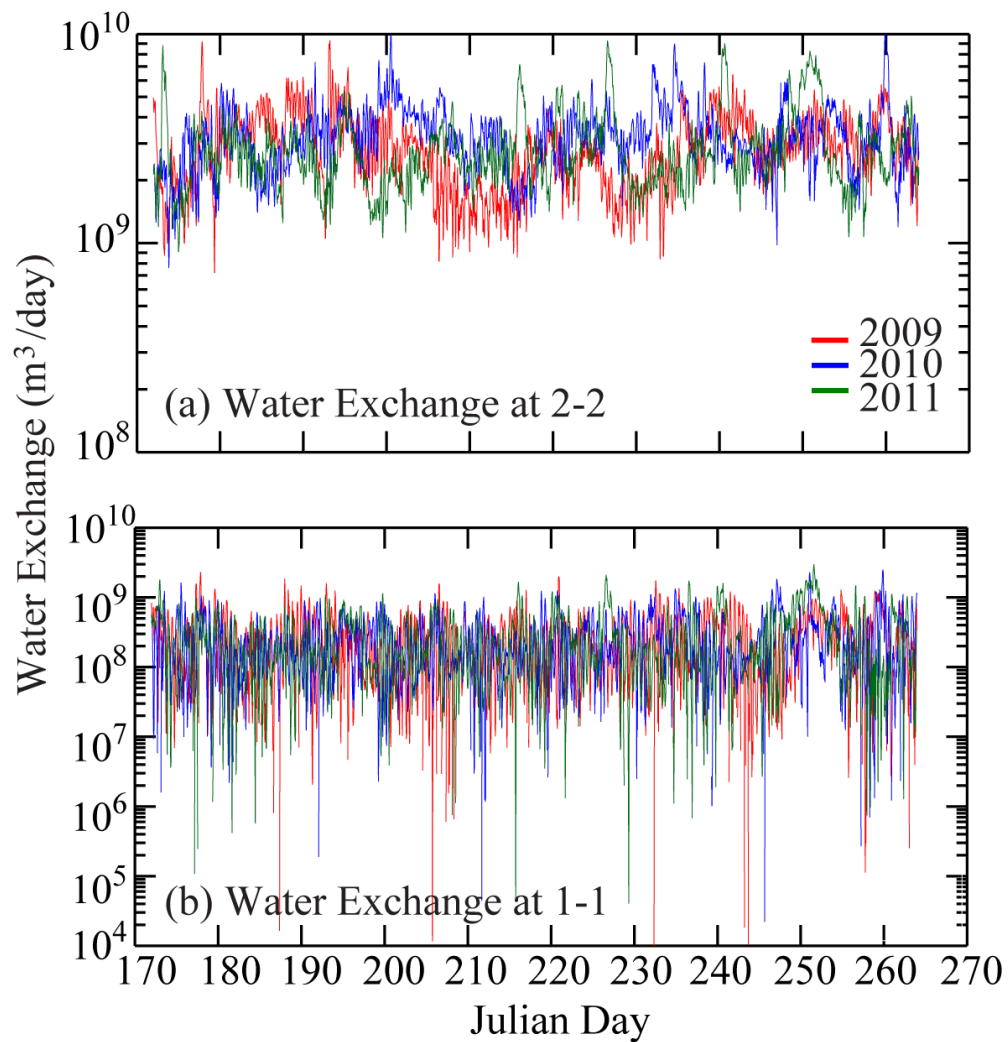
Figure 52: Time series of water exchange rates for the inner transect (1-1 in Figure 3) and the outer transect (2-2 in Figure 3) in Saginaw Bay in summer season.

Table 15: Mean flushing time T_f (in days) for inner and entire Saginaw Bay in summer months

Year	Areas	July	August	September
2009	Inner Bay	23.9	26.2	19.7
	Entire Bay	8.8	13.9	9.1
2010	Inner Bay	26.3	25.0	19.5
	Entire Bay	9.1	8.9	8.6
2011	Inner Bay	25.1	24.4	16.8
	Entire Bay	11.6	10.1	9.2
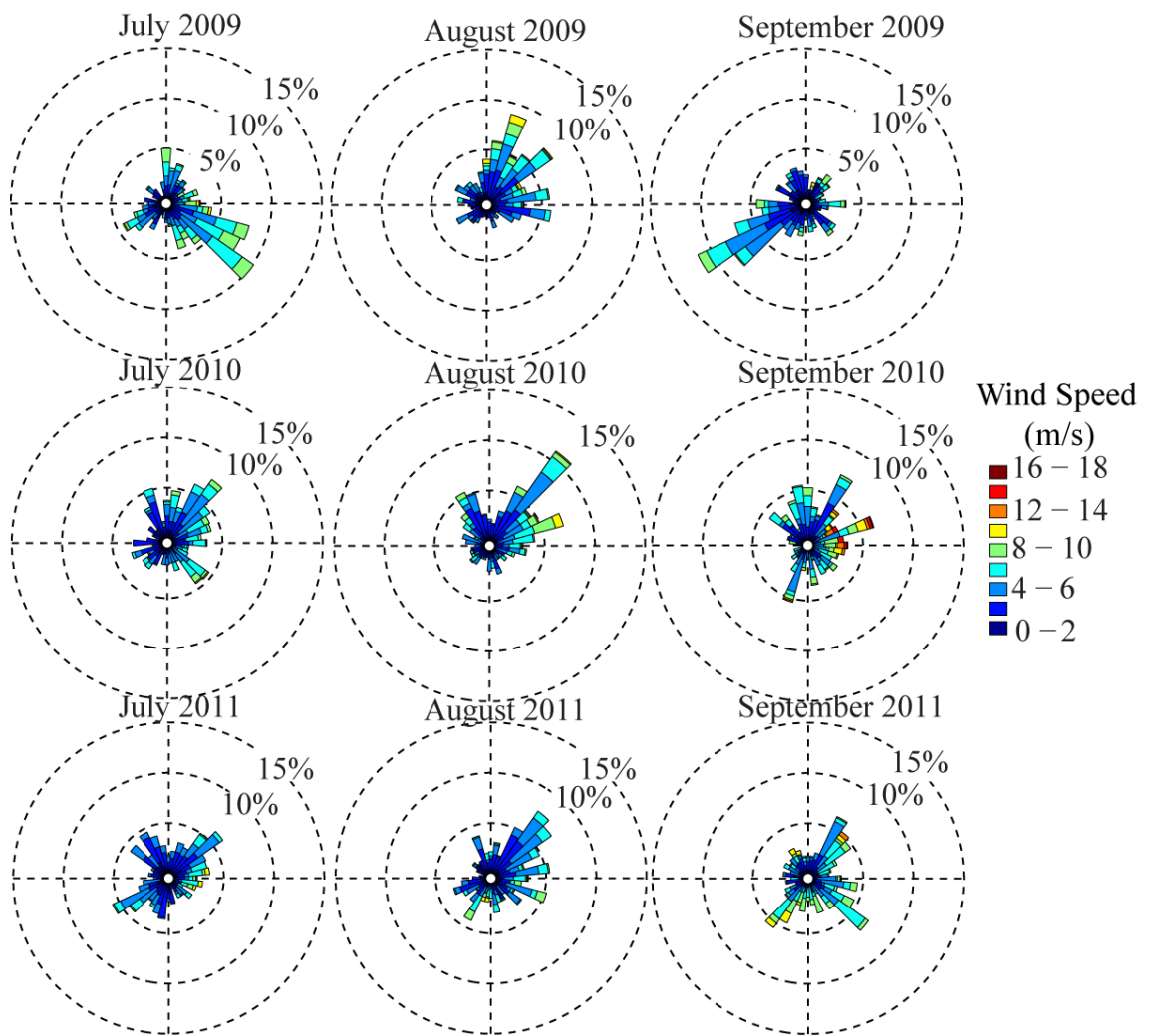
Figure 53: Wind rose plots for summer months during the years 2009-2011.

As stated in chapter 3, the circulation in Saginaw Bay is complex with either clockwise or counterclockwise circulation depending on the wind direction. The important feature of circulation in the bay was also characterized by the difference between hydrodynamics in the inner and outer bays and the effect on exchange between the two. The complexity of the circulation suggests that the hydrodynamics in both the inner and outer bays plays a significant role in the flushing time distribution. Here, the flushing time varies from one grid cell to other.

In order to find "*Dead-Zones*" and "*Flusing-time Maps*" we calculated the flushing time based on the results from the hydrodynamic model for every grid cell within the bay. Following this approach, the eastward and northward velocities obtained from the hydrodynamic model were interpolated into a high resolution structured grid of 200mx200m. Interpolated velocities were then used to calculate the mean volume inflow into each box with consideration of flux between adjacent boxes (Figure 54).
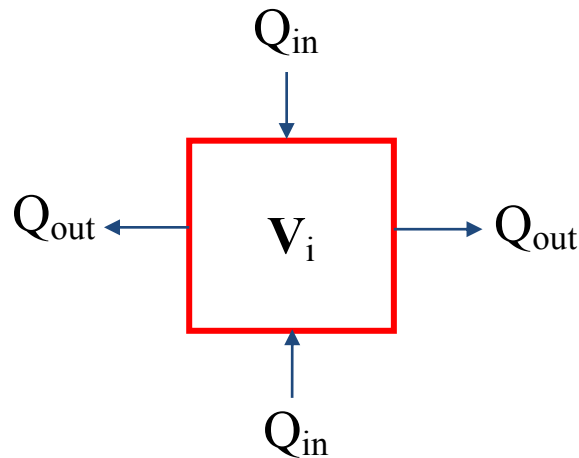
Figure 54: Example of a diagram depicting the water exchanges in a structured grid.

The flushing time for each structured grid cell can be calculated as the volume of each cell divided by the rate of inflow:

$$\tau_i = \frac{V_i}{q_i} \qquad\qquad (48)$$

Where: τ_i, V_i, and q_i are the flushing time, volume, and volumetric flow rate into box i[th], respectively. It should be noted that the calculation is based on the assumptions of steady-state, and constant-volume.

The flushing times were calculated for each summer month for 3 constitutive years (2009-2011) based on vertically integrated currents in the Saginaw Bay. The spatial map in Figure 55 shows the flushing time is mostly closely associated with the bathymetry map. The shallower areas have a shorter flushing time. The variability in estimates of flushing times within the bay can have important implications for stagnation areas between two large recirculating cells within the inner bay. It is important to recognize that the method of obtaining the total flushing time for the bay by accumulating flushing times from individual cells cannot be relied upon.
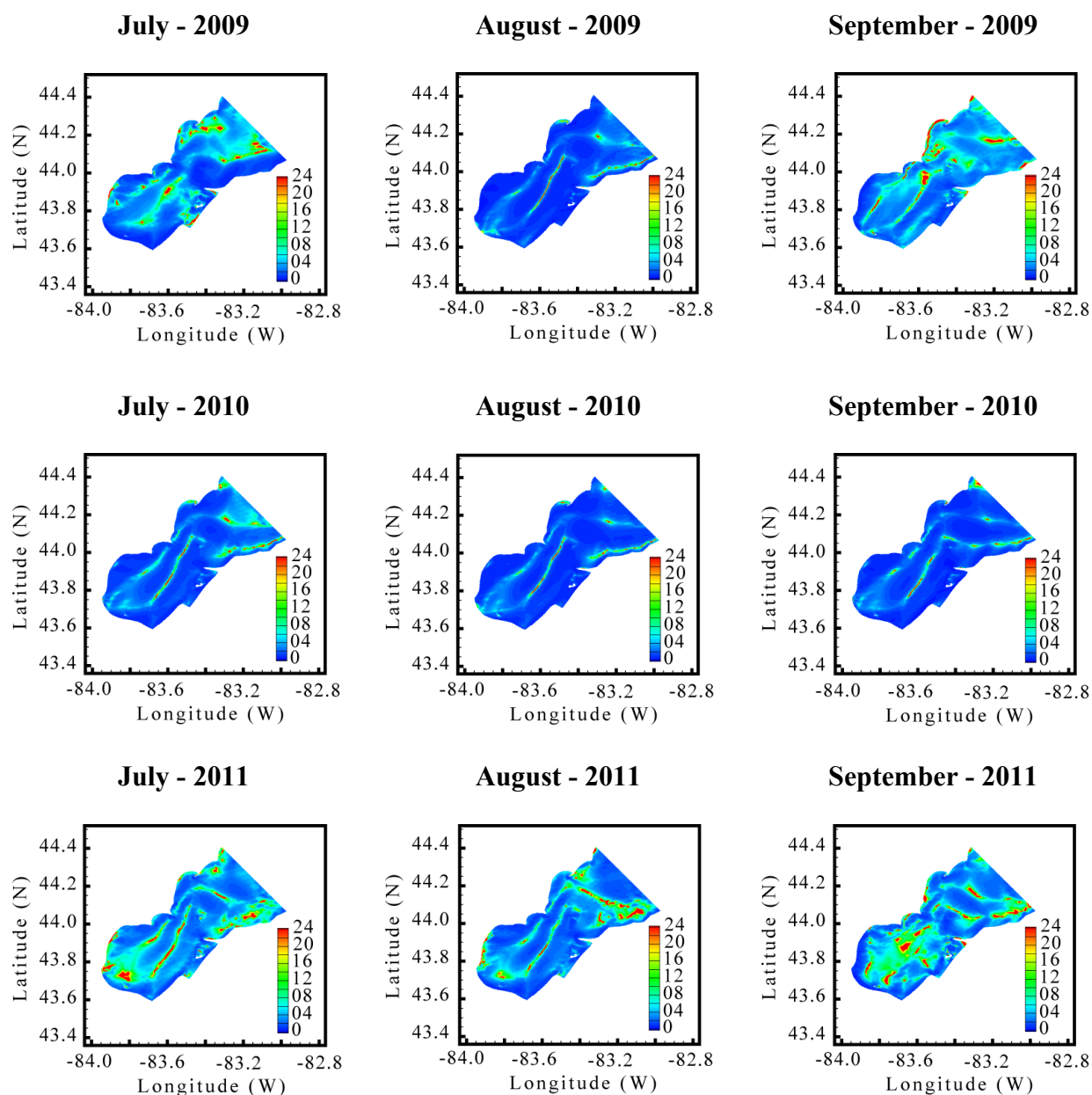
Figure 55: Map of Saginaw Bay showing the contour of flushing time in hours within the Bay calculated based on monthly average velocity.

133

Circulation in the Saginaw Bay in winter months was characterized by two large recirculating cells in the inner bay just as is observed in the summer months. The same approaches and equations were applied to calculate the water exchange and flushing time for the bay for winter in the years 2010 and 2013. Since the vertically integrated current velocity in winter is lower than in summer as shown in Figure 46, Figure 47, the flushing times are expected to be longer than in summer time. The vertically averaged volumetric inflow as a function of time in winter at the transect 1-1 and transect 2-2 are presented in Figure 56. The complexity of the exchange rates at outer transect in winter time can be seen by the fluctuation of volumetric influx and the difference of this index between the two winters (Figure56b).

Table 16: Mean flushing time T_f (in days) for inner and entire Saginaw Bay in winter months

| Year	Areas	Dec-2009/2012	Jan	Feb	Mar
2010	Inner Bay	15.2	33.9	108.0	18.1
	Entire Bay	13.9	11.7	18.5	11.2
2013	Inner Bay	20.8	27.0	75.7	46.9
	Entire Bay	18.8	19.7	16.6	14.5
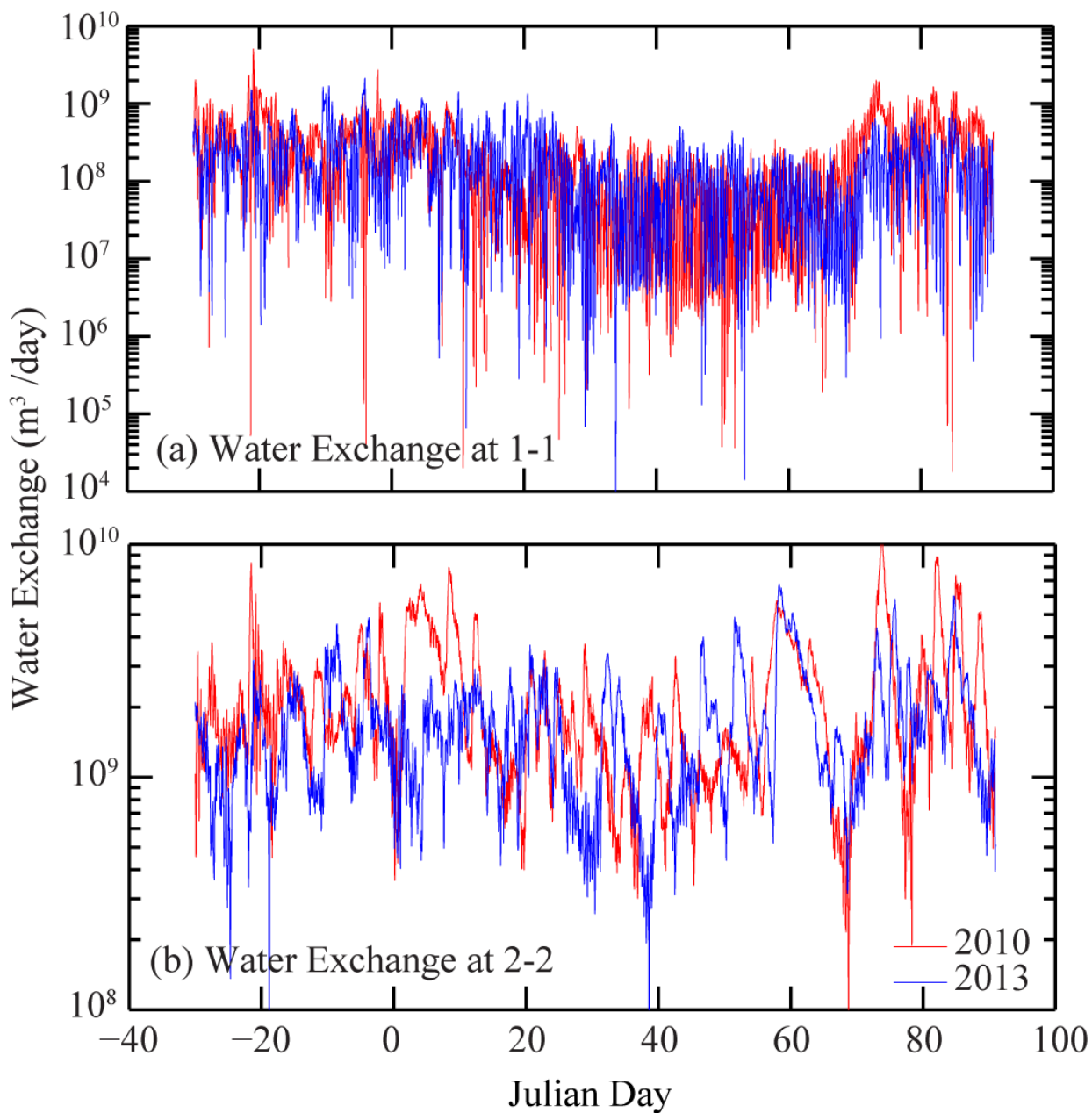
Figure 56: Time series of water exchange rates for the inner transect (1-1 in Figure 3) and the outer transect (2-2 in Figure 3) in Saginaw Bay in winter season.

135

5.3.1.2 The Eulerian Approach

In this approach, the bay was treated as a CSTR (continuously stirred tank reactor, [*Chapra, 2008*]). The residence time for every grid cell in the domain is then calculated as the time it takes for only 36.78% (e^{-1}) of the initial mass to remain within the bay. It is important to recognize that, due to zero-dimensionality and instantaneous mixing assumptions, the ideal CSTR case do not exactly represent real systems. However, the measures are still useful for understanding and interpreting the behavior of contaminants within the bay.

The same hydrodynamic model used for calculating the flushing time ($\boldsymbol{T_f}$) was used to calculate the residence time (expressed as the e-folding flushing time) assuming that the Saginaw Bay was a CSTR. Here it is possible to use different approaches as described in [*Burwell et al., 2000*]. A Lagrangian approach in which particles are released and tracked in every grid cell and an Eulerian approach in which the residence time is calculated based on dye concentration modeling are both options. We have used the second approach.

In this method, the dye concentration was calculated following the instantaneous dye release at an initial concentration of C_0 = 100 ppm in every grid cell in the bay area. The residence time is defined as the time it takes for each element's vertically-integrated concentration to decrease below 1/e of its initial vertically-integrated concentration [*Burwell et al., 2000*]. Since the residence time ($\boldsymbol{\tau_R}$) calculated using this definition would be different for every grid cell, an integrative system measure ($\boldsymbol{\tau_R}$) can be obtained by computing the spatial average of the vertically-integrated concentrations for all grid cells in the domain. This average concentration is only a function of time and does not depend on space. The residence time for the bay ($\boldsymbol{\bar{\tau}_R}$) is then calculated as the time it takes for the average vertically-integrated concentration

in the bay to fall below (1/e) of its initial concentration (i.e., below an average (C/C₀) value of 0.3678).

To understand the effect of the Saginaw River on the residence time, we calculate residence times with and without river flow entering the bay. For each case, the hydrodynamic model was run with flow (or no inflow) from the river and an initial concentration of 100 ppm in every grid cell. For the case with river inflow, the bay was subjected to the initial concentration of 100 ppm but the river water was assumed to be at a zero concentration; therefore, the residence time estimated for this case represents the effect of flushing of the initial water in the bay by the river. It is important to recognize that flushing time and residence time as calculated here can be expected to yield different estimates of transport timescales since the flushing time concept assumes that advective exchange is the only mechanism of transport, while the concentration-based residence time estimate considers the processes of both advection and dispersion in the modeling.

In order to investigate the effect of the ice cover on the residence time, we also calculated the residence times with and without ice model. The results will provide the ranges of the residence time for the winter with less ice coverage to the case of the severe winter with high ice cover.

The summer contour map of residence times in the inner bay and the entire bay with and without river inflow and the relationship between the vertically-integrated concentration averaged over the entire and inner bay and the residence time are presented in Figures 57 and 58 respectively. Similar contour maps for winter season are shown in Figure 59 and 60 for the case of without ice model and Figure 61 and 62 for the case of with ice model.
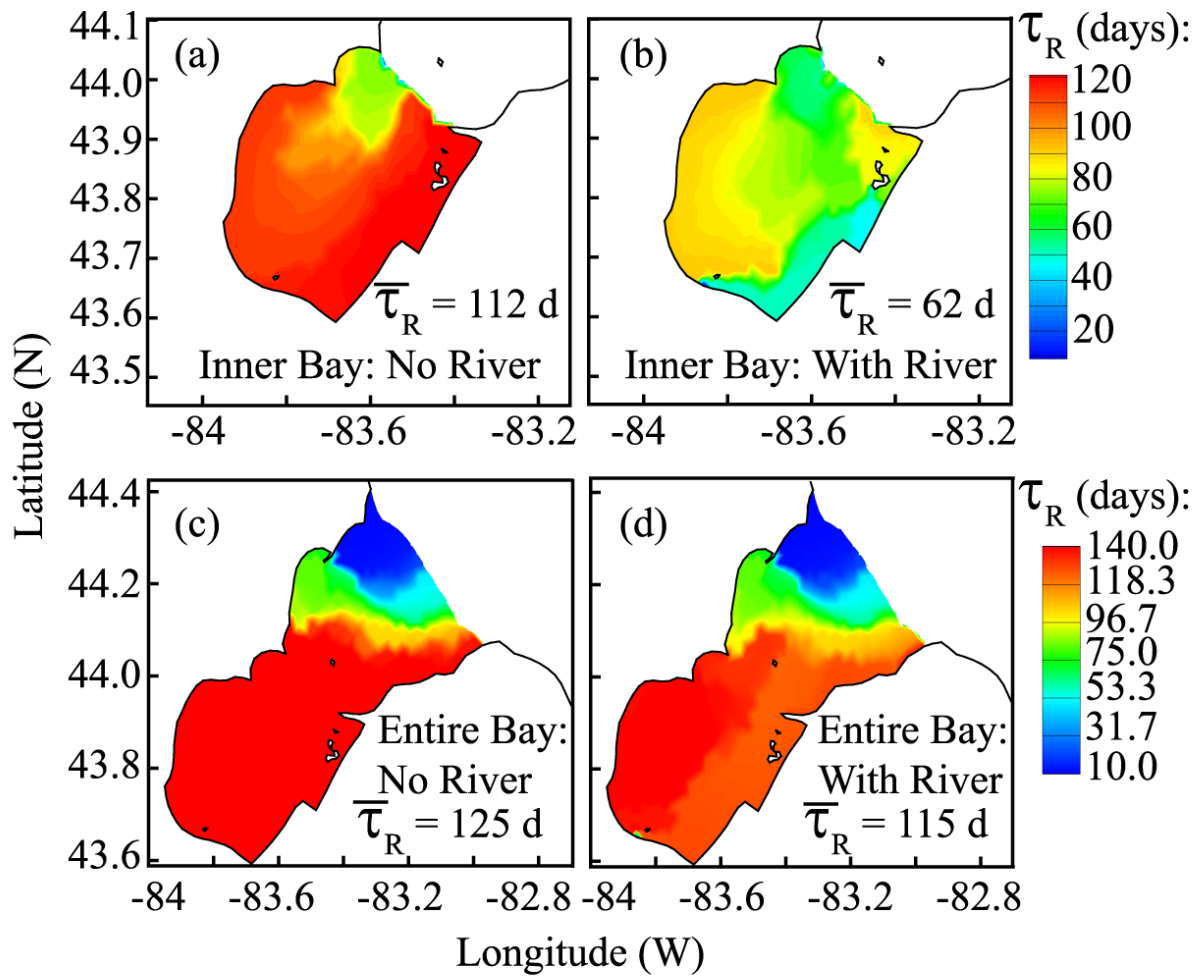
Figure 57: Contour plots of residence time for Saginaw Bay based on dye concentration modeling. Figures (a) and (b) are for inner bay dye releases with (a) no river inflow and (b) with river inflow. Figures (c) and (d) are results based on dye releases for the entire bay with (c) no river flow and (d) with river flow. (Summer season).

Figure 58: Average vertically-integrated concentration in the Saginaw Bay as a function of time. The red solid lines represent the model results while the blue dashed lines represent an exponential decay model fit to the data. The concentration value corresponding to a value of (1/e) is also marked. (Summer season).

The empirical relation curves between the residence time and average vertically-integrated concentration for the inner and entire bay in summer season are as follow:

For Inner Bay:

With River Inflow: ($R^2 = 0.85$)

$$\frac{c}{c_0} = 0.743 e^{-0.01095t} \qquad (49)$$

Without River Inflow: ($R^2 = 0.79$)

$$\frac{c}{c_0} = 0.767 e^{-0.00803t} \qquad (50)$$

For Entire Bay:

With River Inflow: ($R^2 = 0.95$)

$$\frac{c}{c_0} = 0.889 e^{-0.00816t} \qquad (51)$$

Without River Inflow: ($R^2 = 0.93$)

$$\frac{c}{c_0} = 0.926 e^{-0.00624t} \qquad (52)$$

where t is the residence time in day.

Table 17: Mean residence time (e-folding flushing time) in days for Inner and Entire Saginaw Bay in summer season

Year	Areas	Case	
		No river inflow	With river inflow
2011	Inner Bay	112	62
	Entire Bay	125	115
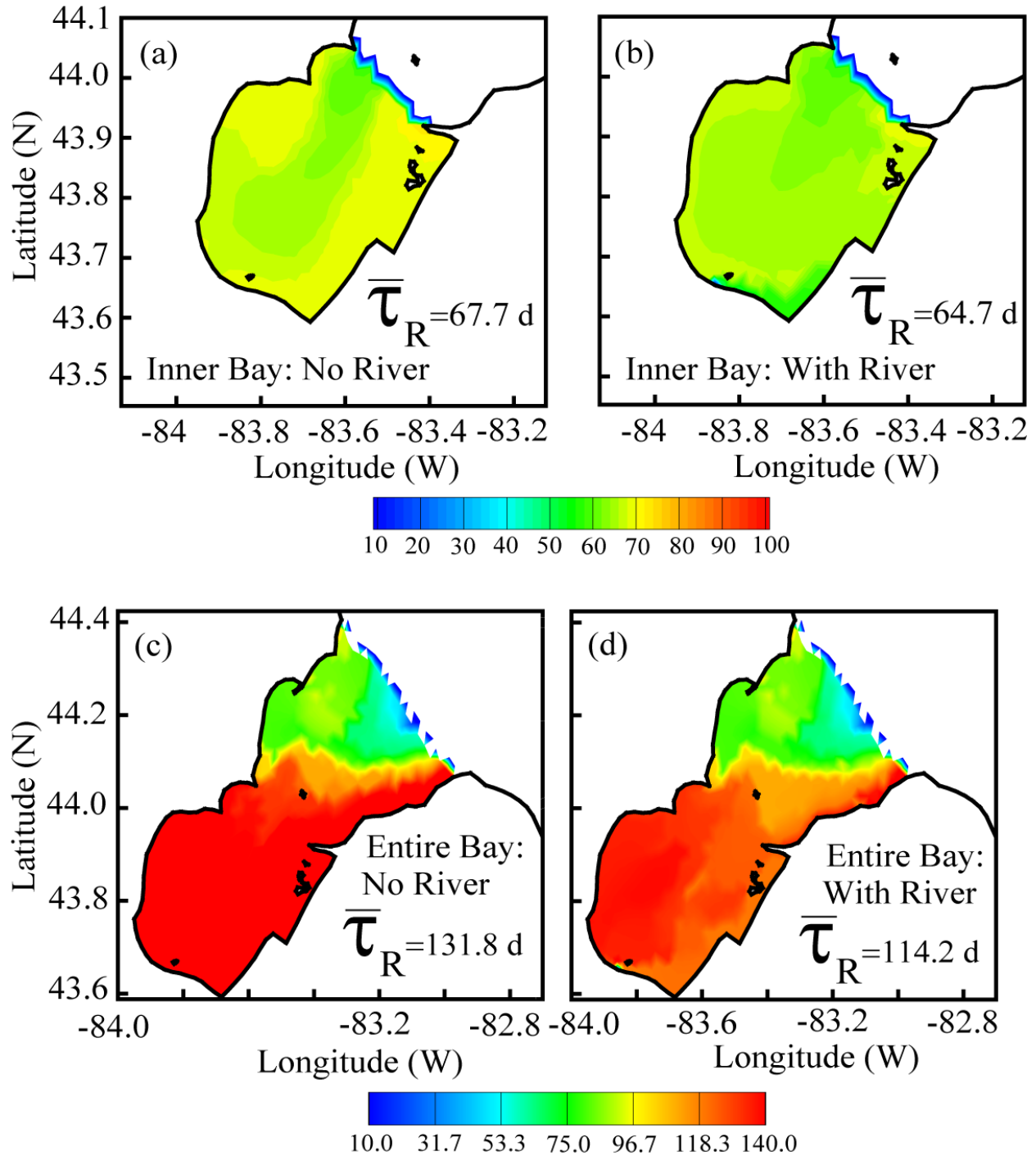
Figure 59: Contour plots of residence time for Saginaw Bay based on dye concentration modeling. Figures (a) and (b) are for inner bay dye releases with (a) no river inflow and (b) with river inflow. Figures (c) and (d) are results based on dye releases for the entire bay with (c) no river flow and (d) with river flow. (Winter season without Ice Model).
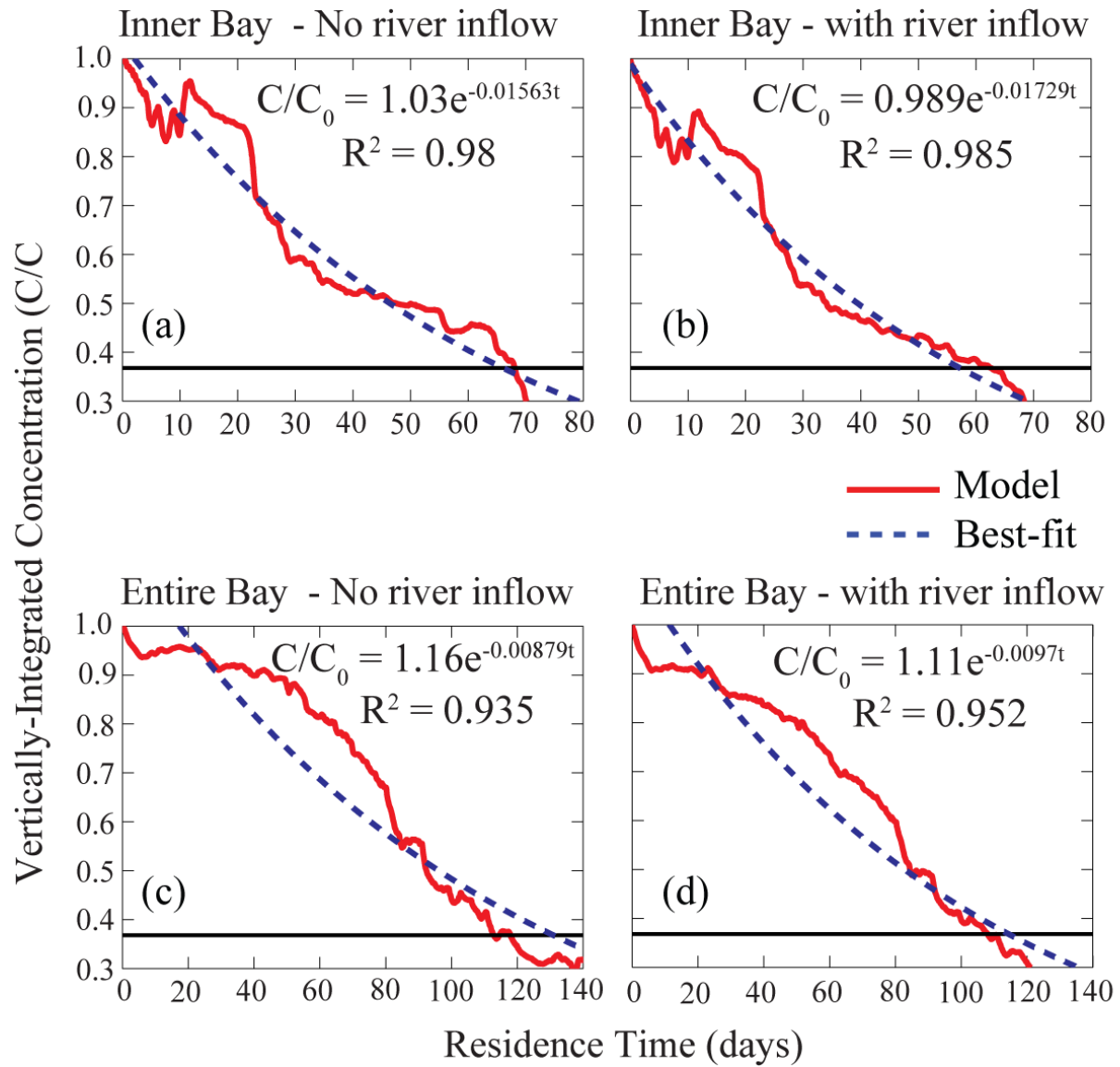
Figure 60: Average vertically-integrated concentration in the Saginaw Bay as a function of time. The red solid lines represent the model results while the blue dashed lines represent an exponential decay model fit to the data. The concentration value corresponding to a value of (1/e) is also marked. (Winter season without Ice Model).

The empirical relations curves for winter season for the case of without ice model are as follow:

For Inner Bay:

With River Inflow: ($R^2 = 0.985$)

$$\frac{c}{c_0} = 0.989e^{-0.01729t} \tag{53}$$

Without River Inflow: ($R^2 = 0.98$)

$$\frac{c}{c_0} = 1.03e^{-0.01563t} \tag{54}$$

For Entire Bay:

With River Inflow: ($R^2 = 0.952$)

$$\frac{c}{c_0} = 1.11e^{-0.0097t} \tag{55}$$

Without River Inflow: ($R^2 = 0.935$)

$$\frac{c}{c_0} = 1.16e^{-0.00879t} \tag{56}$$

| **Table 18:** Mean residence time (e-folding flushing time) in days for Inner and Entire Saginaw Bay in winter season (Without Ice Model)			
Year	**Areas**	**Case**	
		No river inflow	With river inflow
2013	Inner Bay	67.7	64.7
	Entire Bay	131.8	114.2
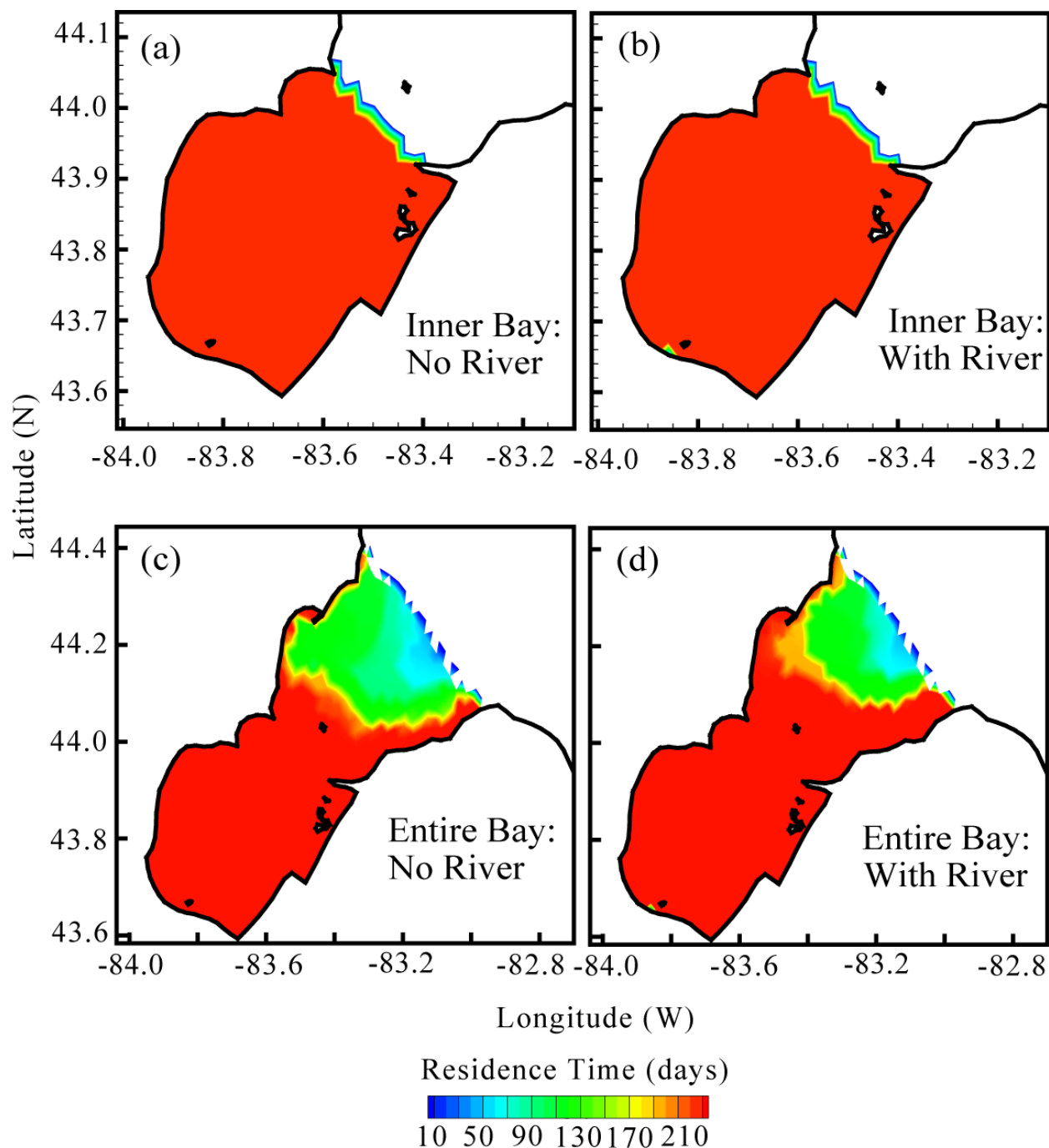
Figure 61: Contour plots of residence time for Saginaw Bay based on dye concentration modeling. Figures (a) and (b) are for inner bay dye releases with (a) no river inflow and (b) with river inflow. Figures (c) and (d) are results based on dye releases for the entire bay with (c) no river flow and (d) with river flow. (Winter season with Ice Model).
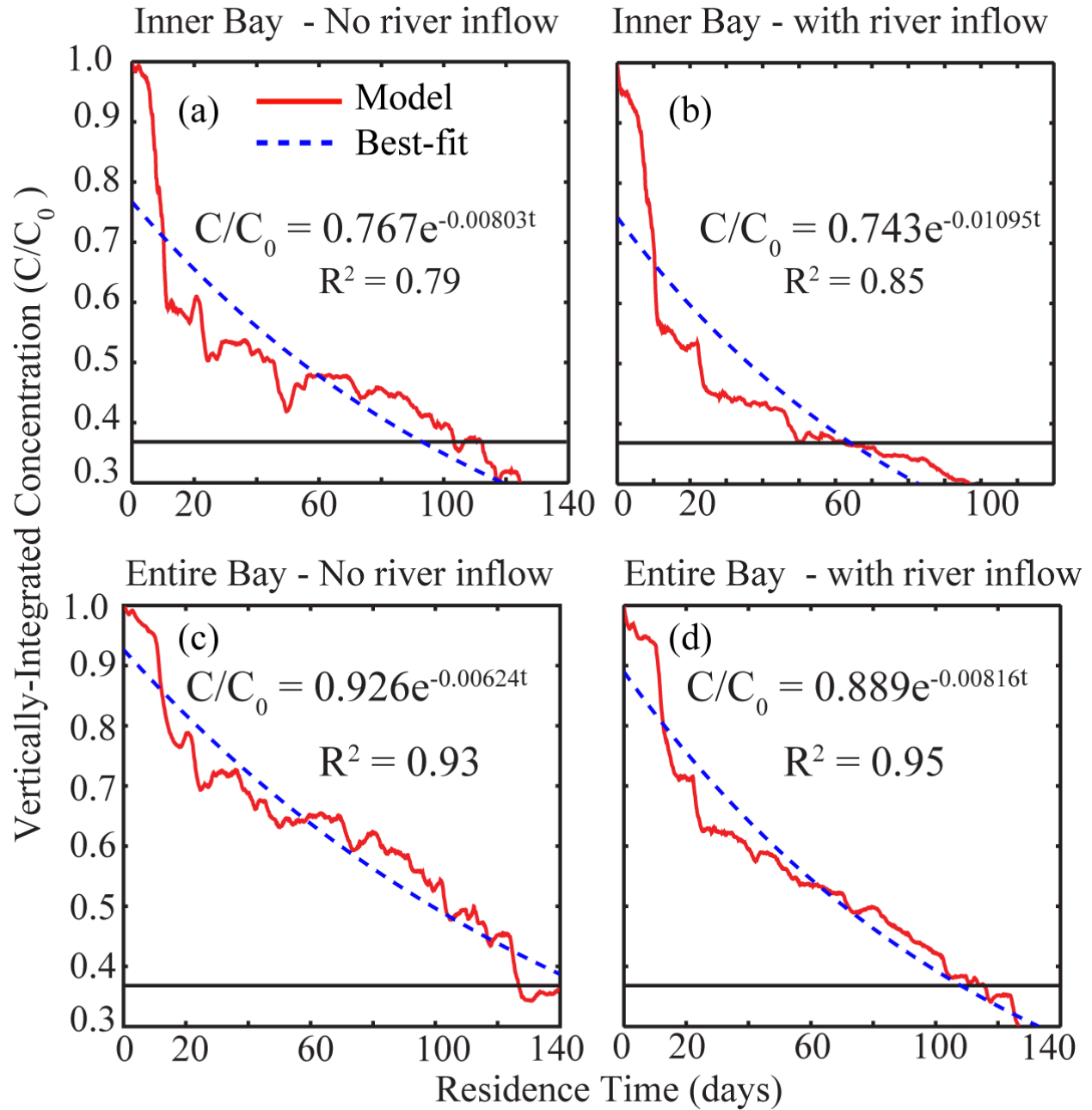
144
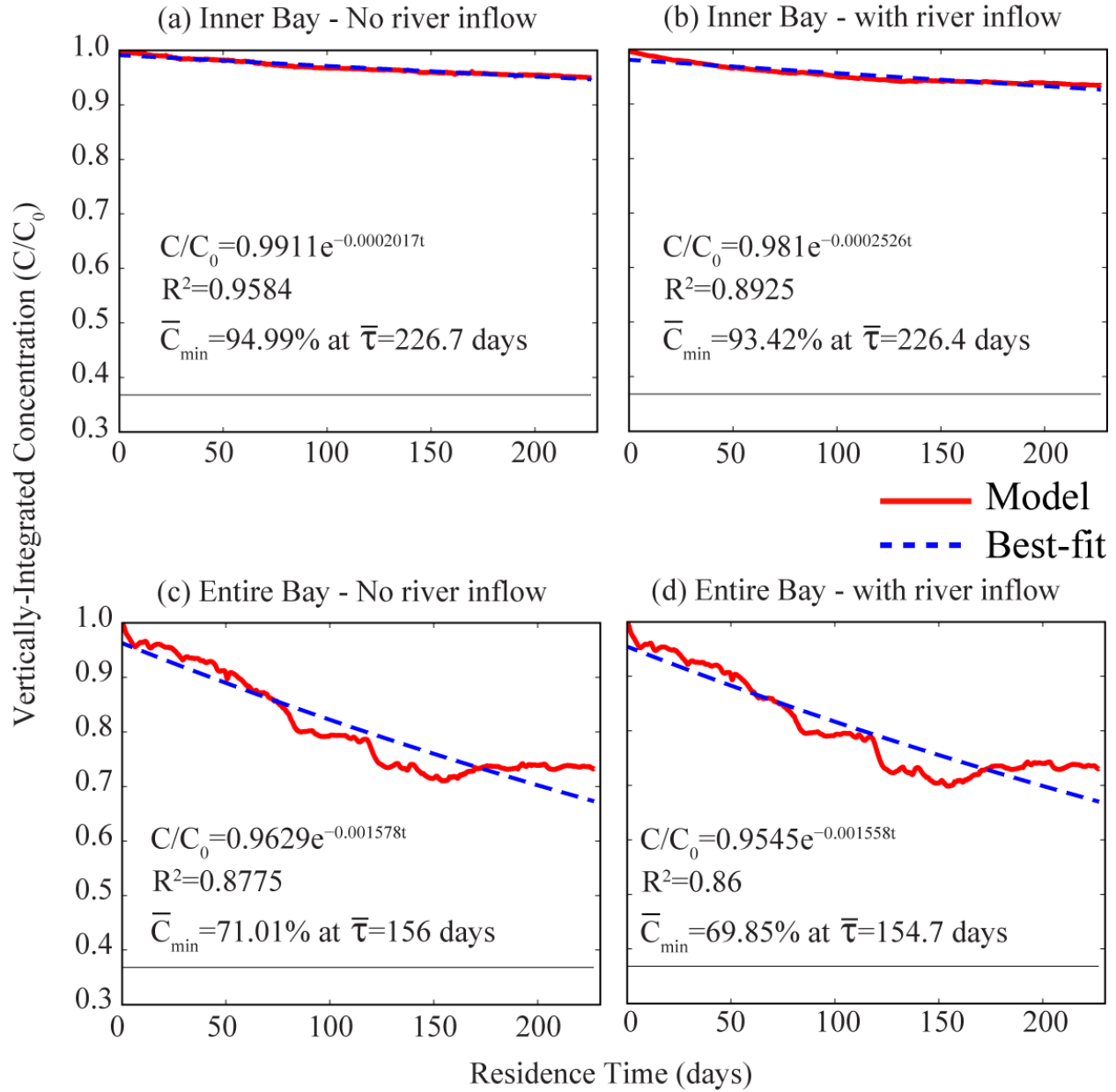
Figure 62: Average vertically-integrated concentration in the Saginaw Bay as a function of time. The red solid lines represent the model results while the blue dashed lines represent an exponential decay model fit to the data. The concentration value corresponding to a value of (1/e) is also marked. (Winter season with Ice Model).

The relations between the residence time and average vertically-integrated concentration in winter season for the inner and entire bay for the case of with ice model are shown in Figure 62. The results are quite different from the case of without ice model. For the case of with ice model, after about 226 days, the mean vertically-integrated concentration in the inner bay drop to 95% and 93.4% with no river inflow and with river inflow, respectively. Corresponding number for the entire bay are 71% and 69.8% after 156 days and 154.7 days, respectively.

Considering the residence time including mixing processes revealed the behavior of the bay under real meteorological conditions. Considerably different residence times were found for the cases with the river and without the river. This leads to the suggestion of the relationship between the residence time and the river discharge that will be presented in the next session.

5.3.2 Discussion

The mean residence time for contaminants entering the Saginaw Bay from point and non-point sources in the bay was estimated from two different methods. The first method used results from the lake-wide numerical model. The flushing rates for water (and dissolved contaminants) in the inner and outer bay were calculated using Equation (45) for different summer months during 2009-2011 and winter months during 2010, 2013 are presented in Table 15 and Table 16, respectively.

The mean flushing time for all three summers (and all 3 years) was 23.0 days for the inner bay and 9.9 days for the entire bay. In an earlier study, *Saylor et al*. [1976] estimated a mean flushing time of 26.5 days for the inner bay. This difference is explained by the change in volume of the inner bay (from 8.5 km^3 in 1976 to 6.5 km^3 in 2012) over the past four decades

146

due to falling lake levels. The results presented in Table 15 clearly show that flushing rate for the outer bay is almost twice as much as for the inner bay. This could be due to the role played by lake-wide circulation on flow in the outer bay. Currents within the Saginaw Bay are strongly affected by the direction of wind. Wind blowing out of the southwest or northeast is associated with higher mean current speeds and therefore, greater mixing and dilution as well as a smaller mean residence time. No such trend is apparent for the mean flushing rate for the outer bay, which is affected to a greater degree by the large-scale circulation. Exchange at the outer transect 2-2 (Figure 52a) is significantly higher compared to the exchange at the inner transect 1-1 (Figure 52b). We also notice that the rate of exchange between the inner and outer bays (Figure 52b) shows a significantly larger variation in summer time (varies by nearly four orders of magnitude) compared to the exchange between the outer bay and the lake (Figure 52a). One of the reasons for this large difference in the variability of exchange rates is the widely different cross-sectional areas at sections 1-1 and 2-2 in Figure 3a as well as the presence of an anticyclonic gyre in the outer bay (shown in Figure 19). The cross-sectional area for the inner bay transect 1-1 is approximately 0.09 km^2 while the area is 1.31 km^2 at the outer transect 2-2.

While in summer months the flushing time in the inner bay is nearly twice as much for the entire bay, the flushing time is almost similar in the inner and entire bay in the beginning of winter (in December) (Table 16). As the cooling air continues and with the presence of ice in January, February, and March there is a significant difference for the flushing time between the inner bay and entire bay. The maximum value of flushing time for the inner bay reached to 108 days in 2010. The difference can be explained by the role of ice cover during the winter time especially in inner bay area. The mean flushing time for two winters was 43.2 days for the inner bay and 15.6 days for the entire bay.

Using the First-Order transport time scale approach we calculated the flushing time for each structured grid cell within the bay as described in Figure 54 and Equation 48. The results show that as the month progresses in summer, the spatially flushing time distribution does not change except for the year 2011 (Figure 55). The areas with higher values of flushing times were found in the inner bay. It is clearly shown that the role of two gyres within the inner bay causes the occurrence of stagnation areas where there are longer flushing times.

Using an Eulerian dye concentration-based approach, we calculated the mean residence time (e-folding flushing time) in the bay as described earlier for both summer and winter seasons. The residence time results are shown in Table 17 and Table 18 for summer and winter season respectively. For summer season, the range of values is from 62 days to 125 days depending on whether inflow from the Saginaw River is considered or not. An earlier study by *Dolan* [1975] calculated a residence time of 110 days for the inner bay and 52 days for the entire bay based on a time-variable chloride model. Their results, based on "well-mixed" mass balance models [*Chapra*, 2008], allow the bay to be divided into a few (e.g.,three) segments taking both advective and dispersive exchange across segments into account. Since the present work is based on fully three-dimensional hydrodynamic and transport models, our residence time estimates can be expected to differ from those of *Dolan* [1975]. The results presented in Table 17 and Table 18 show that residence times calculated by the Eulerian dye concentration-based model are greater than the mean flushing times calculated using the first method which considers only advective exchange. This difference can be explained by the increased time due to mixing and dilution in the entire bay.

For summer months, the low residence times occur in the middle of the bay, and high residence times occur along the shoreline and the Saginaw river mouth areas (Figure

148

57). With dye release into the entire bay, low residence times were found in the areas near the mouth of the Saginaw Bay (5 to 50 days) while the remaining areas have relatively high residence times (more than 140 days, Figure 57). The figure clearly shows the important role played by the gyres near the mouth of the outer Saginaw Bay on residence times. As can be seen from Figure 57, river inflow has a significant effect on the residence time of the inner bay although the effect is almost insignificant when the entire bay is considered (Figure 57d). This is not surprising since the inner bay is fairly shallow and is readily influenced by riverine discharge while the gyres and the larger lake-wide circulation mainly influence the outer bay residence time. Figure 58 shows the vertically-integrated concentrations within the bay (averaged over the spatial extent of the bay) as a function of time for the different cases considered (inner bay and entire bay with and without river flow). The figure shows the models results and the best exponential-fit to the models results. Generally, the declining concentrations follow an exponential curve with R^2 values ranging from 0.79 to 0.95. The empirical equations between the residence time and average vertically-integrated concentration are shown in the Equation 49 to Equation 52 for inner and outer bay.

For winter months without ice model, the residence time patterns in the inner bay are similar for the case of with river and no river inflow with mean residence times of 67.7 days and 64.7 days respectively. The low residence times occur in the middle of the inner bay with the value of about 60 days. For the case of dye release into the entire bay, the longer mean residence times were found for the case of with and no river inflow of 131.8 days and 114.2 days respectively. The lowest residence times were found in the areas in the northwest of the mouth of the Saginaw Bay of about 75 days. This value is relatively higher the results from summer season (5 to 50 days). The results from the winter simulation clearly show the important role of

the gyres near the mouth of the Saginaw Bay on residence time. The empirical equations between the residence time and average vertically-integrated concentration are shown in the Equation 53 to Equation 56 for inner and outer bay.

For winter months with ice model, the minimum of average vertically-integrated concentration is 69.8% for the entire bay. For the inner bay, the dye concentration decrease only 5% through winter months. In this case, we still see the effect of the gyres near the mouth of the Saginaw Bay where the residence times are about 130 days in the outer bay area.

The results of residence time from the Eulerian method above indicate large variation in residence time between the cases includes river inflows and no river inflows. It implies the significance role of the Saginaw River discharge to the residence time in the Saginaw Bay. A very important question concerns the residence time in the Saginaw Bay under different Saginaw River inflows, but this is still poorly understood. The variation of residence times are expected to be consistent with how much the river discharge flows into the bay. In other words, there should be a relationship between the residence time of the Bay and the river discharge.

The experimental investigations were undertaken to provide additional insights into the relationship between river discharge and residence time. No difference is made in the dye concentration modeling except the input of river discharge in which the river discharge was kept as a constant through the whole simulation. Although, it may be not a real condition, it is very seldom that there is a steady river flow rate for a long time but it is still useful for understanding and interpreting the behavior of system to the river inflow.

Table 19: Statistical data for daily discharge in m^3/s					
Min	25th percentile	Median	Mean	75th percentile	Max
15.2	49.55	81.27	114.9	140.01	523.86

We used a statistical data of the USGS station on Saginaw River listed in Table 19. The residence time estimated from dye concentration analysis versus fresh water input rate from the Saginaw River shown in Figure 63. Exponential least-squares regression fit to the results are also given for each case of simulation.

The correspondence between river flow rate and the mean residence time is high with R^2 of about 0.97 (Figure 63). For the entire bay, the residence time is nearly 115 days at minimum of flow rate from river of 15.2 m^3/s, while under maximum of flow rate at 523.86 m^3/s the residence time to be 93 days. For the inner bay, the residence times are 85 days and 55 days, respectively. There is not large difference in the residence time index at the long-term mean and at the minimum flow rate for both entire and inner bay cases. While the residence time is expected to be strongly influenced by the wind speed and wind direction, the strong connection between the mean residence time and river discharge could be caused by other factors such as mixing processes and dilution as well. It should be noted that there is no significant difference in mean residence times for cases where the value of river discharge is less than the 75th percentile, as illustrated in Figure 63. The declining mean residence time as a function of river discharge follows an exponential curve with relatively high value of R^2 of 0.97 as shown in Equation 57 and Equation 58.

For Inner Bay: ($R^2 = 0.976$)

$$\bar{\tau} = 88.63e^{-0.0008288Q} \qquad (57)$$

For Entire Bay: ($R^2 = 0.971$)

$$\bar{\tau} = 117.7e^{-0.0004192Q} \qquad (58)$$

Where Q is river discharge (unit: m^3/s); $\bar{\tau}$ is mean residence time (unit: in day).
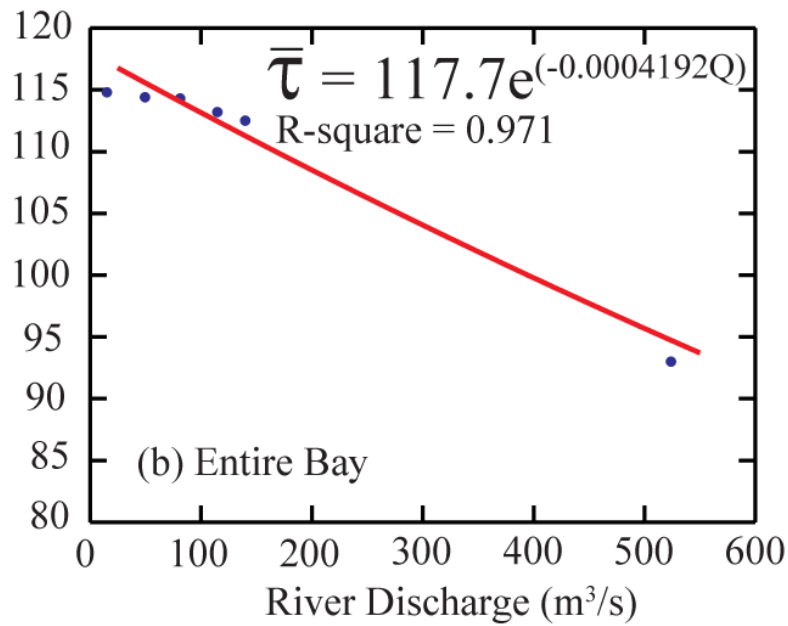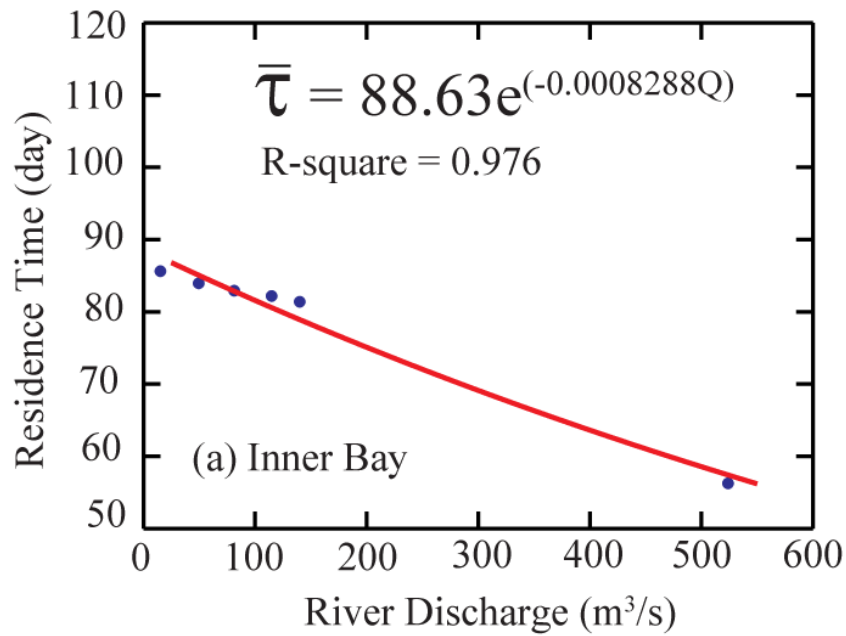
Figure 63: Mean residence time as a function of river discharge for (a) Inner Bay and (b) Entire Bay. The blue solid dots represent the model results while the red line represents an exponential equation fit to the data. The residence times were calculated based on the dye concentration model under summer meteorological conditions.

5.4   Conclusions

Residence time, an important environmental attribute of the bay is determined for both summer and winter seasons. The data and interpretations in the study will bring about a broader understanding of the residence time in Saginaw Bay. The numerical model result is used to calculate the water mass exchange rates and residence time for Saginaw Bay. The influx rates (m^3/s) at two transects (1-1 and 2-2 in Figure 3a) across Saginaw Bay were used to estimate the mean flushing times for the inner and outer Saginaw Bay. The mean flushing time for the inner bay (~23.0 days) was approximately twice that for the entire bay (~9.9days) in summer season. This difference is explained by the topographical features (sill) and the gyres that limit exchange in the inner bay along with the large-scale circulation features that increase the exchange rate for the outer bay. Comparing our results with earlier studies [*Saylor et al.,* 1976] on the exchange rate for Saginaw Bay, we found that the difference is explained by the change in volume of the inner bay in the last four decades due to falling lake levels. There is a notable feature that the mean flushing time for the inner bay (~ 43.2 days) was a significant difference from the corresponding number for the entire bay (~15.6 days) for winter months.

In the summer, the mean e-folding flushing time was found to be 62 days (2 months) for the inner bay and 115 days (3.7 months) for the entire bay. While in winter, the mean e-folding flushing time was 64.7 days and 114.2 days for the inner and entire bay respectively. The declining mean residence time as a function of river discharge was found as an exponential curve with high value of R^2 of 0.97 for both case of inner and entire bay.

Chapter 6

Conclusions

The aim of this study was to describe lake circulation, thermal structure, and exchange in the Saginaw Bay - Lake Huron system under summer and winter conditions. The summer and winter circulations were examined using an unstructured grid hydrodynamic model based on the FVCOM. Several field datasets based on ADCP, thermistor chain and Lagrangian drifters as well as satellite-based datasets for ice cover extent were used to test the numerical models. The comparisons between the simulated and observed results show that the model was able to reproduce the circulation patterns and temperature distribution in the lake very well. The model was run for 3 constitutive years in summer and 2 years in winter seasons.

The hydrodynamic model was able to reproduce the anti-cyclonic (counterclockwise) lake-wide circulation patterns that have been observed in earlier numerical and field studies on Lake Huron for both summer and winter seasons. We found that mean current speeds in Lake Huron were 3 cm/s and 1.14 cm/s during summer and winter periods respectively. The complex topography coupled with stratification and rapid warming of the southern part of the lake results in high inter-annual variability in surface temperature values during summer. Several potential upwelling regions have been identified where topographically-driven upwelling brings cold water from the deeper layers to the surface. One such region is in the strait connecting Lake Huron with Georgian Bay. In addition to upwelling, our simulations show that in the surface

layer (epilimnion) mean flow during summer is from Lake Huron into Georgian Bay, which sets up a return flow in the deeper layers (hypolimnion) from the bay into the lake. Since the hypolimnion is 3-4 times thicker than the epilimnion in this part of the lake, surface velocities are several times larger in magnitude than the velocities in the deeper layers.

In winter time, the simulations show that there is reverse flow at the mouth of Georgian Bay with the outflow from Georgian Bay to Lake Huron at the surface layer and inflow at the bottom layer. The results show that the ice model was able to reproduce the thermal evolution, presence of ice cover, ice concentration, and ice thickness reasonably well. The effects of ice cover on the circulation were also demonstrated where the inner bay was almost in a stagnation state during February.

Based on the model results, the water mass exchange rates for Saginaw Bay were calculated. The influx rates (m^3/s) at two transects (1-1 and 2-2 in Figure 1) across Saginaw Bay were used to estimate the mean flushing times for the inner and outer Saginaw Bay. The mean flushing time for the inner bay (~23.0 days) was approximately twice that for the entire bay (~9.9days) in summer time. This difference is explained by the topographical features (sill) and the gyres that limit exchange in the inner bay and the large-scale circulation features that increase the exchange rate for the outer bay. Comparing our results with earlier studies [*Saylor et al.,* 1976] on the exchange rate for Saginaw Bay, we found that the difference is explained by the change in volume of the inner bay in the last four decades due to falling lake levels. The mean flushing time for the inner and entire bay in winter time was found is 43.2 days and 15.6 days, respectively. The mean e-folding flushing time was 62 days for summer and 64.7 days for winter for the inner bay and 115 days for the summer and 114.2 days for the winter conditions for the entire bay.

Results from the Lagrangian drifter study in Saginaw Bay showed the highly anisotropic and time-variable nature of dispersion near the mouth of Saginaw River. The numerical model was able to predict the drifter trajectories and dispersion coefficients reasonably well.

BIBLIOGRAPHY

BIBLIOGRAPHY

Andréfouët, S., Pages, J., & Tartinville, B. (2001). Water renewal time for classification of atoll lagoons in the Tuamotu Archipelago (French Polynesia).*Coral reefs*, 20(4), 399-408.

Andutta, F. P., P. V. Ridd, and E. Wolanski (2012), The age and the flushing time of the Great Barrier Reef waters. *Continental Shelf Research*.

Allender, J. H. (1975), Numerical simulation of circulation and advection-diffusion processes in Saginaw Bay, Michigan. (Doctoral dissertation, University of Michigan).

Allender, J. H., & A. W. Green (1976), Free mode coupling of Saginaw Bay and Lake Huron. *Journal of Great Lakes Research*, 2(1), 1-6.

Alm, E, W, Janice Burke, and Erin Hagan (2006), Persistence and Potential Growth of the Fecal Indicator Bacteria, Escherichia coli, in Shoreline Sand at Lake Huron. *J. Great Lakes Res.* 32:401–405.

Anderson, E. J., D. J. Schwab (2013), Predicting the oscillating bi-directional exchange flow in the Straits of Mackinac. *Journal of Great Lakes Research* 39(4):9 pp.

Andradóttir, H. Ó., F. J. Rueda, J. Armengol, and R. Marcé(2012), Characterization of residence time variability in a managed monomictic reservoir. *Water Resources Research*, 48(11).

Annear, R. L., and S. A. Wells (2007), A comparison of five models for estimating clear-sky solar radiation. *Water Resources Research*, 43(10).

Assel, R. A. (2005). Classification of Annual Great Lakes Ice Cycles: Winters of 1973–2002. *Journal of climate*, 18(22).

Assel, R. A., Robertson, D. M., Hoff, M., & Selgery, J. (1995). Climatic change implications of long-term (1823–1994) ice records for the Laurentian Great Lakes. *Ann. Glaciol*, 21, 383-386.

Assel, R., Cronk, K., & Norton, D. (2003). Recent trends in Laurentian Great Lakes ice cover. *Climatic Change*, 57(1-2), 185-204.

Bai, X., J. Wang, C. Sellinger, A. Clites, and R. Assel (2012), Interannual variability of Great Lakes ice cover and its relationship to NAO and ENSO, *J. Geophys. Res.*, 117, C03002.

Bai, X., J. Wang, D.J. Schwab, Y. Yang, L. Luo, G. A. Leshkevich, and S. Liu (2013),Modeling 1993-2008 climatology of seasonal general circulation and thermal structure in the Great Lakes using FVCOM. *Ocean Modeling,* 65:40-63.

Beletsky, D., J. H. Saylor, and D. J. Schwab (1999), Mean circulation in the Great Lakes. *J. Great Lakes Res.*, 25,78–93.

Beletsky, D., & Schwab, D. J. (2001). Modeling circulation and thermal structure in Lake Michigan: Annual cycle and interannual variability. *Journal of Geophysical Research: Oceans* (1978–2012), 106(C9), 19745-19771.

Bennett Jr, T. J. (1982). A coupled atmosphere-sea ice model study of the role of sea ice in climatic predictability. *Journal of the Atmospheric Sciences*, 39(7), 1456-1465.

Berliand, T. C. (1960). Method of climatological estimation of global radiation.*Meteorol. Gidrol*, 6, 9-12.

Bierman, V. J, Jr. Jagjit Kaur, Joseph V. DePinto, Timothy J. Feist, and David W. Dilks, Modeling the Role of Zebra Mussels in the Proliferation of Blue-green Algae in Saginaw Bay, Lake Huron. *J. Great Lakes Res.* 31:32–55

Bolin, B., and , H. Rodhe (1973), A note on the concepts of age distribution and transit time in natural reservoirs. *Tellus*, 25(1), 58-62.

Brown, J., J. MacMahan, and A. Reniers (2009), Surf zone diffusivity on a rip-channeled beach. *Journal of Geophysical Research* 114.C11: C11015.

Boyce, F. M., M. A. Donelan, P. F. Hamblin, C. Murthy, T. Simons (1989), Thermal structure and circulation in the Great Lakes. *Atmosphere-Ocean* 27, 607–642.

Bunker, A. F. (1976), Computations of surface energy flux and annual air-sea interaction cycles of the North Atlantic ocean.

Burwell, D., M. Vincent, M. Luther, and B. Galperin (2000), Modeling residence times: Eulerian versus Lagrangian, in *Estuarine and Coastal Modeling*, eds. M.L. Spaulding and H.L. Butler, ASCE, Reston, VA, pp. 995-1009.

Camacho, R. A., and J. L. Martin (2012), Hydrodynamic Modeling of First-Order Transport Timescales in the St. Louis Bay Estuary, Mississippi. *Journal of Environmental Engineering*, 139(3), 317-331.

Chapra, S. C. (2008), *Surface Water-Quality Modeling*, Waveland Press, Long Grove, IL, USA.

Chen, C., H. Liu, R. C. Beardsley (2003), An unstructured, finite-volume, three-dimensional, primitive equation ocean model: application to coastal ocean and estuaries. *J. Atmos. Oceanic Technol.*, 20, 159–186.

Chen, C. et al, An unstructured, finite-volume, three-dimensional, primitive equation ocean model: FVCOM user manual (2013).

Danek, L. J., and J. H. Saylor (1977), Measurements of the summer currents in Saginaw Bay, Michigan.*Journal of Great Lakes Research*, 3(1), 65-71.

Delhez, E. J. M., G. Lacroix, E. Deleersnijder (2004b), The age as a diagnostic of the dynamics of marine ecosystem models. *Ocean Dynamics* 54, 221–231.

Dolan, D. M. (1975), Saginaw Bay residence time. Internal Working Paper, US EPA, Large Lakes research Station, Grosse Ile, Michigan.

Fahnenstiel, G. L., Lang, G. A., Nalepa, T. F., & Johengen, T. H. (1995). Effects of Zebra Mussel (Dreissena polymorpha) Colonization on Water Quality Parameters in Saginaw Bay, Lake Huron. *Journal of Great Lakes Research*, 21(4), 435-448.

Fairall, C. W., Bradley, E. F., Rogers, D. P., Edson, J. B., & Young, G. S. (1996). Bulk parameterization of air- sea fluxes for tropical ocean- global atmosphere coupled- ocean atmosphere response experiment. *Journal of Geophysical Research: Oceans* (1978– 2012), 101(C2), 3747-3764.

Figueroa, D., & Moffat, C. (2000). On the influence of topography in the induction of coastal upwelling along the Chilean coast. *Geophysical Research Letters*, 27(23), 3905-3908.

Fischer, H. B. (Ed.). (1979). Mixing in inland and coastal waters.

Fishman, D. B., Adlerstein, S. A., Vanderploeg, H. A., Fahnenstiel, G. L., & Scavia, D. (2009). Causes of phytoplankton changes in Saginaw Bay, Lake Huron, during the zebra mussel invasion. *Journal of Great Lakes Research*,35(4), 482-495.

Galperin, B., Kantha, L. H., Hassid, S., & Rosati, A. (1988). A quasi-equilibrium turbulent energy model for geophysical flows. *Journal of the Atmospheric Sciences*, *45*(1), 55-62.

Ge, Z., R. L. Whitman, M. B. Nevers, M. S. Phanikumar, and M. N. Byappanahalli (2012b), Nearshore hydrodynamics as loading and forcing factors for*Escherichiacoli*contamination at an embayed beach,*Limnol. Oceanogr.*,57(1), 362– 381, doi:10.4319/lo.2012.57.1.0362.

Geyer, W. R. (1997), Influence of wind on dynamics and flushing of shallow estuaries. Estuarine, *Coastal and Shelf Science*, 44(6), 713-722.

Go´mez-Gesteira, M., M. deCastro, and R. Prego (2003), Dependence of the water residence time in Ria of Pontevedra (NW Spain)on the seawater inflow and the river discharge. *Estuarine Coastal and Shelf Science* 58, 567–573.

Harrington, M. W. (1894), Currents of the Great Lakes as deduced from the movements of bottle papers during the seasons of 1892 and 1893. U.S. Weather Bureau, Washington, D.C.

Heath, R. T., Fahnenstiel, G. L., Gardner, W. S., Cavaletto, J. F., & Hwang, S. J. (1995). Ecosystem-Level Effects of Zebra Mussels (Dreissena polymorpha): An Enclosure Experiment in Saginaw Bay, Lake Huron. *Journal of Great Lakes Research*, 21(4), 501-516.

Hecky, R. E., Smith, R. E., Barton, D. R., Guildford, S. J., Taylor, W. D., Charlton, M. N., & Howell, T. (2004). The nearshore phosphorus shunt: a consequence of ecosystem engineering by dreissenids in the Laurentian Great Lakes. *Canadian Journal of Fisheries and Aquatic Sciences*, 61(7), 1285-1293.

Hsu, K., M. T. Stacey, and R. C. Holleman (2011), Exchange between an estuary and an intertidal marsh and slough. Estuaries and Coasts, 1-13.

Hunke, E. C., & Lipscomb, W. H. (2010). CICE: the Los Alamos sea ice model, documentation and software user's manual, Version 4.1.

Kraines, S. B., Isobe, M., & Komiyama, H. (2001). Seasonal variations in the exchange of water and water-borne particles at Majuro Atoll, the Republic of the Marshall Islands. *Coral Reefs*, 20(4), 330-340.

Leppäranta, M. (2005). The drift of sea ice. Springer.

Liu, Z., H. Wang, X. Guo, Q. Wang, and H. Gao (2012), The age of Yellow River water in the Bohai Sea. *Journal of Geophysical Research: Oceans* (1978–2012), 117(C11).

Jouon, A., P. Douillet, S. Ouillon, and P. Frauni'e (2006), Calculations of hydrodynamic time parameters in a semi-opened coastal zone using a 3D hydrodynamic model. *Continental Shelf Research*, 26(12), 1395-1415.

Marvin C, S. Painter, and R. Rossmann (2004), Spatial and temporal patterns in mercury contamination in sediments of the Laurentian Great Lakes. *Environmental Research 95* (2004) 351–362.

McCormick, Miller, G.S., Murthy, C.R., Rao, Y.R., and Saylor, J.H. 2002. Tracking coastal flow with surface drifters during the episodic events Great Lakes experiment. *Verh. Internat. Verein. Limnol*. 28:365–369.

McCormick, M. J., Manley, T. O., Beletsky, D., Foley III, A. J., & Fahnenstiel, G. L. (2008). Tracking the surface flow in Lake Champlain. *Journal of Great Lakes Research*, 34(4), 721-730.

Mellor, G. L., and T. Yamada (1982), Development of a turbulence closure model for geophysical fluid problems, *Rev. Geophys*., 20, 851–875,1982.

Miller, G. S., & Saylor, J. H. (1981). Winter temperature structure in Lake Huron. *Journal of Great Lakes Research*, 7(3), 201-206.

Monsen, N. E., J. E. Cloern, L. V. Lucas, and S. G. Monismith (2002), A comment on the use of flushing time, residence time, and age as transport time scales, Limnology and Oceanography, 47(5), pp. 1545-1553.

Nalepa, T. F., Fanslow, D. L., Pothoven, S. A., Foley III, A. J., & Lang, G. A. (2007). Long-term trends in benthic macroinvertebrate populations in Lake Huron over the past four decades. *Journal of Great Lakes Research*, 33(2), 421-436.

Nekouee, N. (2010), Dynamics and Numerical Modeling of River Plumes in Lakes, NOAA Technical Memorandum GLERL-151, Great Lakes Environmental Research Lab, Ann Arbor, MI, USA.

Niemelä, S., Räisänen, P., & Savijärvi, H. (2001). Comparison of surface radiative flux parameterizations: Part I: Longwave radiation. *Atmospheric Research*, 58(1), 1-18.

Nixon, S. W., J. W. Ammerman, L. P. Atkinson, V. M. Berounsky, G. Billen, W. C. Boicourt, W. R. Boynton, T. M. Church, D. M. Ditoro, R. Elmgrens, J. H. Garber, A. E. Giblin'o, R. A. Jahnke, N. J. P. Owens, M. E. Q. Pilson, S. P. Seitzinger (1996), The fate of nitrogen and phosphorus at the land-sea margin of the North Atlantic Ocean,*Biogeochemistry,* 35: 141-180.

Ojo, T. O., J. S. Bonner, and C. Page (2006), Observations of shear-augmented diffusion processes and evaluation of effective diffusivity from current measurements in Corpus Christi Bay, *Cont. Shelf Res.*,26(6), 788–803.

Okubo, A. (1971), Oceanic diffusion diagram,*Deep Sea Research*,18, 789–902.

Parkinson, C. L., and Washington, W. M. (1979), A large-scale numerical model of sea ice. *Journal of Geophysical Research*: Oceans (1978–2012), 84(C1), 311-337.

Peeters, F., A. Wüest, G. Piepke, and D. M. Imboden (1996), Horizontal mixing in lakes, *J.Geophys.Res.*, 101, 18-18.

Phelps, J. J., J. A. Polton, A. J. Souza, and L. A. Robinson (2013), Hydrodynamic timescales in a hyper-tidal region of freshwater influence.*Continental Shelf Research*.

Pickett, R. L. (1980). Observed and predicted Great Lakes winter circulations. *Journal of Physical Oceanography*, 10(7), 1140-1145.

Plattner, S., D. M. Mason, G. A. Leshkevich, D. J. Schwab, and E. S. Rutherford (2006), Classifying and forecasting coastal upwellings in Lake Michigan using satellite derived temperature images and buoy data. *Journal of Great Lakes Research*, 32(1), 63-76.

Pope, S. B. (2000), Turbulent flows. Cambridge University Press.

Rao, D. B., & Murty, T. S. (1970). Calculation of the steady state wind-driven circulations in Lake Ontario. *Archiv für Meteorologie, Geophysik und Bioklimatologie, Serie A, 19(2),* 195-210.

Robertson, D. M., Ragotzkie, R. A., & Magnuson, J. J. (1992). Lake ice records used to detect historical and future climatic changes. *Climatic Change*, 21(4), 407-427.

Saylor, J. H., and L. J. Danek (1976), Wind-Driven Circulation of Saginaw Bay, Coastal Engineering, pp. 3262-3275, ASCE.

Saylor J. H and G. S. Miller (1979), Lake Huron winter circulation, *J.Geophys. Res. Oceans,*84:3237–3252.

Schwab D.J (1999), Lake Michigan Mass Balance Study: Hydrodynamic Modeling Project, *NOAA Technical Memorandum ERL GLERL-108.*

Schertzer, W. M., R. A. Assel, D. Beletsky, T. E. Croley II, B. M. Lofgren, J. H. Saylor, D. J. Schwab (2008), Lake Huron climatology, inter-lake exchange and mean circulation. Aquatic Ecosystem Health & Management, 11(2):144–152.

Sheldon, J. E., and M. Alber (2006), The calculation of estuarine turnover times using freshwater fraction and tidal prism models: A critical evaluation. Estuaries and *Coasts*, 29(1), 133-146.

Sheng, J., Wright, D. G., Greatbatch, R. J., & Dietrich, D. E. (1998). CANDIE: A new version of the DieCAST ocean circulation model. *Journal of Atmospheric & Oceanic Technology*, 15(6).

Sheng, J., Y. R. Rao (2006), Circulation and thermal structure in Lake Huron and GeorgianBay: Application of a nested-grid hydrodynamic model, *Continental Shelf Research,* 26 1496–1518.

Simons, T. J., Murthy, C. R., & Campbell, J. E. (1985). Winter circulation in lake Ontario. *Journal of Great Lakes Research*, 11(4), 423-433.

Sloss, P. W., and J. H. Saylor (1976), Large-scale current measurements in Lake Huron, *J.Geophys. Res*.81:3069–3078.

Smagorinsky, J. (1963). General circulation experiments with the primitive equations: I. The basic experiment*. *Monthly weather review*, 91(3), 99-164.

Spydell, M., F. Feddersen, R. T. Guza, and W. E. Schmidt (2007), Observing surf-zone dispersion with drifters*, Journal of Physical Oceanography*, 37(12), 2920-2939.

Spydell, M. S., F. Feddersen, and R. T. Guza (2009),Observations of drifter dispersion in the surfzone: The effect of sheared alongshore currents, *J. Geophys. Res. Oceans,*114: C07028.

Stocker, R., and J. Imberger(2003), Horizontal Transport and Dispersion in the Surface Layer of a Medium-Sized Lake,*Limnology and Oceanography*, 48(3), 971-982.

Takeoka, H. (1984), Fundamental concepts of exchange and transport time scales in a coastal sea. *Continental Shelf Research* 3, 311–326.

Taylor, G. I. (1921), Diffusion by continuous movements, *Proc. London Math. Soc.*,20,196–212.

Thupaki, P., M. S. Phanikumar, D. Beletsky, D. J. Schwab, M. B. Nevers, and R. L. Whitman (2010). Budget analysis of Escherichia coli at a southern Lake Michigan beach. *Environmental science & technology*, 44(3), 1010-1016.

Thupaki, P., M. S. Phanikumar and R. L. Whitman (2013), Solute dispersion in the coastal boundary layer ofsouthern Lake Michigan,*J. Geophys. Res. Oceans*, 118(3),pp. 1606-1617, doi:10.1029/2012JC008286.

Wan, Y., C. Qiu, P. Doering, M. Ashton, D. Sun, and T. Coley (2013). Modeling residence time with a three-dimensional hydrodynamic model: Linkage with chlorophyll a in a subtropical estuary. *Ecological Modelling*, 268, 93-102.